Investigate the Possible use of Hybrid Solar and Wind Energy Power Supply for Local Recreational Boat

Tigist Andarge Yeshitila

Office of Graduate Studies

Adama Science and Technology University

January, 2022

Adama, Ethiopia

Investigate the Possible use of Hybrid Solar and Wind Energy Power Supply for Local Recreational Boat

Tigist Andarge Yeshitila

A Thesis Submitted to
The Department of Mechanical Engineering
School of Mechanical, Chemical and Materials Engineering

Presented in Partial Fulfillment of the Requirement for Master of Science in Automotive Engineering

Office of Graduate Studies
Adama Science and Technology University

January, 2022
Adama, Ethiopia

Investigate the Possible use of Hybrid Solar and Wind Energy Power Supply for Local Recreational Boat

Tigist Andarge Yeshitila

Advisor: Dr. Addisu Bekele

Co-Advisor: Dr. N.Ramesh Babu.

A Thesis Submitted to

The Department of Mechanical Engineering

School of Mechanical, Chemical and Materials Engineering

Presented in Partial Fulfillment of the Requirement for Master of Science in Automotive Engineering

Office of Graduate Studies

Adama Science and Technology University

January, 2022

Adama, Ethiopia

DECLARATION

I hereby declare that this Master Thesis entitled "Investigate the Possible use of Hybrid Solar and Wind Energy Power Supply for Local Recreational Boat" is my original work. That is, it has not been submitted for the award of any academic degree, diploma, or certificate in any other university. All sources of materials that are used for this thesis have been duly acknowledged through citation.

Tigist Andarge Yeshitila	__________________	__________________
Name of student	Signature	Date

RECOMMENDATION

We, the advisors of this thesis, hereby certify that we have read the revised version of the thesis entitled **“**Investigate the Possible use of Hybrid Solar and Wind Energy Power Supply for Local Recreational Boat” prepared under our guidance by Tigist Andarge submitted in partial fulfillment of the requirements for Master of Science in automotive engineering. Therefore, we recommend the submission of the revised version of the thesis to the department following the applicable procedures.

Dr. Addisu Bekele	______________	____________
Major Advisor	Signature	Date
Dr. N. Ramesh Babu	______________	____________
Co-Advisor	Signature	Date

APPROVAL PAGE

We, the advisors of the thesis entitled **"**Investigate the Possible use of Hybrid Solar and Wind Energy Power Supply for Local Recreational Boat" and developed by Tigist Andarge, hereby certify that the recommendation and suggestions made by the board of examiners are appropriately incorporated into the final version of the thesis.

Major Advisor	Signature	Date
Co-advisor	Signature	Date

We, the undersigned, members of the Board of Examiners of the thesis by Tigist Andarge have read and evaluated the thesis entitled **"**Investigate the Possible use of Hybrid Solar and Wind Energy Power Supply for Local Recreational Boat" and examined the candidate during the open defense. This is, therefore, to certify that the thesis is accepted for partial fulfillment of the requirement of Master of Science in Automotive Engineering.

Chairperson	Signature	Date
Internal Examiner	Signature	Date
External Examiner	Signature	Date

Finally, approval and acceptance of the thesis is contingent upon submission of its final copy to the Office of Postgraduate Studies (OPGS) through the Department Graduate Council (DGC) and School Graduate Committee (SGC).

Department Head	Signature	Date
School Dean	Signature	Date
Office of Post Graduate studies, Dean	Signature	Date

ACKNOWLEDGMENT

I would like to start by extending my deepest gratitude to God for enabling me to undertake my studies and this research.

I would like to sincerely thank my advisor Dr. Addisu Bekele (Associate Professor) who continually conveyed constructive advice and scholarly support, without his persistent advice and guidance this research paper would not have been possible. I would also like to thank my co-advisor Dr. Ramesh Babu, for supporting and helping me.

In addition, I would like to thank a boat manufacturer Mr. Abel Chane, and last but most definitely not least, I am grateful for my teachers who have emotionally encouraged me to complete my studies. My friends and my sisters Tsedeniya and Bethlehem for your significant contribution, support, and advice.

TABLE OF CONTENTS

Contents **Page**

LIST OF TABLES

LIST OF FIGURES

ACRONYMS

ANSYS	Analysis of Systems
CAD	Computer-Aided Design
CATIA	Computer Aided Three Dimensional Interactive Application
CFD	Computational Fluid Dynamics
DNS	Direct Numerical Simulation
EPSs	Electric Propulsion System for Boat.
GHG	Green House Gas
HPS	Hybrid marine propulsion system
HRES	Hybrid Renewable Energy Systems
IC	Internal combustion
ITTC	International Towing Tank Committee
LES	Large Eddy Simulation
MPPT	Maximum point tracking system
PEM	Polymer electrolyte membrane
PMSM	Permanent magnet synchronous motors
PWM	Pulse Width Modulation
PV	Photovoltaic
RANS	Reynolds Averaged Navier - Stokes Simulation
SST	Shear Stress Transport
TSR	The Tip speed ratio
VOF	Volume of fluid
WECS	Wind energy conversion device transforms

NOMENCLATURE

A	Projected Area (m^2)
As	a Swept area of turbine (m^2)
C_d	Drag Coefficient (-)
C_l	Lift Coefficient (-)
CA	Coefficient of Air Resistance (-)
Ct	The torque Coefficient (-)
Cp	The power coefficient (-)
CT	Coefficient Total of Hull Resistance (-)
CV	Coefficient of Viscous Resistance (-)
C_R	Residual resistance coefficient (-)
CW	Coefficient of Wave Making Resistance (-)
d	The diameter of the semi-cylindrical Savonius rotor (m)
D	Rotor diameter (m)
Fr	Froude Number (-)
H	Rotor height (m)
$\bar{I}$	Hourly solar irradiance ($\mathrm{Watts/m^2}$)
I	Rotor moment of inertia ($kg.m^2$)
I_b	Moment of inertia for two blades of savonous rotor ($kg.m^2$)
I_s	Shaft moment of inertia ($kg .m^2$)
I_p	End plates moment of inertia (kg)
k	Radius of gyration
L	Length of the Hull (m)
m	Total mass of turbine (kg)
PE	Effective power (W)
P_w	Extracted power from the wind (Wh)
P_a	Available power from the wind (Wh)
Pp	Propulsion Power (Wh)
P_p	Solar power Energy (Wh)
r	Effective radius of turbine (m)
RA	Air Resistance (-)

Rn	Reynolds number (-)
RT	Total Resistance (-)
RV	Viscous Resistance (-)
RW	Wake Making Resistance (-)
S	Wetted Surface Area of the Hull (m^2)
R_b	Ratio of beam radiation on the tilted surface (-)
V	Velocity of Boat (m/s)
V_{rotor}	Velocity of Savonius rotor (m/s)
T	The rotor torque (N.m)
Tw	The wind available torque (N.m)

GREEK SYMBOLS

ϕ	Latitude (°)
δ	Angle of declination of the sun (°)
θ	Angle of incidence (°)
θz	Zenith angle of the sun
β	Tilt angle (°)
ω	Hour angle (°)
η	Efficiency (%)
ρ	Density (kg/m^3)
ρ	Ground albedo (reflectivity)
φ	Latitude of the site under study
λ	The Tip speed ratio
ω	The angular velocity of Savonius rotor (rad/sec).
α	Angular acceleration
ν	Kinematic viscosity of water

ABSTRACT

The fuel economy has been one of the dominant issues in the transportation sector. Combustion engines in boats bring several environmental problems, such as greenhouse gas emissions and acidification of oceans. Air and water pollution is rapidly increasing and affecting most of the major cities of the world. In addition to that developing country like Ethiopia has a great scarcity of oil fuel. To address these issues the combined utilization of renewable energy sources is becoming increasingly attractive and is being widely used as alternative sources of energy. The main aim of this thesis work to investigate the possible use of hybrid solar and wind energy power supply for recreational boats manufactured locally. To achieve the objectives of this thesis the data about solar radiation and wind speed was gathered from the Ethiopian Meteorological Agency. For the numerical analysis, the boat was modeled in CATIA V5 and the CFD analysis is carried out in ANSYS Fluent. The simulations were based on the Reynolds Average Navier-Stokes equations with SST k-ω as turbulence model together with the volume of a fluid method describing the two-phased flow of both water and air surrounding the boat. In addition to this ANSYS hydrodynamic was done for testing the stability of the boat. Moreover, the model was also constructed for demonstration purposes. The Propulsion Power was determined as 5hp. The average energy output from the solar system is 6.66 kWh in February and the average energy obtained from the wind turbines was 1.3 kWh in May. However, the energy produced by the integration is insufficient to run the boat, as a result, it was concluded to propel the boat by integrating solar energy with a grid system that uses energy stored in batteries. This produces the required 20 kWh power used to drive the boat. Besides the results of the hydrostatic and hydrodynamics stability testing confirms the stability hence the metacenter height of the designed boat is more than the recommended (0.75m). The life cycle cost of the proposed PV solar system and electric grid system is 847,726.65 birr which is low compared to gasoline, which its life cycle cost is 3,500,160 birr. Finally, the testing of the constructed model was functional and shows a more stable condition when the keel is installed.

Keywords: ANSYS, Boat, Hydrodynamic, Propulsion, Resistance, Solar-wind.

CHAPTER ONE

INTRODUCTION

1.1 Background of the study

A boat is a watercraft of a large range of types and sizes but generally smaller than a ship. Small boats are typically found on inland waterways such as rivers and lakes, or in protected coastal areas. The boat is intended to be used for recreational and tourism purposes (Sunaryo & Ramadhani, 2018). In today's fast-developing world, air pollution is rapidly increasing and affecting most of the major cities of the world. This increase is mainly due to the emission of carbon dioxide and other toxic gases from the different transportation systems. This leads to a gradual increase in global warming. In addition, demand for utilization of fossil. Consequently, to overcome the dependency on those fuels many technologies and solutions are now developing and hybrid technology is one of them.

Hybrid technology is that uses two or more distinct power sources to maneuver the vehicle. Today, boats using solar and wind energy are being developed as alternatives to fuel-dependent vehicles. Technologies and materials are advancing in a way that enables high performance yet clean and inexpensive sea vessels. Instead of fuel-dependent sailing crafts, eco-friendly water vessels with near-zero emissions are being developed, because of the pre-industrialized sailboats (Gürsu, H.2014). Hybrid Renewable Energy Systems (HRES) are becoming popular as stand-alone power systems for providing electricity (Shirsath et al., 2016).

Wind and solar power are omnipresent, freely available, and environmentally friendly. The wind energy systems might not be technically viable in the least sites due to low wind speeds and being more unpredictable than solar power. The combined utilization of those renewable energy sources is therefore becoming increasingly attractive and is being widely used as an alternative to oil-produced energy. Economic aspects of those renewable energy technologies are sufficiently promising to incorporate them for rising power generation capability in developing countries (Nema et al., 2009).

It is important to form an accurate prediction of the hull resistance to be ready to choose an appropriate engine power of the propulsion unit. Traditionally, the hull resistance and running attitude are determined by performing experiments by scaled-down the model hulls in towing tanks. These experiments have proved to predict the full-scale hull very well, but the method is time-consuming, expensive, and only applicable to the tested model. A more universal method for hull performance predictions is to use computational fluid dynamics (CFD) which is a branch of computer simulations (Frisk & Tegehall, 2015).

1.1.1 Electric Propulsion System for Boat

Electrically propelled recreational boats offer a viable way to lessen the environmental and health impacts of recreational boating. The environmental and health effect was lower when it was powered by non-renewable fossil fuel electricity than when it was powered by nuclear, wind, or solar energy (Hemez et al., 2020). EPS technologies have been developed for a variety of applications, particularly in the transportation industry. The prime mover, synchronous generator, power transformer, motor drive, motor propeller, and other load needs were described as components of the EPS for boats, as shown in Figure 1.1.

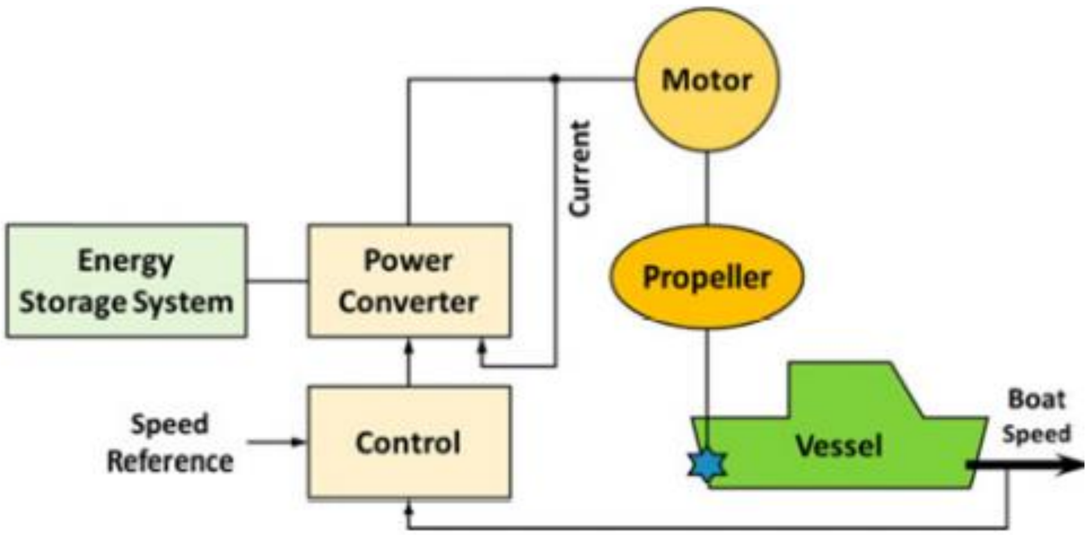

Figure 1.1. Basic components of direct EPS (Lee et al., 2014)

1.1.2 Solar Energy System

It is a form of energy that is derived directly from sunlight. Photovoltaic solar panels can be used for both small and large-scale applications to harvest solar energy. Panels are used in small and large applications to provide electricity for equipment (Nyanya, & Vu, 2019).

Most solar applications are now land-based, as opposed to marine applications. On maritime applications, solar panels can be engaged for main propulsion or auxiliary. Photovoltaic modules can easily implement in remote areas since the electrical power production comes from a reliable, free from pollution. They can produce electric current during cloudy days (Chun, 2015).

1.1.3 Wind Energy System

Wind is an environment-friendly source of energy that possesses huge potential to satisfy energy needs for people and also to mitigate the global climate change from greenhouse gasses emitted by the burning of fossil fuels (Maisuria, et al., 2016). A wind energy conversion device transforms wind energy into electrical energy (WECS). The wind turbine is a vital component of the WECS because it collects kinetic energy from the wind and transforms it into electrical energy. The kinetic energy from the flow of a mass of air is transformed to rotational kinetic energy (Aymane et al., 2017).

1.2 Drawbacks of Using Fuel as an Energy Source

Oceans and lakes around the world are impacted by environmental degradation and fuel combustion. The main reason for this problem is the shipping industry. The shipping industry is the most important transport mode for world trade. It consumes more fuel in comparison with other transport modes. Its Emissions contribute significantly to global air pollution and long-term global warming (Sui et al., 2020). It was predicted that maritime CO_2 emissions will increase significantly by 50% to 250% in the period up to 2050 (Faber et al., 2020). As a result, the shipping industry is striving to reduce its fuel consumption and emissions (Sui et al., 2020). Otherwise, the shipping industry will create high air pollution and affect human health (Walker et al., 2019). Moreover, in today's fast-growing economy the need for energy demand is increasing, and this leads to an increase in energy costs, limited reserves, and environmental pollution, as a result, renewable energy is the most attractive energy source and best solution (Mengi et al., 2015).

1.3 Statement of the Problem

The fuel economy and the adverse environmental effect of the internal combustion engine (ICE) is one of the dominant concerns in the transport sector in recent years. Achieving minimum fuel consumption helps to conserve natural resources and minimize emissions. The earliest boat utilizes manpower, while modern boat technologies utilize ICE for providing propulsive force to the boat. Currently, in Ethiopia, local recreational boats are propelled both man-powered and ICE. The propulsion of the boat using ICE consumes imported fuels which leads to environmental pollution and dependence on fuel-producing countries. On other hand, the man-powered type has a very limited carrying capacity and is not ergonomic. To address the adverse effect of ICE propelled boats, several innovative works are carried out in the past. In this study, investigate the possible use of hybrid solar and wind energy power supply for local recreational boat is carried out utilizing the wind and solar radiation data of a specific location, Bahir-Dar city.

1.4 Objectives of the Study

1.4.1 General objective

The general objective of this thesis work is to investigate the possible use of hybrid solar and wind Energy power supply for local recreational boat.

1.4.2 Specific objectives

The specific objectives of this thesis work are:

- To study the solar potential and wind potential of the site analytically (Lake Tana).
- To size the photovoltaic (PV) system for an alternative power supply to the boat.
- To design and size a wind turbine system for an alternative power supply to the boat.
- Numerical analysis of the boat using computational tools.
- Stability analysis of the boat at different wind speeds and directions.
- To develop a model of the boat for demonstration purposes.

1.5 Significance of the Study

The significances of this thesis work are as follows:

- Mitigate environmental pollution caused by ICE propelled boats.
- Helps in reducing the country's dependence on imported oils.
- Reduction in the operating cost of the recreational boat and, helps owners of the boat to get benefited.

1.6 Scope and Limitation of the Study

1.6.1 Scope of the study

The scope of this thesis work includes the design of a boat that can be propelled by wind and solar energy sources. The boat models were designed by using CATIA software and then transferred to ANSYS software to study the simulation of the fluid motion around the boat and to predicate the resistance force to determine propeller power. ANSYS AQWA was used to study the Static and hydrodynamic Stability Tests. Finally, a small-scale model for demonstration purposes was developed. The proposed work does not include the structural design of the boat.

1.6.2 Limitation of the Study

Experimental evaluation of the actual boat is inquired for the validity of the result. Nevertheless, hence experimental setups inquire a high amount of budget and lab facility. In this study, the experimental evaluation is not carried out.

Estimation of boat resistance using a CFD analysis conducted using SST k-ω turbulence model. Since it is difficult to get a high-performance PC.it was vastly challenging and time-consuming. Single results were obtained by waiting for more than a week. Due to that, it is difficult to conduct the study with a better turbulence model.

1.7 Organization of the Thesis

This thesis is organized into eight chapters. The **First Chapter** presents the introduction of the study including the drawback of using fuels as an energy source, statement of the problem, the general and specific objectives, significance, Scope and Limitation of the Study, and finally organization of the thesis. Literature about solar energy, wind energy, hybrid energy, resistance force prediction, computational fluid dynamics analysis, and stability for a boat are reviewed in **Chapter Two**. **Chapter Three** elaborates on the materials and methodology of the work including data collection. **Chapter Four** presents the radiation estimation and wind potential of the site. **Chapter Five** elaborates the theoretical analysis of solar and wind energy integrated for the boat and presented the sizing of energy. **Chapter Six** presents the numerical analysis of energy demand using the drag coefficient and stability of the boat. Results and discussions are presented in **Chapter Seven**. **Chapter Eight** presents the major conclusions of the work conducted in this thesis, highlighting the findings and concluding with recommendations for further work.

CHAPTER TWO

LITERATURE REVIEW

2.1 Introduction

In this chapter, various studies related to solar powered boats, wind powered, hybrid powered and CFD analysis on the boat reviewed in - depth.

2.2 Previous literature on related work

2.2.1 Previous works on solar assisted boats

Cancela et al. (2016), constructed and simulated a notional zero-emission electric sailboat to develop an energy-independent sailing boat powered by an electric motor. It includes a simulation and validation of a sailing yacht with an integrated renewable energy system designed to reduce pollutants and emissions. Solar panels were employed to provide electrical energy for the engine, and batteries were used for the storage system. The simulation of the electrical installation and independent modular models for each energy system was done in Matlab® Simulink® and embedded to test the system under varied situations. All of the simulations are controlled by a logic controller written in Matlab®. The primary issue with solar energy is its seasonality.

Nasirudin et al. (2017), carried out a Solar Powered Boat Design Optimization. A strategy for designing a solar-powered boat is to determine the size of the photovoltaic (PV) system with the least amount of money. Two-stage optimization procedures have been proposed. The first stage involves applying the golden search section technique to simplify ship size optimization based on the existing ship design to acquire the lowest possible propulsion power. The second stage involves utilizing the Simplex algorithm to optimize the size of the PV system to achieve the most PV modules and batteries at the lowest cost. When they compare the existing ship, the optimum ship gives higher PV power and smaller battery capacity, which means that the optimum ship utilizes more solar energy and reduces the dependency on grid energy.

Sunaryo et al. (2018), designed a solar-powered electrical recreational boat for Indonesian waters to support the government's program in developing maritime tourism and to promote the use of green and renewable energy. Based on the appliances and equipment placed in the boat, the required electrical power was determined and the optimum attachment of solar panels on the boat structure is also calculated. The findings reveal that solar electricity is stored in a battery and used by electrical devices on board the vessel. The electrical power required for each trip is 24.17 kWh.

Freire and Pruna (2009), a Solar Powered Model Boat can also be designed and built. Solar energy is commonly assumed to be limited to sunny places. The boat was tested and found to operate directly off the solar panels, giving it a pleasant appearance.

Tamunodukobipi et al. (2018), studied the design of a flexible lightweight solar-powered marine vessel that can be used in the Rivers State Peace Park and the Nigerian interior. The hull of a catamaran was chosen because of its low resistance and stability. For the hydrodynamic analysis of the hull, two alternative methodologies were applied. In addition, the boat resistance was determined using comparable methods. A method and algorithm for determining the best solar PV module for a boat.

Postiglione and Colleagues (2012), studied Permanent magnet synchronous motors and advanced power electronics are used in the propulsion system for an all-electric passenger boat. The main objective was to build a zero-emission electric power boat that could be utilized for both public transportation and water activities. It was powered partly by photovoltaic panels for an extended range and partially by lithium-ion batteries charged at the harbor. A DC-DC converter was utilized to provide a constant DC-bus for a voltage source inverter based on multistate switching cells that drives two 12 kW permanent magnet synchronous motors (PMSM). This article focuses on the speed of the boat, the duration of the battery power and does not describe the procedures for charge control and engine control.

2.2.2 Previous works on wind power assisted boats

Garbe, (2017), designed a Wind turbine integrated boat system to scale back the pollution of the environment as its renewable energy. The Energy extracted from the wind was converted into electricity which will be stored within the capacitor. The stored energy is used to drive the motor that's attached to the propeller of the boat or the shaft of the water jet pump. This technique was Modeled on CatiaV5 software and ANSYS hydrodynamic software for stability testing. All basic dimensions and propulsion power were determined by written java code.

Moreover, a shrouded airborne turbine, capable of generating 70 kW to propel a leisure boat with a capacity of 8-10 passengers was designed. The model has been analyzed numerically by CFD, by Star CCM+ software. The Unsteady Reynolds Averaged Naiver Stokes Simulation (URANS) has been analyzed. Turbulence model has been selected, to review the physical properties of the flow, with emphasis on the performance of the turbine and thus the rise in air velocity at the throat (Zefreh, 2016).

2.2.3 Previous works on hybrid technology assisted boats

Banjarnahor et al., (2017), proposed a hybrid solar and wind energy harvester to be installed on the fishing smack to power a refrigerator. Solar panels with a power output of 100 watts and a wind turbine with a power output of 300 watts were used. The solar panels can harvest 815-817 watts of electricity per day, while the turbine can harvest 43-62 watts per day, according to the testing. As a result, the system is capable of achieving its goals.

A Hybrid marine propulsion system (HPS) consisting of an internal combustion engine and an electric engine coupled with a battery pack was also done. The HPS performance, varying the battery pack capacity, was provided alongside an estimation of its impact on the system efficiency (Barelli et al., (2018).

(Scurtu et al., 2020), they proposed a hybrid power grid system for electric boats. As the first renewable energy power source, the system uses a turbine that drives an induction generator, solar PV panels with a Maximum Point Tracking (MPPT) system as the second renewable energy power source, and a polymer electrolyte membrane (PEM) cell as the third renewable energy power source. As a result, the design problem is one of establishing a balanced and flexible system with the fewest possible uncertainties. Stability values are shown and calculated for a specific load of 20 people using the SolidWorks produced 3D model. Computer-based programs can be used in all phases of the design process.

Zhang & Xu, (2020), carried out a motor-screw-slide-rack-and-pinion gear structure is integrated with the solar panels to create electromechanical-solar panels. The application of automatic control technology, while optimizing the hull design and component coordination, further increases the use efficiency of wind and lightweight energy, achieving the difference in sail angle of attack and the efficient coupling of the two energies.

Obaid et al., (2019), an electric boat was designed with a three-phase asynchronous motorpowered by a solar and diesel hybrid system. They use the MPPT system for maximum PV array output to drive the electric boat. However, when solar irradiance is insufficient, a diesel generator is used as an auxiliary power source. They also demonstrated previous predictions of solar irradiance by using a neural network that helps plan hybrid operations to drive electric boats.

2.2.4 Previous works on CFD analysis of the boat

Aldas et al. (2019), analyzed the performance of a ship mono hull at Galapagos real conditions using ANSYS FLUENT. The analyses were made to validate ships behavior existing in Galapagos Islands. The hydrodynamic analysis of a mono hull was simulated in static and dynamic conditions. The static analysis considers water and airflow hitting the boat bow which is resting (anchored boat). While dynamic analysis considers both the boat and water flow speed (sailing boat). The result showed that as marine current speed increases from 2.06 to 4.12 m/s, the values of static and dynamic pressures reach a maximum value of 1.63 and 5.96 MPa. From the results, the maximum error between calculated and simulated static pressure at a speed of 3.6 m/s is 2% whereas the maximum error of the calculated and simulated values of dynamic pressure is 3.48%.

D. Purnamasari et al. (2017), carried out a numerical simulation to determine free surface flow around a tanker hull form for which experimental results are available. The numerical methodology is found to be appropriate for simulating the turbulent flow around a model to estimate model total resistance and the SST turbulence model was used in Ansys CFX. According to their result, At a Froud number of 0.161, the pressure is ranged from 1.565 kPa to 3.704 kPa and the total resistance (R_T) resulting from the simulation is 26.448N. At Froude number of 0.181, the pressure is ranged from 1.289 kPa to 3.808 kPa and the total resistance (R_T) resulting from the simulation is 33.744N. At the Froud number of 0.202, the pressure is ranged from 1.088 kPa to 3.909 kPa and the total resistance (R_T) resulting from the simulation is 44.548N. The average error between the numerical and experimental resistance components is 2.34%.

Elkafas et al. (2019), presented ship resistance using the CFD simulation method which is ANSYS-CFX software. As a case study, the Container ship scale model is investigated in the paper and the ship resistance is calculated at various ship speeds and Froude number. The predicted results for resistance components at various Froude numbers were compared with resistance results computed by using the Holtrop method. From their result, it is shown that the simulation results agree well with the results computed from the Holtrop method and that ANSYS-CFX code can predict ship resistance. Within the simulated range of Froude Number, the maximum error is 5.15% Froude number of 0.4.

Khaware et al. (2019), employed overset mesh approach to overcome limitations of the traditional dynamic mesh approach, which provides ease of mesh generation and modeling of mesh motion. In their paper, two common marine hydrodynamic problems were simulated using the Volume of Fluid method (VOF) and overset approach. The first problem focuses on the dynamic response of a container ship at open sea. The second problem focuses on the launching of a lifeboat in the calm water. The results of various validation studies showed good agreement with theoretical and experimental data. It can be concluded from their study that numerical simulation of ship motion and lifeboat launching can be achieved robustly and accurately using overset mesh implemented in ANSYS Fluent.

2.3 Types of solar panels

I. Monocrystalline solar panels

They have the highest efficiency and power capacity out of all types of solar panels. The higher efficiency of monocrystalline solar panels means that they require less space to reach a given power capacity Saleem, et al., 2016.

II. Polycrystalline solar panels

Polycrystalline panels have a lower efficiency rate than monocrystalline panels due to this crystal structure. Polycrystalline solar panels, on the other hand, are now far more efficient than monocrystalline solar panels Saleem, et al., 2016.

III. Thin-film solar panels

Thin-film solar cells are mostly utilized in large-scale operations, like utility or industrial solar installations due to their lower efficiency ratings. They are lightweight and, in some cases, flexible. However, it also makes them less efficient than crystalline solar panels. They have shorter lifespans than other types of solar panels Saleem, et al., 2016.

Table 2.1.The efficiency of Solar PV System (Saleem, et al., 2016)

PV Module type	Theoretical efficiency	Practical efficiency	Warranty(Years)
Mono- crystalline	25%	15-20%	25
Poly-crystalline	20.4%	13-16%	25
Thin film	18.7	9-11%	10-25

2.4 Types of wind turbine

There are two general types of wind turbines: horizontal axis and vertical axis. Horizontal axis machines have blades that rotate on an axis parallel to the ground. The blades of a vertical axis machine rotate on an axis perpendicular to the ground.

2.4.1 Horizontal axis wind turbine

Most commercial wind turbines today belong to the horizontal-axis type, during which the rotating axis of blades is parallel to the wind stream. The advantages of this sort of turbine include the high turbine efficiency, high power density, low cut-in wind speeds, and low cost per unit power output (Tong, 2010). The axis faces into the wind and the blades use the aerodynamic lift to spin perpendicular to the direction of wind flow (Winslow, 2017). One of the most significant disadvantages of HAWTs is their high level of noise. As a result, they are typically less socially acceptable than other renewable energy sources and are difficult to design and build. Since there are so many factors to consider when designing the ideal blade for a horizontal wind turbine, they are both costly and difficult to maintain.

2.4.2 Vertical axis wind turbine

Wind turbines with vertical axis blades are perpendicular to the ground and rotate around a vertical axis. Vertical turbines use lift, drag, or a combination of the two to generate power (Winslow, 2017). The fundamental advantage of VAWTs is that they are not affected by wind direction and do not require a yaw mechanism. They are also highly fixed in the sense that they do not vary their or the blade's direction once placed. They don't need a device to adjust the angle of their blades because they can work in any wind direction. VAWTs can better capture turbulent airflow around buildings and other impediments. Their total efficiency, however, is modest.

I .Savonuis vertical axis wind turbines

The simplest type of wind energy conversion system is the Savonius turbine. They are drag-type devices, consisting of two or three blades (vertical – half cylinders). The Finnish engineer Sigurd Savories invented the savonous wind turbine in 1922. The Savonius turbine uses drag to push the curved blades to generate a torque that will make the rotor turn. Aerodynamically it is the simplest wind turbine to design and build which reduces its cost drastically compared to the aero foil blade designs of the other VAWTs and HAWTs.Two blades savonous wind turbine would look like an "S" letter shape in cross-section. The below Figure 2.1 shows the working principle of savonous wind turbine (Ali, 2013).

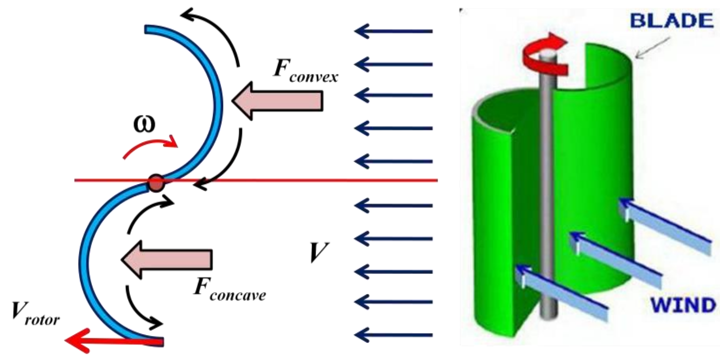

Figure 2.1. Schematic drawing showing the drag forces exert on two blades Savonius (Ali, 2013)

2.5 Charge Controller

It controls the power source, which is kept active or inactive. It simultaneously charges the battery and delivers power to the load. The controller has over-charge protection, short-circuit protection, pole-confusion protection, and automatic dump-load function. It can vary the power as per load demand. It adds both power sources, so that load demand can be fulfilled and when power is not generating, it should extract power from the battery and deliver it to the load.

I. Pulse Width Modulation (PWM) Charge, controller

It is the most effective to achieve constant voltage battery charging by adjusting the duty ratio of the switches (MOSFET). In PWM, the charge controller, the current from the solar panel tapers according to the battery's condition and recharging needs. When a battery voltage reaches the regulation set point, reduces the charging current to avoid heating and gassing of the battery. Because the pulse width modulation technology charges at the same voltage as the battery The PWM, type is unable to capture excess voltage. A PWM controller is not a DC-to DC transformer (Osaretin & Edeko, 2015).

II. Maximum Power Point Tracking (MPPT) Charge Controller

The most advanced solar charge controller available is the Maximum Power Point Tracking (MPPT). It is more sophisticated and more expensive. It has several advantages over the PWM charge controller. It is 30 to 40% more efficient at low temperatures. It will adjust its input voltage to harvest the maximum power from the solar panel and then transform this power to supply the varying voltage requirement of the battery plus load. It is generally accepted to increase photovoltaic (PV) system efficiency by maximizing PV output power in every weather condition. The MPPT charge controller is a DC-to-DC transformer that can transform power from a higher voltage to power at a lower voltage (Vitronenergy, 2014).

2.5.1 Comparison between PWM and MPPT Solar Charge Controllers

PWM helps to get the batteries charged up, longer battery life, reduced battery overheating, PV array and battery voltages should match for PWM, and more of the power generated by the solar panels is stored. Since the batteries store more energy on average, a smaller battery (or less battery in a battery bank) can be used to reduce overall system costs but it is unable to capture excess voltage because the pulse width modulation technology charges at the same voltage as the battery (Majaw et al,2018). MPPT solar charge controllers allow users to use PV modules with a higher voltage output than the operating voltage battery system. Since MPPT units are generally larger in physical size so they are more costly as compared to PWM controllers (Vitronenergy, 2014).

2.6 Converters (AC – DC Conversion)

Converters are a device are used to convert AC power to DC power. Virtually all electronic devices require converters. It increases or decreases the voltage (AC or DC) of a power source depending on the application. A converter that increases voltage is called a step-up converter and a converter that decreases voltage is called a step-down converter. An advantage of using a converter to increase the voltage from the battery is a smaller and less expensive battery may be used while still utilizing an efficient high voltage motor.

2.7 Energy Storage System

A battery is a device that converts the chemical energy of its cell components into electrical energy and is used to store electricity.

2.7.1 Lead acid-based batteries

It is the oldest type of rechargeable battery. Despite having a very low energy-to-weight and a low energy-to-volume, its ability to supply high surge currents means that the cells have a relatively large power-to-weight ratio. Lead-acid batteries are habitually used in the automotive and naval industry to provide the necessary energy to the starter motors and for a storage system. There are three basic types of lead-acid batteries: flooded batteries, absorbed glass mat batteries (AGM), and gel batteries. All Lead Acid Batteries should be ventilated to prevent the buildup of explosive hydrogen gas (Romani, 2021).

2.7.2 Lithium-Ion batteries

Lithium is the lightest of all metals; it has the greatest electrochemical potential and provides the largest specific energy per weight. Accounting for 85.6% of deployed energy storage systems. Li-ion batteries don't require temperature monitoring to make sure effective operation. Many technologies believe lithium-ion batteries, like portable devices, hybrid electric vehicles, and electric vehicles. The advantages of Li-ion batteries may lead to their use in the production of large-scale storage systems, even if such storage will be expensive. Lithium-ion is a new technology that has proven difficult to recycle. However, recent research has shown that lithium batteries can be recycled up to 96%. Lithium is the lightest metal on the planet, and 1 kg of lithium contains 29 times more atoms than lead-acid batteries (Romani, 2021). The comparison of lead-acid and lithium battery are shown in Table 2.2 and Figure 2.2

Table 2. 2. Comparison of Lead-acid and Lithium battery storage systems (Krieger et al., 2013)

	Lead-acid	Lithium-ion
Storage capacity	30-40 Wh/kg	110-250 Wh/kg
Safety	Release of highly toxic gas	Fire/explosion ,highly flammable
Depth of discharge	50%	80%
Charge	6-15 hours	3-5 hours
Total number of cycles	2-5 years	10 years
Efficiency	85%	90% -98%
Availability	More available	Not easily available
Estimated Cost	Cheap	Expensive
Recycle	Recycle up to 100%	Recycle up to 96%

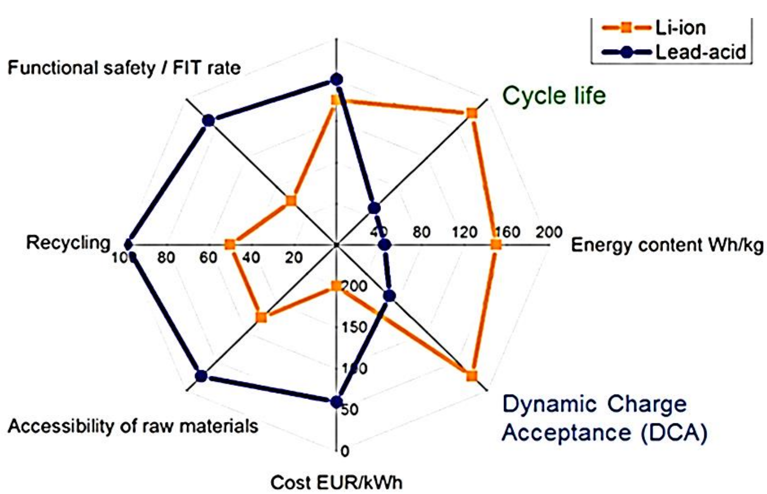

Figure 2.2. Comparison of Lead-acid and Lithium battery storage systems (https://batteryuniveristy.com)

2.8 Electric Motor

Electric outboard motors have got a lot of attention these days. It is silent, clean, and maintenance-free with NO fuel or exhaust smells. A motor is an electro-mechanical device, used to change one form of energy (electrical) to another (mechanical) to generate rotational force. The working principle of the motor mainly depends on the communication of two fields like electrical and magnetic. Basically there are two kinds of electric motors available like AC motors, DC motors.

2.8.1 DC-motors

Currently a wide-ranging of electric motor technologies are in use. Traditional field-wound DC-motors still are used. Today many boats use lightweight permanent magnet DC-motors. The advantage of both types is that the speed can be controlled electronically. The energy used by a DC motor comes from batteries or another generated power source that offers constant voltage. DC motors offer better speed variation and control and produce more torque than AC motors (Asadi, 2018).

2.8.2 AC-motors

Energy comes from magnetic fields generated through coils wrapped around the output shaft. AC motors consist of several parts, including a stator and rotor. The comparison of AC-motor and DC-motor is illustrated in Table 2.3.

Table 2.3. Comparison of AC-Motor and DC-Motor (Asadi, 2018)

AC Motor	**DC Motor**
Complicated because DC power from the battery must be converted to AC	Simpler as they use battery power directly
Generates more heat comparatively	Generates less heat, less energy is wasted
Motor/controller/Inverter blocks are expensive.	Motor controller blocks are less expensive
Single-speed transmission	Multi-speed transmission.
lightweight	Heavier for the same power.
Average starting torque	Very high starting torque
Simpler to install	Complicated to install
AC Inverter fails and car stops	Can short-circuit the battery-pack, mostly causing the motor to catch fire.

AC motors are efficient, durable, quiet, and flexible, making them a viable solution for many power generation needs. Some boats are use AC motors or permanent magnet brushless motors. The advantages of these AC motors are lack of commutators which can wear out or fail and lower currents allowing thinner cables and, the disadvantages are the total reliance on the required electronic controllers and the usually high voltages which require a high standard of insulation (Bhatt, et al., 2013).

2.9 Resistance

The force acting on the hull in the opposite direction of motion, i.e. in the horizontal direction, is known as resistance. The resistance forces operating on a hull are caused by both the water and the hull's features. During the design process, there are several methods for predicting resistance. Computational fluid dynamics is the most well-known method (CFD) (Skupień and Prokopowicz, 2014).

2.9 1 Total resistance

The ship's total resistance is made up of air and hydrodynamic resistances. According to two perspectives, it can be separated into two primary components. It is made up of either frictional or viscous components, as well as wave resistance (Skupień and Prokopowicz, 2014). There are three basic components to total resistance: viscous resistance of the water acting on the hull, wave-producing resistance, and air resistance. As shown in Figure 2.3, the total hull resistance increases as speed increases. It's worth noting that the resistance curve isn't linear and that it steepens as you go faster.

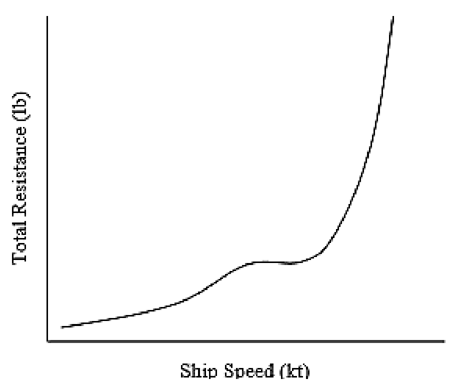

Figure 2.3. Total hull resistance (https://www.usna.edu/NAOE)

I. Viscous hull resistance

Figure 2.4 shows the ideal flow around a submerged body and is defined by the fluid flowing smoothly over the entire surface with a pressure distribution that is normal to the body. There is a component of pressure resisting motion in the forward segment of the hull, and a component of pressure assisting motion in the aft section of the body. These pressure forces are equal in a perfect fluid, and the body experiences no resistance.

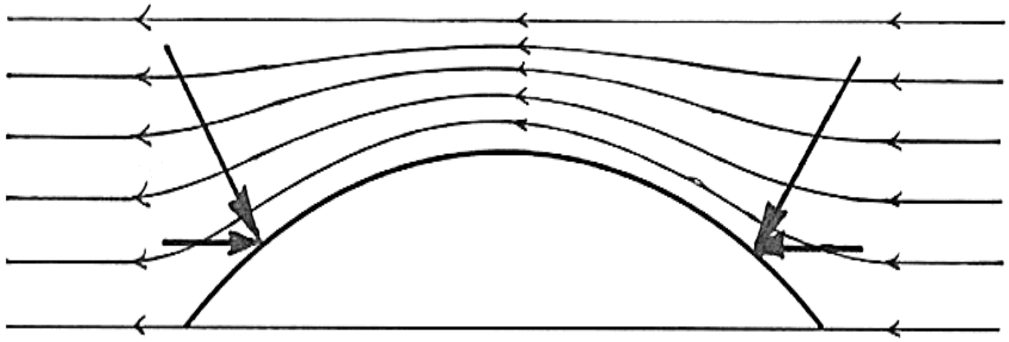

Figure 2.4. Ideal flow around a submerged body (https://www.usna.edu/NAOE)

In reality, a fluid travels over a body, causing drag. As it adheres to the surface, a boundary layer forms, as shown in Figure 2.5 within this layer, the flow speeds rapidly shift from zero near the body's surface to free stream velocity far away from the surface. There are two types of drag as a result of this: viscous friction resistance caused by shear stress within the fluid and viscous pressure resistance caused by a pressure differential.

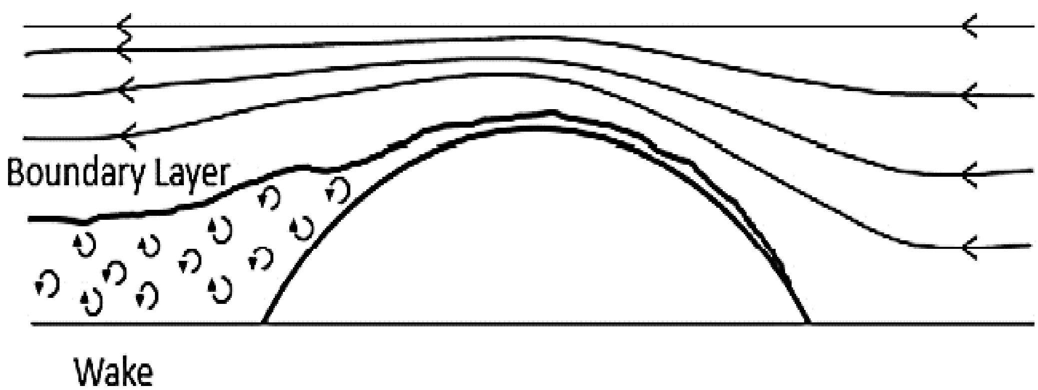

Figure 2.5. Actual Flow around a Body (https://www.usna.edu/NAOE)

- ✓ Resistance is due to the viscous stresses that the fluid exerts on the hull. (due to friction of the water against the surface of the ship)
- ✓ Viscosity, ship's velocity, the wetted surface area of the ship generally affect the viscous resistance.
- ✓ As a boat moves through the water, the velocity of the water at the hull's surface is equal to the speed of the boat.
- ✓ As the distance from the hull increases, the velocity moves toward the free stream velocity. This velocity gradient creates shear stress in the water and thus drag.

II. Wake making resistance

- ✓ Resistance is caused by waves generated by the motion of the ship.
- ✓ Wave-making resistance is affected by beam to length ratio, displacement, the shape of the hull, Froude number (ship length & speed).
- ✓ As ship speed increases, the height of the waves produced by the ship increases, and therefore the energy required to produce these waves also increases.

Divergent waves, which expand outward from the ship, and transverse waves, as shown in Figure 2.6 are created when an object moves through the water.

.

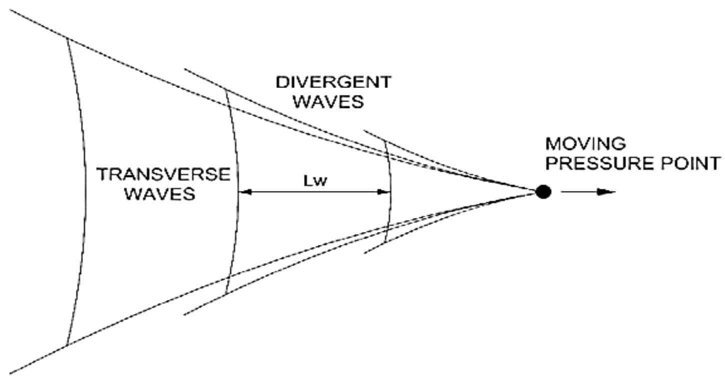

Figure 2.6. A moving object in the water creates a wave pattern (https://www.usna.edu/NAOE)

III. Air resistance

- ✓ Resistance is caused by the flow of air over the ship with no wind present.
- ✓ Air resistance is affected by projected area, the shape of the ship above the waterline, wind velocity, and direction.
- ✓ Resistance due to air is typically 4-8% of the total ship resistance, but maybe as much as 10% in high-sided ships such as aircraft carriers.

2.9.2 Dimensionless coefficient of total hull resistance

Dimensionless coefficients are used to describe the performance of a system or to compare different systems to each other.

2.10 Computational Fluid Dynamics (CFD)

CFD is applied in most disciplines involving a flowing fluid, including the shipping industry. The tool is especially useful when there is a complex fluid flow involved (Voxakis, 2012). It is the analysis of fluid flows, using numerical methods. It is economical in time and cost in comparison with the experimental methods, and allows the designer to estimate and predict some characteristics of the flow pattern around the ship hull form which are not possible to be obtained by model tests. CFD can be used to simulate a flow and analyze the interaction between a fluid and an object. In boat design, it is used to determine lift and drag force and used to simulate boat hydrodynamics (Zhang et al., 2006). It gives an acceptable accuracy compared to experimental data. One of the most advantages of CFD for resistance predictions. The computational domain can be discretized using mesh-based methods or particle-based methods (Andersson et al., 2018).

2.10.1 Laminar and Turbulent Flow

The flow of fluid around a body can be divided into two general types of flow: laminar flow and turbulent flow. The extent of the viscous resistance on a body depends on the type of flow it is experiencing. Laminar flow is characterized by fluid flowing along smooth lines with a minimal amount of frictional resistance. For a typical ship, laminar flow exists for only a very small distance along the hull. Turbulent flow is characterized by the development of a layer of water along the hull moving with the ship along its direction of travel. This layer of water is referred to as the “boundary layer.” Water molecules closest to the ship are carried along with the ship at the ship’s velocity.

2.10.2 Turbulence Model

The turbulent flow is the type of viscous flow that is applied to most industries. It is a flow the main turbulence models are grouped into three families.

1. Reynolds-averaged Navier-Stokes (RANS) equations are obtained by time-averaging equations of motion over a coordinate in which the mean flow does not vary.
    - Solve time-averaged Navier-Stokes equations.
    - All turbulent length scales are modeled in RANS.
    - Extensively used approach for calculating industrial flows.
2. Large Eddy Simulation (LES) solves large-scale flow motion while approximating small-scale motions.
    - Solves the spatially averaged N-S equations.
    - Less expensive than DNS, but the number of computational resources and efforts are still too large for most practical applications
3. Direct Numerical Simulation (DNS), in which Navier-Stokes equations are solved for all scales of turbulent flow motion, increasing accuracy as well as the time required for the calculation.

- Theoretically, all turbulent flows can be simulated by numerically solving the full Navier-Stokes equations.
- Resolves the whole spectrum of scales. No modeling is required.
- The cost is too excessive and not practical for industrial flows.

I. Reynolds-averaged Navier Stokes (RANS)

Spalart-Allmara model: It's a low-cost RANS model for solving a modified eddy viscosity transport equation. It is useful for aerodynamics and transonic flows over airfoils because it is stable and has good convergence. Its limitation does not promise to apply to all sorts of complex engineering flows.

Standard k–ε (SKE) model: The Standard k–ε e is the most extensively used turbulence model for industrial applications. It has good convergence and cheap memory requirements. Compressible and incompressible flow are both supported. No-slip walls, unfavorable pressure gradients, severe curvature into a flow, and jet flows are not correct.

RNG k– ε: Suitable for complex shear flows involving rapid strain, moderate swirl, vortices, and locally transitional flows (e.g. boundary layer separation, massive separation, and vortex shedding behind the bluff body.

Realizable k–ε: Offers largely the same benefits and has similar applications as RNG. Possibly more accurate and easier to converge than RNG.

Standard k–ω model: This model is utilized for good convergence, minimal memory requirements, and enhanced accuracy for internal flows, curvatures, separated flows, and jets. However, it is difficult to converge and sensitive to initial conditions.

Shear Stress Transport k-omega (SST k–ω): The SST (Shear Stress Transport) k-omega turbulence model is a two-equation eddy viscosity model. It is a combination of both the k-epsilon and the k-omega turbulence models, using the former in the free-stream and the latter near the walls.

2.11 Stability of Boat

The capacity of a vessel to recover to its upright position after being heeled by an external force such as the wind, a wave, or the strain of its fishing gear is referred to as stability. It is determined by the vessel's characteristics, such as hull design and weight distribution, as well as how it is operated. When a fishing vessel has enough positive stability to withstand the external forces created by current weather and fishing conditions, it is said to be stable and will return to its upright position. Figure 2.7 depicts the vessel's fishing stability for easy comprehension.

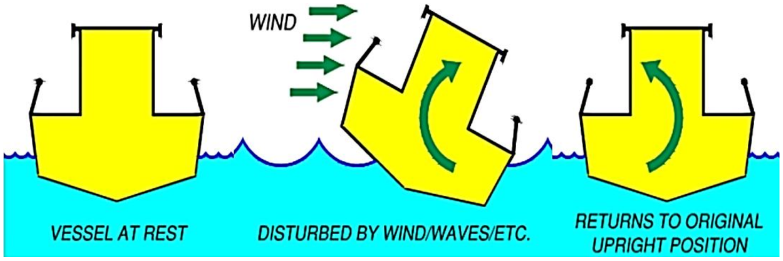

Figure 2.7. Stable vessel with sufficient righting forces

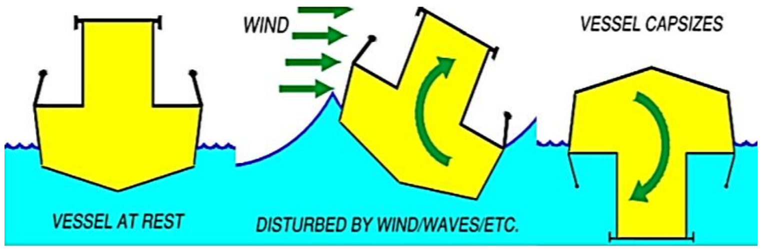

Figure 2.8. Unstable vessel with insufficient righting forces

Figure 2.8 shows when a fishing vessel lacks sufficient positive stability to withstand the external forces caused by current weather and fishing circumstances. Stability is determined by the relationship between three things, the center of gravity (CG), a center of buoyancy (CB), and Meta centric height (GM). The weight of the boat acts vertically downwards at its center of gravity. As a result, the boat acts as though all of its weight is concentrated at the center of gravity. The lower the center of gravity of the vessel, the more stable it is. The center of buoyancy is assumed to be the area where all upward/vertical force acts. It's in the middle of the submerged shape of the hull. The metacentric height is calculated as the distance between the ship's center of gravity (G) and its metacenter (M), where a larger metacentric height suggests greater initial stability.For different types of vessels, different Meta centric heights are desired. For fully-loaded "General cargo ships", the typical Meta centric height is 0.3 - 0.5 meters, for "Container ships" the value is 1.5 - 2 meters, and for "Double-hull supertankers", the Meta centric height is 2 - 5 meters. The Meta centric height should never be less than 0.15 meters for any type of vessel (ITTC, 2011). In Figure 2.9 boat with a keel is illustrated.

2.11.1 ANSYS AQWA for Stability of Boat

ANSYS AQWA is provides an engineering toolset for the investigation of the effects of wave, wind, and current on floating and fixed offshore and marine structures (Garbe, 2017). Stability is divided into two different types of stability, hydrostatic and hydrodynamic stability (AQWA Theory Manual, 2013).

- Hydrostatic stability refers to a body being affected by nothing more but the buoyancy force and the gravitational force still in the water.
- Hydrodynamic stability gives a more detailed look of the stability; it considers the waves that interact with the body, the forces acting on the body while the body is in motion, and similar dynamic effects.

AQWA Hydrodynamic Diffraction can also generate pressure and inertial loading for use in structural analysis as part of the vessel hull design process. The results from a diffraction analysis can be mapped onto an ANSYS Mechanical finite element model for further structural assessment and detailed design of boats (Samaei, etal.2016).

2.12 Boat keel

In boats and ships, keel can state either two parts, a structural element, or a hydrodynamic element. In sailboats, keels use the forwarding motion of the boat to get a lift to respond to the leeward force of the wind. Keels are also fixed, or non-movable, or they will retract to permit sailing in shallower waters. The primary purpose of Hydrodynamic keels is for interacting with the water and are typical of certain sailboats. Fixed hydrodynamic keels have the structural strength to support the weight of the boat (Barrass and Derrett, 2011).

The general purpose of the keel is:

- Convert the sideways motion of the wind when it's abeam into motion.
- Provides much more stability when lowered than when retracted (due to the greater moment arm involved) and Provide an extra stability by providing a weight low enough to significantly lower the center of gravity and helps the hull to move forward.

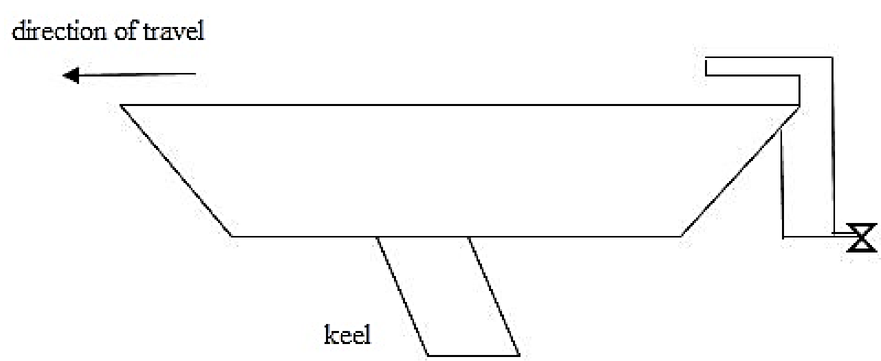

Figure 2.9. Diagram of a boat with a keel

2.13 Overall literature summary and research gaps

The literature reveals that different renewable energy has a significant role in the martin sector. Solar-powered, wind-powered vessels have reduced carbon emissions, reduce noise levels and eliminate the cost of fuel. The marine solar panels are installed on a boat and they, in turn, convert the sun's renewable energy into electric energy. From the above papers, it can be seen that the boats which only operated by wind were subjected to the fluctuation of energy because sometimes the wind does not blow constantly, as a result, there would be a shortage of power or energy. On another hand, if it only operates by solar energy the battery capacity needs to be improved for facilitating the working under varying weather conditions and requires improvement on the number of solar panels but the space available for the installation of the panels that will power the boat was limited. Moreover, it is possible to use hydrogen energy by combining with solar panels to power the boat but this lead to high energy storage system requirement, in addition, it was tried to combine an ICE with an electric motor but this would result in more battery pack price and an increase in the weight of the boat and also contribute to environmental pollution. To overcome the above problems the combination of solar with wind energy is believed to be the best option compared to the others for the location of Bahirdar city, Ethiopian on Lake Tana. Lake Tana is the largest lake in Ethiopia and it is the source of the Blue Nile and it is truly spectacular. The lake is approximately 84 km long and 66 km wide. Tourism at Lake Tana is very high and attractive there is a significant potential for the development and promotion of ecotourism to encourage visitors to see the area's beautiful mosaic of interchanging landscapes in a sustainable way (Zur Heide, 2012).

CHAPTER THREE

MATERIALS AND METHODS

3.1 Introduction

In this chapter, the material used for the proposed project is listed and followed by methodology. Moreover, the collected data required for this study and the conceptual design presented.

3.2 Materials

The materials that have been used to complete this thesis work are illustrated in Table 3.1.

Table 3.1. Materials used for the proposed project

Item	Specification
Solar panel	Polycrystalline (YL250P-29b)
Aluminum sheet	Thickness 0.7 mm
Shaft	Steel, AISI 1045
Generator	DC115
Charge controller	MPPT (48v)
Litum - ion battery	2V/200AH

3.3 Methods

To achieve the thesis's general and specific objectives, a series of steps or methodology are to be followed. Various steps included in the methodology are listed and summarized in Figure 3.1.

- **Literature review and problem identification**

To have the full image of the project such as what others have done in this area, their drawbacks, and gaps literature surveys were carried out. The latest reviews and research works in the area related to solar and wind energy for propelling the boat are collected and surveyed.

- **Data collection**

To get reliable information and necessary data about the local recreational boat from the study area (Bahirdar) is collected by using primary or secondary data collection methods. The data is collected from Abel Chane General metals and boat works and the owner of the boat.

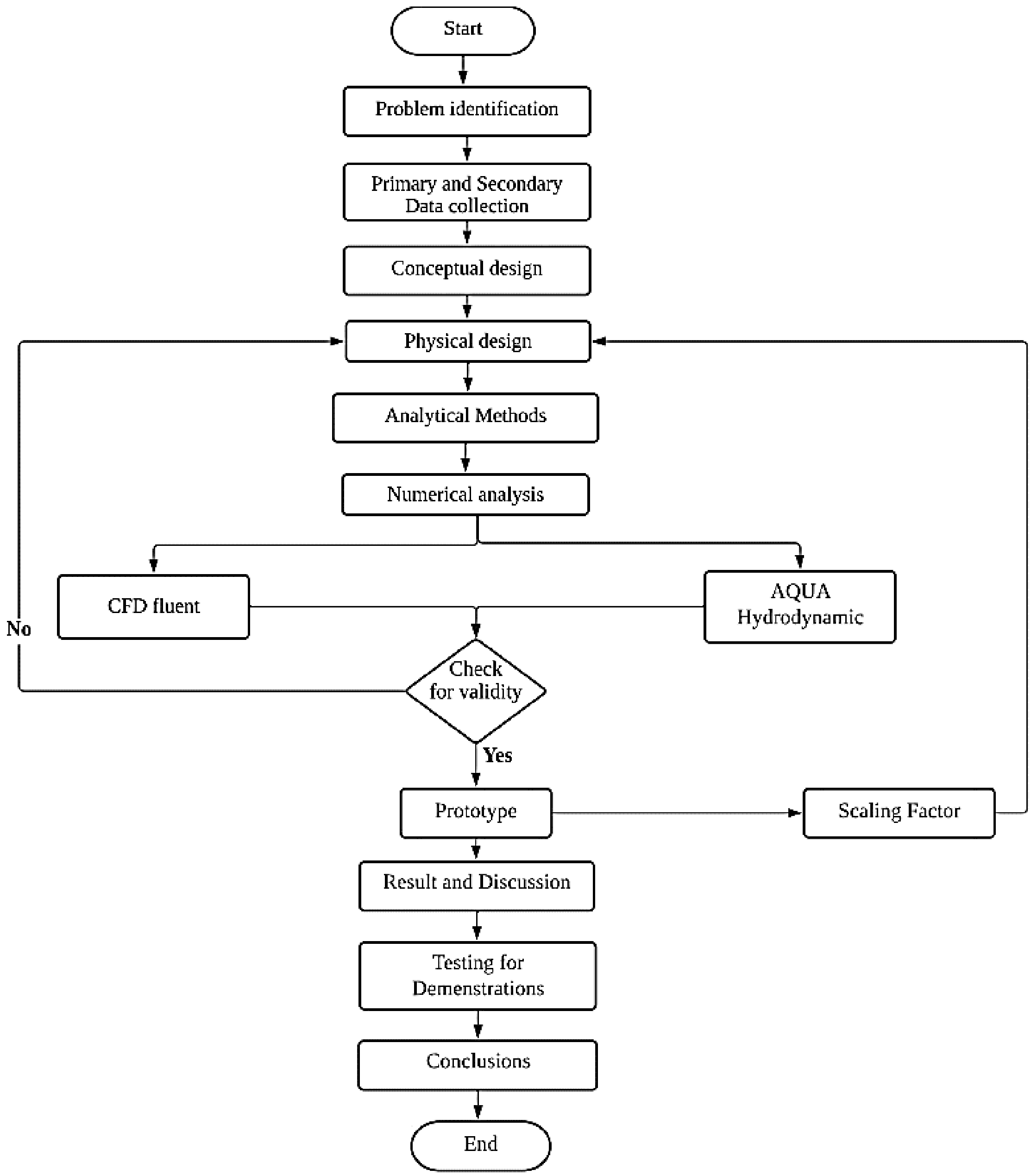

Figure 3.1. Block diagram of the methodology

3.3.1 Data Collection

- ✓ To get reliable and valid data both primary and secondary data are very important. The primary sources of data are data obtained from interviewing the owner of the boats, from the manufacturers of a boat (Abel chane metals and boats works plc) in Bahirdar city, and the meteorological data which is collected from the National Meteorology Agency of Ethiopia, Addis Ababa. The secondary sources of data are from reference books, journals, and the internet.

3.3.1.1 The Collected Data and Gathered Information

- The shallow Lake Tana (average) depth is 9 m and the maximum depth is 14m (Vijverberg et al., (2009).
- The service of the boat on Lake Tana any time from 8:00 AM to 5:00 PM. This was used to estimate the service allowance for the boat. Estimation was done based on per-day service. This is approximately determined as in equation 3.1.based on (ITTC).

$$\text{service allowance}=\frac{\text{Time (hours)}}{\text{Unit day(hour)}}=\frac{5}{24}=20\% \qquad (3.1)$$

- The hull shape used mostly is on this lake is V flat bottom.
- The material of the boat was used sheet metal mild steel.
- On the lake, there were different sizes of boats are found. Out of those, three boats were selected as a sample and one out of them was selected for this thesis work.
- The horsepower of the boat motor was increased when the size of the boat increased.

The dimensional boat data is given in Table 3.2 and shown in Figure 3.2. (Abel chane metals and boats works plc).

Table 3.2.Dimensional details of selected three boats manufactured at Bahirdar city

Parameters	Size of boats		
	Boat 1	Boat 2	Boat 3
The overall length of the (L_{OA}) (m)	6	7	8
Breadth (B) (m)	2	2.10	2.25
Height (H)(m)	0.6	0.65	0.7
Draught before load (D) (m)	0.15	0.15	0.17
Draught after load (D) (m)	0.30 - 0.38	0.35 - 0.38	0.40
Mass (with full load) (kg)	2300	2500	2700
Bottom corner fillet radius (m)	0.15	0.17	0.18
Motor horsepower (hp)	9.9	15	25

A 6m length boat was selected for this design.

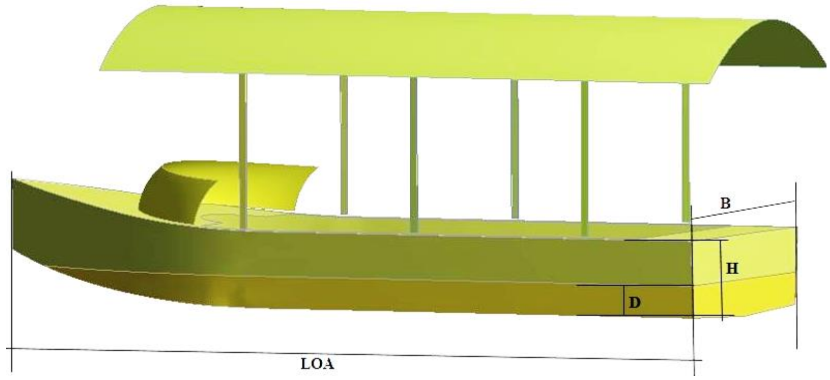

Figure 3.2. Boat dimensions

The Material of this boat was mild steel and the total structural weight is 800 kg and the number of passengers is 12. Figure3.3 shows the existing recreational local boat used in Bahirdar city.

Figure 3.3. Existing boat (Bahirdar, Lake Tana)

3.4 Conceptual design of solar and wind integrated boat

The proposed hybrid energy will be designed to install on the recreational boat. The system includes solar PV panels, wind turbine, battery bank, charge controller, and AC to DC converter for wind turbine and DC motor to propel the boat. The solar PV panel can be combined with a maximum point tracking system (MPPT) system to get the maximum power. Solar and wind energy are used to charge the battery bank. A battery management system that controls the operation based on measurements is required to switch between the hybrid power system components since solar irradiance levels change depending on daytime and weather conditions the overall hybrid system is used to drive the boat by the electric motor propulsion. The conceptual design of the solar panel and wind turbine integrated boat system is shown in Figure 3.4.

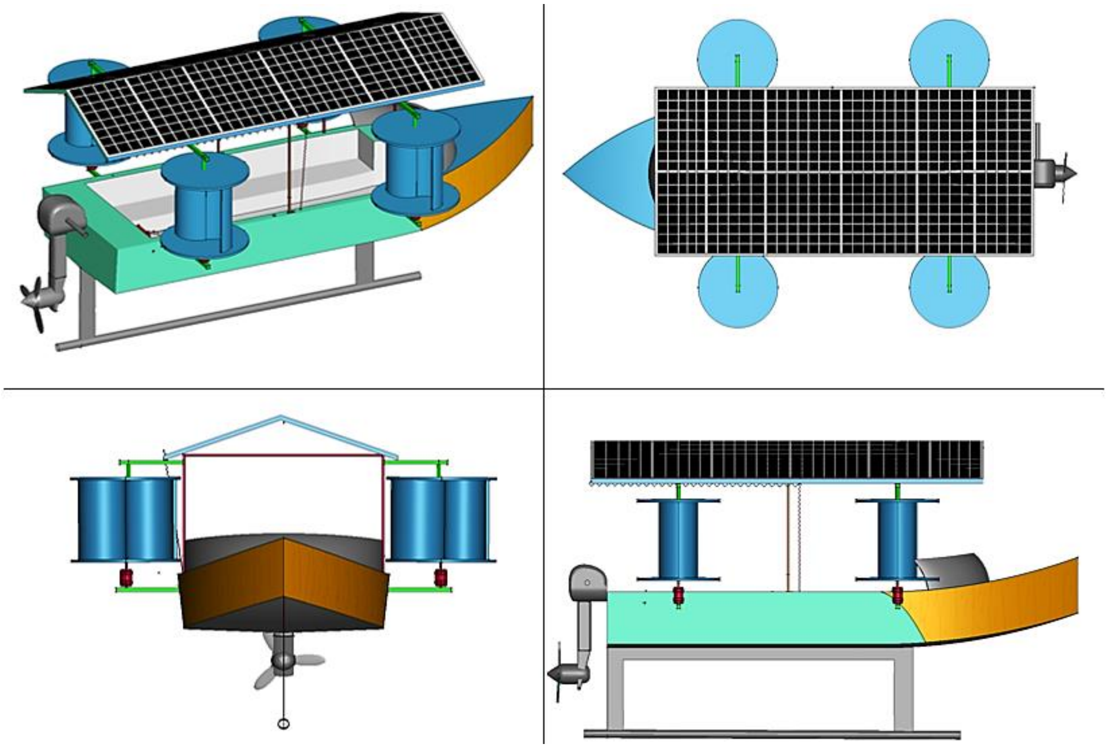

Figure 3.4. Conceptual design of solar panel and wind turbine integrated boat

CHAPTER FOUR

SOLAR AND WIND ENERGY POTENTIAL ANALYSIS OF THE SITE

4.1 Introduction

In this chapter, the collected data from Ethiopian Meteorological Agency are analyzed by using emphatically relations on an Excel spread sheet. The solar radiation and wind energy potential are analyzed. The geographical coordinates of the meteorological stations were captured at a height of 2 m.

4.2 Solar Radiation Estimation

It is energy emitted by the sun from a fusion reaction that makes electromagnetic energy. The spectrum of radiation is on the brink of that of a black body with a temperature of about 5800 k. About half the radiation is within the visible short wave a part of the spectrum. Solar radiation at the earth's surface is the principal and fundamental energy for several physical, chemical, and biological processes. Solar radiation data at ground level are important for a good range of applications in meteorology, engineering, agricultural sciences particularly for soil physics, agricultural hydrology, crop modeling, and estimating crop, in the health sector and research of the many fields in natural sciences.

In most developing countries, there are not any properly recorded radiation data. What is usually available is sun-shine duration data obtained by a sunshine recorder. Ethiopia is one such country, which lacks properly recorded solar radiation data like many other countries. However, from the given number of sunshine hours and local atmospheric conditions data (relative humidity, rainfall, maximum and minimum temperature) with the help of an empirical model the daily average solar radiation can be estimated. Ethiopia may be a high incident radiation country that receives high radiation, with a mean potential of 5.26 kWh per square meter per day (Woldegiyorgis, 2019). Solar radiation data are a fundamental input for solar power applications like photovoltaic and solar thermal systems (Pandey & Katiyar, 2013).

The amount of solar radiation on the surface of the earth is estimated using several correlations that relate the radiation outside of the earth's atmosphere (extraterrestrial radiation) with the radiation inside the earth's atmosphere (terrestrial radiation) the geometric relationship between a plane is fixed or moving relative to the earth and incoming beam solar radiation and this can be determined in terms of several angels (Duffie and Beckman, 2020).

4.2.1 Fundamental angles of the sun with the earth

Major angles of the sun are hour angle, latitude, and declination. Other angles like those that solar incidence; azimuth etc. must be related to these fundamental angular quantities

Latitude (ϕ): the angular location north or south of the equator, north positive; $-90^\circ \leq \varphi \leq 90^\circ$.

Declination (δ): the angular position of the sun at solar noon (i.e., when the sun is on the local meridian) concerning the plane of the equator, north positive; $-23.45^\circ \leq \delta \leq 23.45^\circ$.

$$\delta = 23.45 \sin\left[\frac{360}{365}(284+n)\right] \tag{4.1}$$

Slope or tilt angle (β): the angle between the inclined plane surface under consideration and the horizontal; $-180° \leq \beta \leq 180°$.

Hour angle(ω): the angular displacement of the sun east or west of the local meridian due to rotation of the earth on its axis at 15° per hour; morning negative, afternoon positive (Duffie and Beckman, 2020).

$$\omega = [\text{solar time} - 12{:}00]\ (\text{in hours}) \times 15° - 12{:}00 \tag{4.2}$$

Zenith angle (θz): the angle between the vertical and the line to the sun, that is, the angle of incidence of beam radiation on a horizontal surface (Duffie and Beckman, 2020).

$$\cos\theta z = \cos\delta\cos\phi\cos\omega + \sin\phi\sin\delta \tag{4.3}$$

Sunset hour angle (ωs): the hour angle at sunset is determined using Equation 3.4.

$$\omega_s = \cos^{-1}[-\tan(\varphi)\tan(\delta)] \tag{4.4}$$

The angle of incidence (θ): the angle between the sun's rays' incident on the plane surface and normal to that surface (Duffie and Beckman, 2020).

$$\cos\theta = (\cos\phi\cos\beta + \sin\phi\sin\beta\cos\gamma)\cos\delta\cos\omega + \cos\delta\sin\omega\sin\beta\sin\gamma + \sin\delta\,(\cos\beta\sin\phi + \cos\phi\sin\beta\cos\gamma) \tag{4.5}$$

4.2.2 Geographic coordinates of designated location

A geographic coordinate system (GCS) uses a three-dimensional spherical surface to define locations on the earth. Using latitude, longitude, and elevation. The following geographical coordinates are the Bahirdar city site. The geographic location of the specific study area is shown in Figure 4.1.

Latitude: 11.57°N Longitude: 37.39° and

Elevation above sea level: 1800 m = 5902 ft.

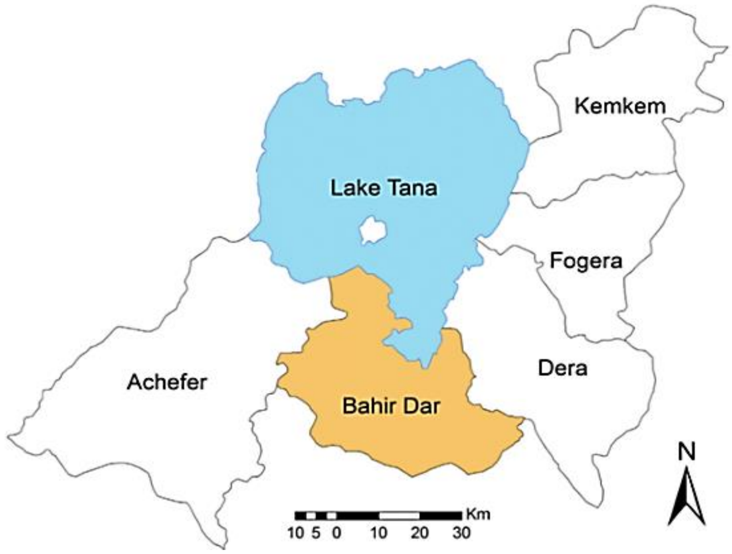

Figure 4.1. The geographic location of the study area (Meshesha, D et al., 2019)

4.2.3 Estimation of solar radiation based on sunshine based model

For many developing countries, particularly in Ethiopia, global solar radiation measurements are not easily available due to the cost of measuring equipment, therefore, it is necessary to use empirical equations for estimating the worldwide radiation supported by the readily available meteorological parameters like a sunshine hour. In this study, the prediction of monthly daily mean global solar radiation from sunshine hours was used to estimate global solar radiation in Bahirdar, Amhara region, Ethiopia.

The estimation of solar radiation by using the sunshine hour data set was accessible to collect sunshine duration. The daily solar radiation can be estimated by using the Angstrom-Prescott method follows the other parameters, daily extraterrestrial solar radiation, empirical coefficients, are calculated (Keawsang 2018, December).

Addisu et al., (2013) solar radiation were estimated by using the sunshine data of the different sites based on the well-known Angström model for successfully designing a large-scale solar water heating system in Ethiopia. Due to the lack of or breakdown of measuring equipment in poor countries such as Ethiopia, Solar radiation data that is dependable is not accessible due to a lack of instruments. The most commonly used parameter for estimating global solar radiation is sunshine duration. Because, it can be easily and reliably measured, and data are widely available at the weather stations**.** Figure 4.2 shows the monthly average sunshine hours of Bahirdar for ten years (2010-2019).

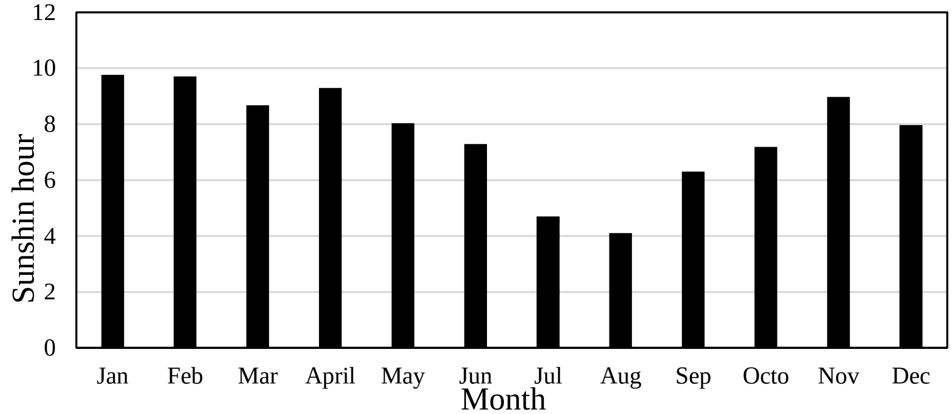

Figure 4.2. Monthly average sunshine hours of Bahirdar for ten years (Meteorology)

I. Estimation of daily extraterrestrial radiation on a horizontal surface

Extraterrestrial radiation on a surface normal to the sun's rays, measured at the real sun-earth distance at a certain day and hour, with the distance between the sun and the earth adjusted to allow for variations in the distance (Duffie and Beckman, 2020). The daily extraterrestrial solar radiation on a horizontal surface can be found by integrating Equation 4.6 from sunrise to sunset and expressed as:

$$\overline{H}_o = \frac{24 \times 3600}{\pi} I_{sc} \left[1 + 0.033 \cos\left(\frac{360\,(n)}{365}\right)\right] \left(\cos\phi \cos\delta \sin\omega_s + \frac{\pi \times \omega_s}{180} \sin\phi \sin\delta\right) \tag{4.6}$$

Where: n = day of the year,

I_{sc} = is solar constant =1367 W/m^2

φ = the latitude of the site under study

II. Estimation of global monthly average daily radiation on a horizontal surface

Monthly average daily global solar radiation statistics are crucial in the design and research of solar energy conversion systems. In this regard, several empirical models based on the Angstrom-Prescott model were used to estimate the monthly average daily global solar radiation, $\overline{H}$ on a horizontal surface (Duffie and Beckman, 2020).

$$\frac{\overline{H}}{\overline{H}_O} = a + b\left(\frac{\overline{n}_s}{\overline{N}_s}\right) \tag{4.7}$$

Where: $\overline{H}$ = the monthly average daily global radiation on a horizontal surface

$\overline{H}_O$= the daily extraterrestrial radiation on a horizontal surface

$\overline{n}_s$=the monthly average daily hours of bright sunshine

$\overline{N}_s$= the day length is the number of hours of sunshine within the 24 hours a and b values are angstrom empirical constant or regression coefficients

$$a = -0.110 + 0.235\cos(\varphi) + 0.323\left(\frac{\bar{n}_s}{\bar{N}_s}\right) \tag{4.8}$$

$$b = 1.449 - 0.553\cos(\varphi) - 0.694\left(\frac{\bar{n}_s}{\bar{N}_s}\right) \tag{4.9}$$

The day length ($\bar{N}_s$) is the number of hours of sunshine within the 24 hours on a given day. The mean day length is expressed as (Duffie and Beckman, 2020)

$$\bar{N}_s = \frac{2}{15}\cos^{-1}[-\tan(\varphi)\tan(\delta)] \tag{4.10}$$

III. Prediction of monthly average daily diffuse radiation on a horizontal surface

The monthly average daily diffuse radiation on a horizontal surface can be determined from the monthly average daily global radiation on a horizontal surface and the number of bright sunshine hours (Angström 1924).

$$\frac{\bar{H}_d}{\bar{H}} = 0.931 - 0.814\left(\frac{\bar{n}_s}{\bar{N}_s}\right) \tag{4.11}$$

IV. Monthly average daily Beam radiation

Beam solar radiation is direct solar radiation that reaches the piles of the earth's surface without scattering in the atmosphere. The difference between the monthly average daily global and diffuse radiations on a horizontal surface is the monthly average daily beam radiation.

$$\bar{H}_b = \bar{H} - \bar{H}_d \tag{4.12}$$

Figure 4.3 shows the variations of monthly average daily global, diffuse, and beam radiations on a horizontal surface.

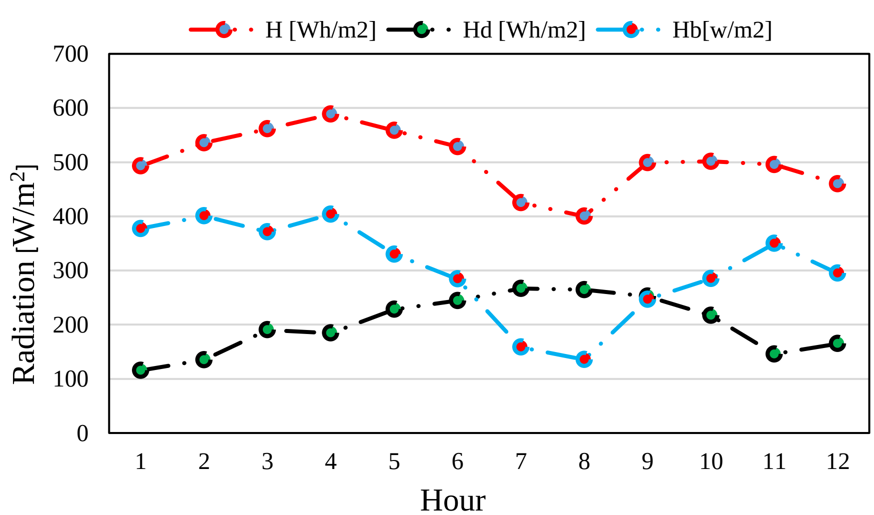

Figure 4.3. Monthly average daily global, diffuse, and beam radiations on the horizontal surface

V. Prediction of monthly average hourly global radiation on a horizontal surface

The monthly average hourly global radiation on a horizontal surface can be calculated from the information of the monthly average daily global radiation on a horizontal surface (Angstrom 1924) as shown in Figure 4.4. The mean hourly global solar radiation for Bahirdar has been calculated using Equation 4.13 (Duffie and Beckman, 2020) with measured values of daily solar radiation, which reveals the estimated values for the period 2010-2019.

$$\frac{\bar{I}}{\bar{\bar{H}}} = \frac{\pi}{24}(a + b\cos\omega)\left(\frac{\cos\omega - \cos\omega_s}{\sin\omega_s - \frac{\pi}{180}\,\omega_s\cos\omega_s}\right) \tag{4.13}$$

Where: $a_2 = 0.409 + 0.5016\sin(\omega_s - 60)$

$b_2 = 0.6609 - 0.4767\sin(\omega_s - 60)$

Figure 4.4. Monthly average Hourly Global Radiation on Horizontal surface

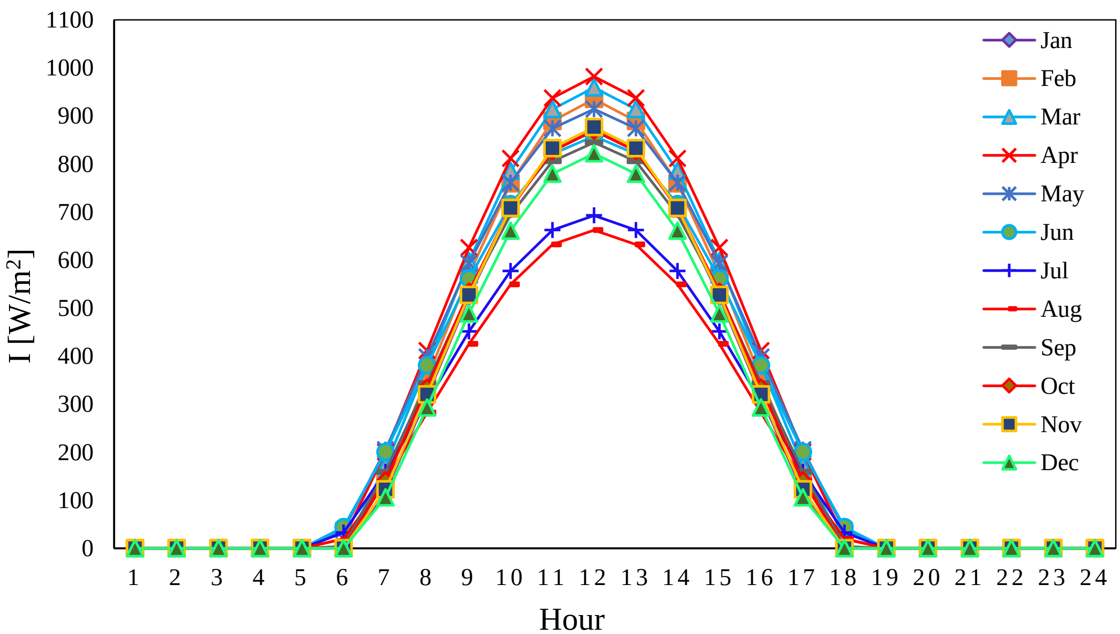

VI. Prediction of monthly average hourly diffuse radiation on a horizontal surface

The monthly average hourly diffuse radiation on a horizontal surface can be calculated from the knowledge of the monthly average daily diffuse radiation on a horizontal surface (Duffie and Beckman, 2020) and presented in Figure 4.5.

$$\frac{\bar{I}_d}{\bar{\bar{H}}_d} = \frac{\pi}{24}\left(\frac{\cos\omega - \cos\omega_s}{\sin\omega_s - \frac{\pi}{180}\,\omega_s\cos\omega_s}\right) \tag{4.14}$$

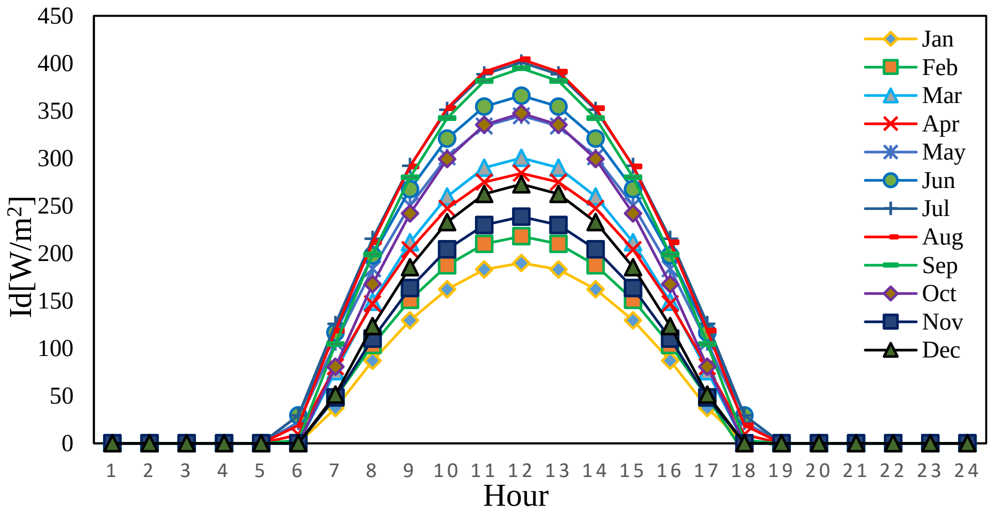

Figure 4.5. Monthly average Hourly Diffuse Radiation on Horizontal surface

VII. Monthly average hourly beam solar radiation estimation

The difference between the monthly average hourly global and diffuse radiations on a horizontal surface is the monthly average hourly beam radiation as shown in Figure 4.6.

$$\bar{I}_b = \bar{I} - \bar{I}_d \quad (4.15)$$

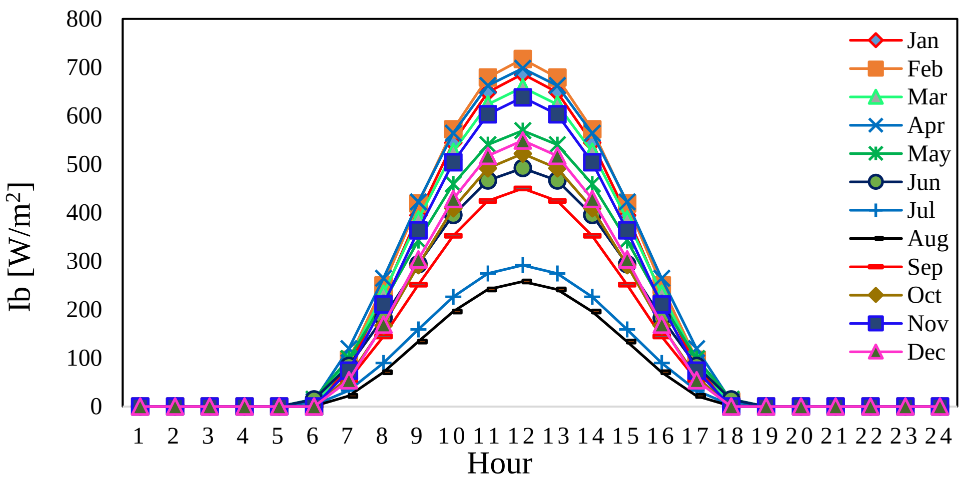

Figure 4.6. Monthly average Hourly Direct Radiation on Horizontal surface

VIII. Monthly average hourly estimation on a tilted surface

The monthly average hourly irradiance on tilted surface expressed in equation 4.16 (Duffie and Beckman, 2020)

$$\bar{I}_T = \bar{I}_b R_b + \bar{I}_d \left(\frac{1 + \cos\beta}{2}\right) + (\bar{I}_b + \bar{I}_d)\rho\left(\frac{1 - \cos\beta}{2}\right) \quad (4.16)$$

Where: $\bar{I}_T$= Total hourly irradiance on a tilted surface (W/m^2)

R_b=ratio of beam radiation on the tilted surface to that on a horizontal surface

β-Surface slop angel and ρ-Ground albedo (reflectivity) – 0.2 for bare earth

$$R_b = \frac{\cos\theta}{\cos\theta_z} \tag{4.17}$$

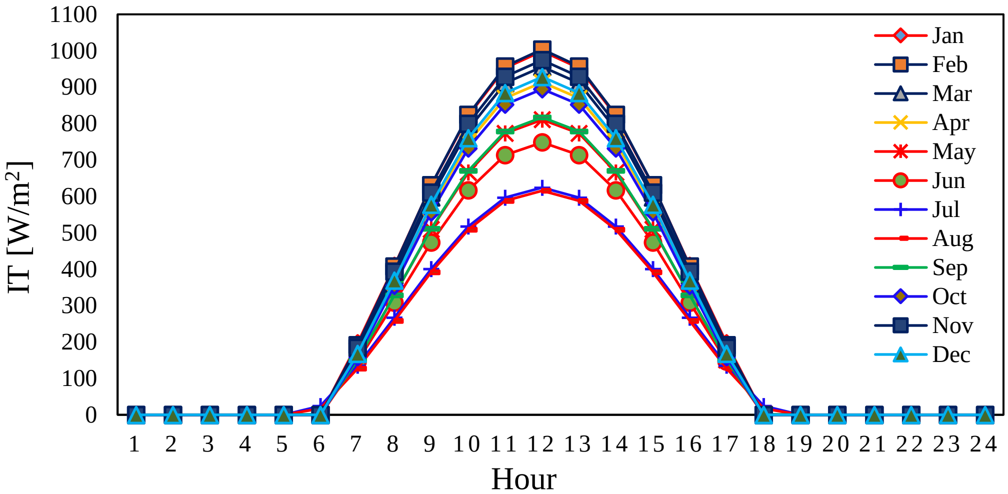

Figure 4.7. Monthly average hourly estimation on a tilted surface

4.3 Wind potential of the site

Today, Ethiopia is one of the countries with the lowest per capita electricity consumption in Africa. Recognizing that energy access and security are important factors for economic growth, Ethiopia needs to address key challenges related to energy security and diversification of energy supply and wind energy is one of the renewable energy sources (Hailu,& Kumsa 2021). The potential of wind energy is a major resource for renewable energy, an alternative resource for possible fuels, and a major sign to mitigate its negative impact on the environment. Renewable energy sources (RES) are increasing day by day, accounting for about 65% of global electricity generation in 2018, and energy sources play an important role in this wind power

4.3.1 Wind speed

Wind speed is the main factor that will determine sites suitability or the available wind spectra of a site. The mean wind of the selected site at a height of 2m is calculated by using the data source from the metrological station. The monthly mean wind velocity distribution for Bahirdar city is shown in Figure 4.8 for the year starting from 2010 - to 2019. The mean velocity (V_m) is given in equation 4.18 (Duffie and Beckman, 2013).

$$V_m = \frac{1}{n}\sum_{i=1}^{n} \times V_i \tag{4.18}$$

Where: V_i = wind velocity (m/s)

n= number of wind data

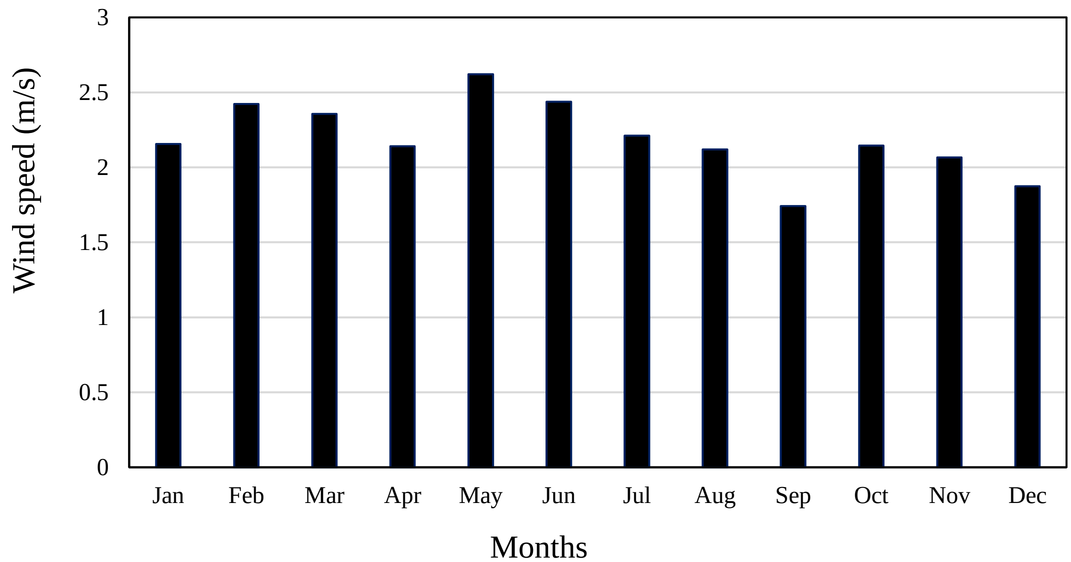

Figure 4.8. Monthly average wind Speed distribution (2010-2019, Meteorology)

Figure 4.9 indicated the mean hourly wind velocity distribution for May 15.

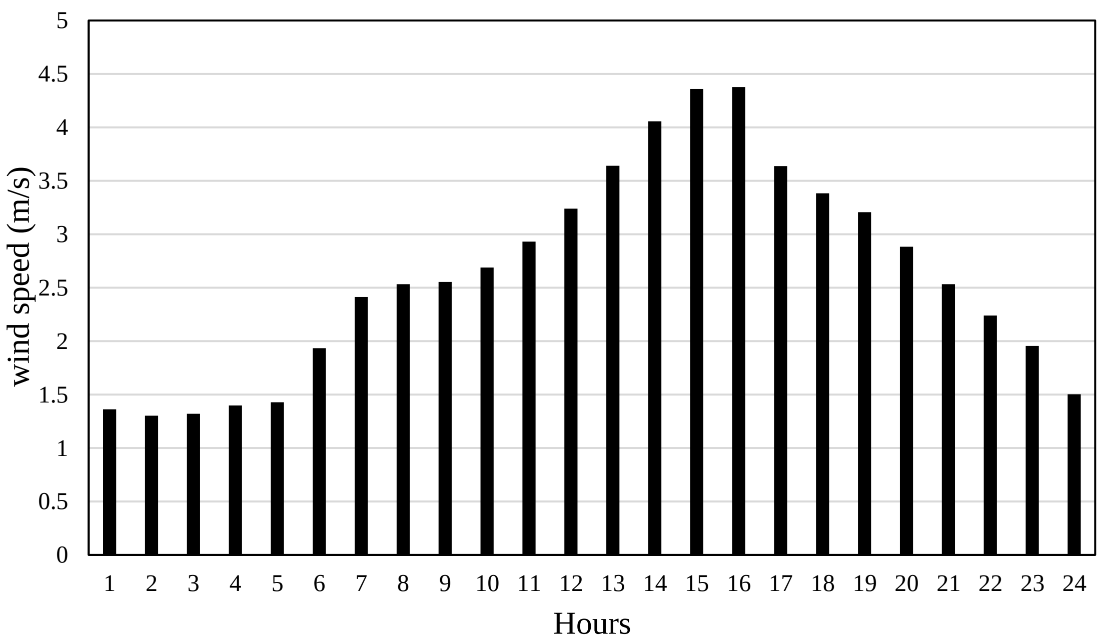

Figure 4.9. Mean monthly hourly wind speed distribution for May 15 (Meteorology)

Figure 4.10 shows an average monthly effective wind velocity which is the sum of the measured wind velocity with the boat velocity when the boat moves in the same direction as wind velocity.

$$V_E = V_w + V_b \tag{4.19}$$

Where: V_E = effective wind velocity (m/s)

V_w =wind velocity and V_b is the velocity of the boat

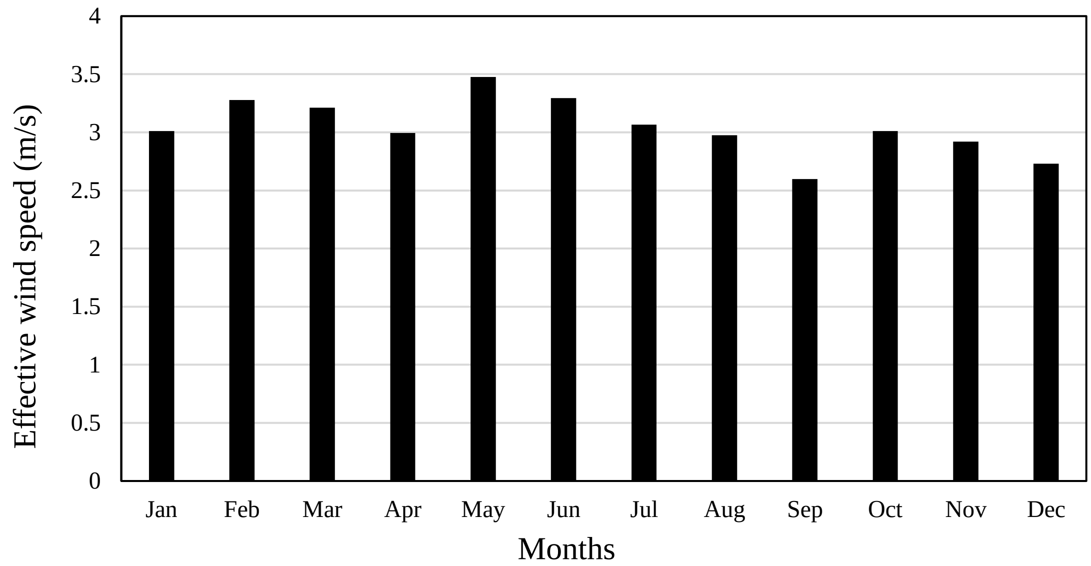

Figure 4.10. Monthly average effective wind speed

Figure 4.11 shows the distributions of the mean hourly effective wind speed for May 15.

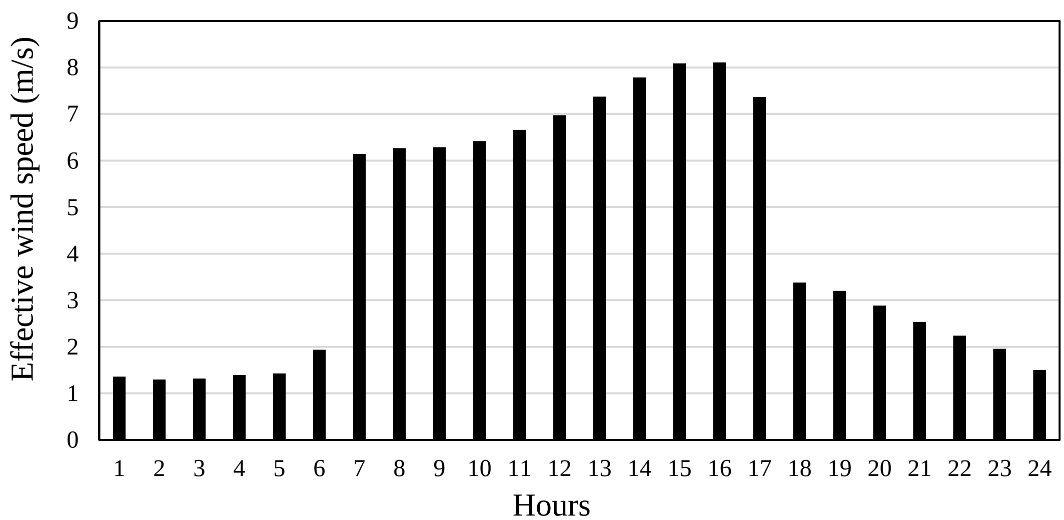

Figure 4.11. Mean hourly effective wind speed distribution for September month

4.3.2 Estimation of Wind Energy

A Wind energy density and energy available in the area over time are usually acquired. Energy density is the energy available in that area in the area and time of the unit rotor. (Duffie and Beckman, 2013).

$$E_D=\frac{1}{2}\times\rho\times V^3 \tag{4.20}$$

Where: E_D= wind energy density

ρ = the air density, kg⁄m3 and V^3 =Wind velocity, m/s

The monthly average wind power density and monthly effective power density are shown in Figure 4.12 and Figure 4.13 respectively.

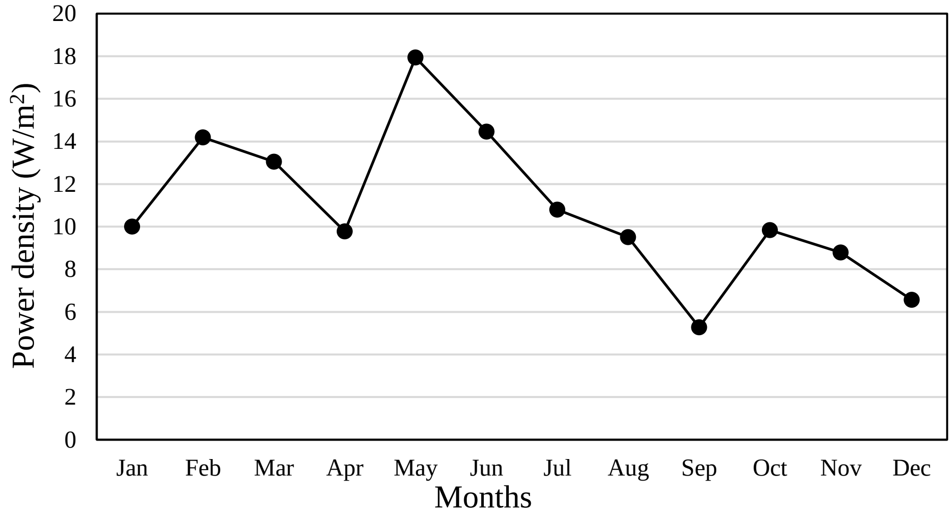

Figure 4.12. Monthly average wind power density

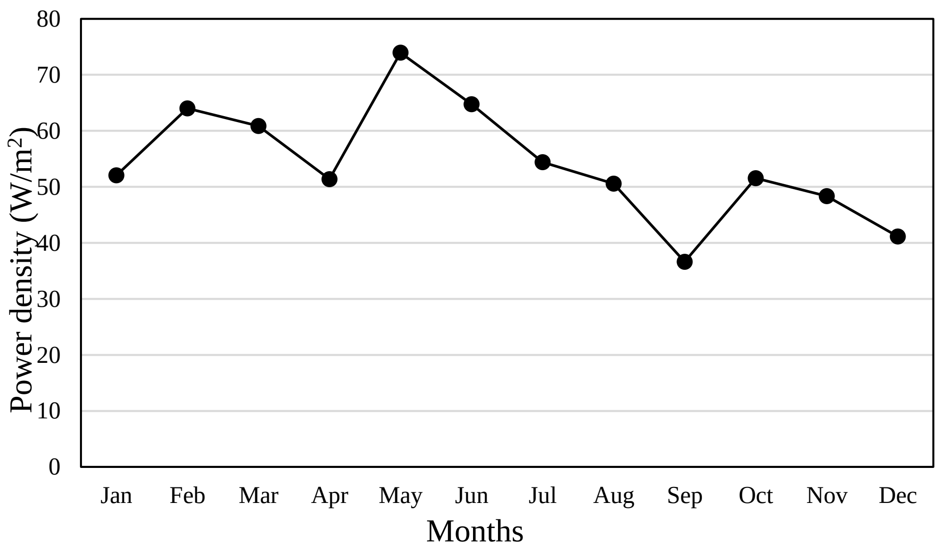

Figure 4. 13. Monthly average effective wind power density

CHAPTER FIVE

ANALYSIS OF SOLAR-WIND HYBRID POWER SYSTEM FOR BOAT

5.1 Introduction

This chapter presents a theoretical analysis of solar and wind hybrid energy sources for local recreational boats. The analysis includes the estimation of solar and wind energy requirements for propulsion vessels, sizing of the solar panel, wind turbine, and battery. The model for the demonstration purpose of the boat has been developed. Available materials are used for developing the model.

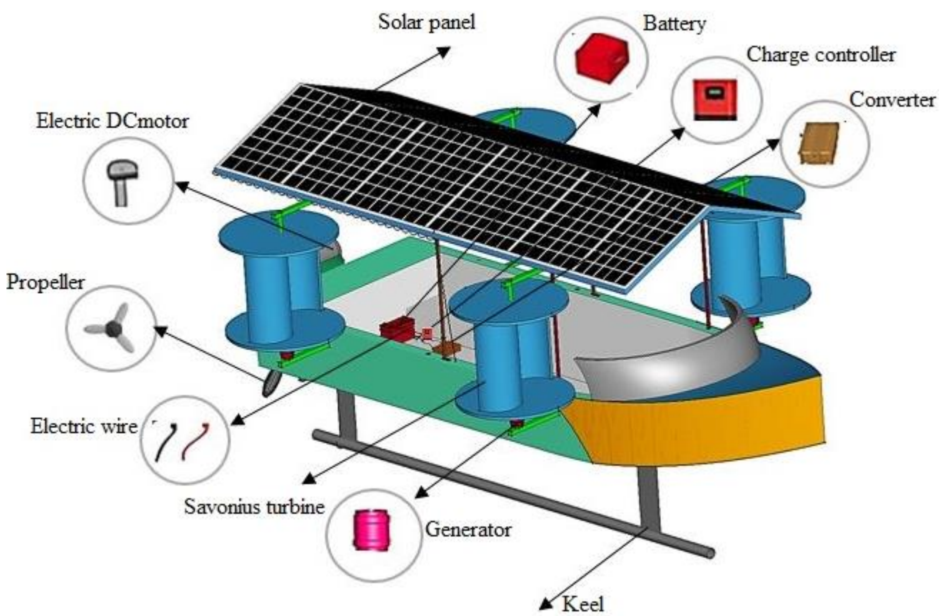

Figure 5.1. Hybrid energy system components on the boat

5.2 Power Transmission Circuit for the Hybrid Local Recreational Boat

Typically, a local recreational boat used on Lake Tana is powered by a 9.9 hp gasoline engine. The goal of this thesis work is to replace the energy demand of a gasoline engine with electricity generation from solar photovoltaic systems and wind turbines, as shown in Figure 5.1. Solar photovoltaic installation is made at an angle of 15 degrees by adjusting the solar panel mechanically to get the sunshine. Four savonous turbines are installed at the four corners of the boat. Since the photovoltaic systems generate direct current and the wind turbine generates alternating current, a charge controller is used for the hybridization system. The wind aerodynamic force (KE) is converted into rotational mechanical energy by the savonous turbine which produces AC and this AC is converted to DC by an AC/DC converter, the charge controller controls the overflow towards the battery. A solar photovoltaic system collects global solar radiation or solar flux. The electrical energy generated by the charging of the photovoltaic system is controlled. The photovoltaic module is selected of the polycrystalline type. All of the electrical energy from solar PV and wind turbines is stored in the battery. This stored energy is then transferred to the DC-electric motor that propels the boat. Figure 5.2 shows the block diagram of the total hybrid system used to drive the boat by electric propulsion.

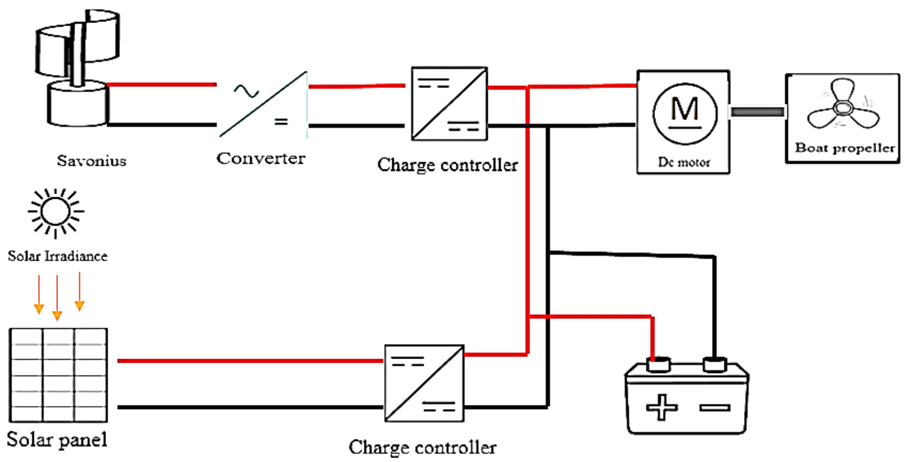

Figure 5.2. System connection schema for the hybrid system

The efficiency of components that are used in this study is listed in below Table 5.1.

Table 5.1. The efficiency of system components

Material	PV-panel	Charge controller	converter	Battery	Electric motor
Efficiency (%)	14.5	95	94.78	99	90

5.3 Sizing of a Solar Integrated Boat

A solar-powered boat is an electrical boat with a clean engine that uses either AC or DC motor. Solar-powered recreational boats for the transportation sector or tourists along the lakes. To do this, a boat solely powered by electricity captured through solar energy will be designed.

5.3.1 Determination of Photovoltaic Power Generation System

To determine the energy available from solar energy, the design data includes the photovoltaic panel, the average efficiency of the solar panels, the solar irradiance, and the area of the boat's structural roof. The solar panel was used to convert sunlight into electrical energy. The charge controller maintains the amount of charge coming from the solar PV panel going into the battery and then the energy is stored in the battery. The efficiency modulus of photovoltaic panels for polycrystalline panels is between 13% and 16% (Saleem et al, 2016). An advanced MPPT

(Maximum Point Tracking System) system was adopted, and the efficiency of the MPPT charge controller is about 93-97% of conversion. To increase the efficiency of solar panels, an MPPT must be installed (Müller et al., 2013). lithium battery is chosen for this study it's due to their high energy and power density, long service life, and environmental friendliness and, thus, has been widely applied in consumer electronics they are dependable and expensive on a cost-per-watt basis (Dunn et al, 2011). Elco electric motor was chosen because of its way in electric mobility on the water. The efficiency of the motor, battery, solar panel, and charge controller efficiency is indicated in Table 5.1. The schematic diagram of a proposed photovoltaic powered boat with a converter is shown in Figure 5.3. Solar cells naturally perform solar energy conversion into electrical power.

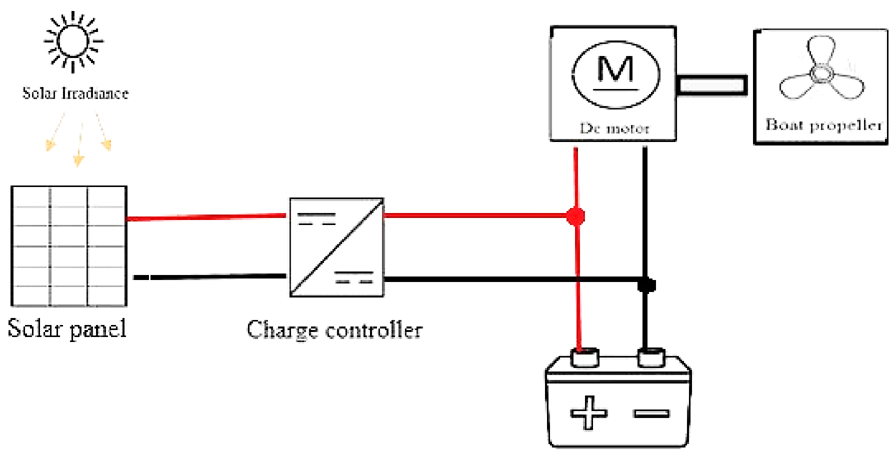

Figure 5.3. Schematic circuit diagram for PV system

Solar power is the electricity generated using solar radiation from the Sun. To measure the output power PV generation, it is necessary to estimate the space available for arranging the solar array on the boat roof. Depending on the design of the boat, the available space is $12m^2$ the output power from the PV module is expressed by using equation 5.1 (Oğuz & Özsoy, 2015)

$$P_{PV} = \bar{I} \times A \times \eta_{PV} \tag{5.1}$$

Where: P_{PV} = photovoltaic array output power (W)

$\bar{I}$ = Hourly solar irradiance (watts/m^2)

A = Total solar panel area (m^2)

η_{PV} = average solar panel yield or efficiency (%)

The energy output after gating into the charge controller is expressed by equation (5.2).

$$P_C = P_{PV} \times \eta_C \tag{5.2}$$

The energy output after gating into the battery is expressed using equation (5.3)

$$P_B = P_C \times \eta_B \quad (5.3)$$

The net electrical power from the solar panel after being stored in a battery is expressed in equation 5.4 (Oğuz & Özsoy, 2015)

$$P_{net} = P_B \times \eta_M \quad (5.4)$$

Where: P_{PV} = Output power the PV module

η_C= Efficiency of the charge controller

η_B= Efficiency of battery

η_M= Efficiency of moto

Measure the hourly energy from the total electrical load from solar energy is calculated using equation 5.5 (Oğuz & Özsoy, 2015)

$$P_{net\ E} = P_{net\ PV,\ boat} \times t \quad (5.5)$$

Where: $P_{net\ E}$ = electrical energy in a given amount of time (Wh)

5.4 Design and sizing of wind turbine integrated boat

A small Savonius vertical axis wind turbine is designed with two blades. The Savonius wind turbine is a drag-based vertical axis wind turbine that utilizes the kinetic power of the wind to create torque on the turbine rotor. The wind hits the surface of the turbine blades creating a force that leads to the creation of torque on the turbine rotor.

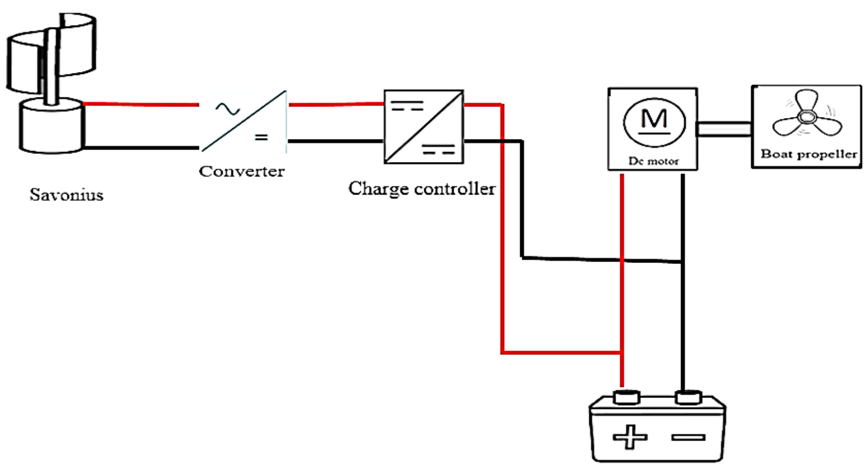

Figure 5.4. Schematic diagram of Savonius rotor wind turbine

Figure 5.4 shows the Schematic diagram of savonous wind turbine to a powered boat with a converter. The wind turbine can’t rotate faster than the wind speed. This means that the tip speed ratio is nearly equal to 1 or smaller (D'Ambrosio & Medaglia, 2010). Aluminum is selected to construct the endplates of the turbine due to its lightweight, corrosion resistance, rigidity, recyclable materials, ease of construction, and low cost (Ali, M., 2013).

5.4.1 Blade design

The design of a savonous wind turbine rotor includes the choice of the number of blades, determination of blade dimensions, and shaft. When the number of blades increases the power coefficient decreases. This is due to as the number of blades increased, more wind is deflected by a blade from entering into the concave side of its adjacent blades (Al-Kayiem et al., 2016). The equation from 5.6 to 5.24 are taken from (Ali, M., 2013)

I. Swept area

The amount of energy produced by a wind turbine primarily depends on the rotor area, thus the area of the turbine is influenced the energy output. The larger it is the more energy will be produced. The swept area for savonous wind turbine can be calculated from the dimensions of the rotor. The dimensions of these rotors were selected to have an aspect ratio (AR = H / D =1). These blades were assembled and mounted on two aluminum disc sheets. The components with their dimensions used to develop the savonous wind turbine are listed in Table 5.2.

Table 5.2. Dimensions of the parts used in savonous turbine

Part	Dimension (m)
End Plate Diameter (Do)	1.4
Rotor Diameter (D)	1.2
Rotor Height (H)	0.6
Shaft outer diameter	0.04
Shaft inner diameter	0.03
Length of shaft	1.4
Thickness of End Plate (t_p)	0.0007
Thickness of Rotor (t_R)	0.001

The material used to construct the savonous materials are listed in the below Table 5.3. (Ali, M., 2013) (Shah, M. H., & Alsibiani, 2020).

Table 5.3. Material Used to design savonous turbine

Components	Materials	Density
End plates of rotor	Aluminum sheet	2700 kg/m^3
Turbine Blades	PVC	1467 kg/m^3
Shaft	Steel, AISI 1045	7800 kg/m^3

The swept area for savonous wind turbine can be calculated from the dimensions of the rotor using equation 5.6 (Ali, M., 2013).

$$A_S = H \times D \quad (5.6)$$

Where: As=Swept area [m^2].

H= Rotor height (m).

D= Rotor diameter (m).

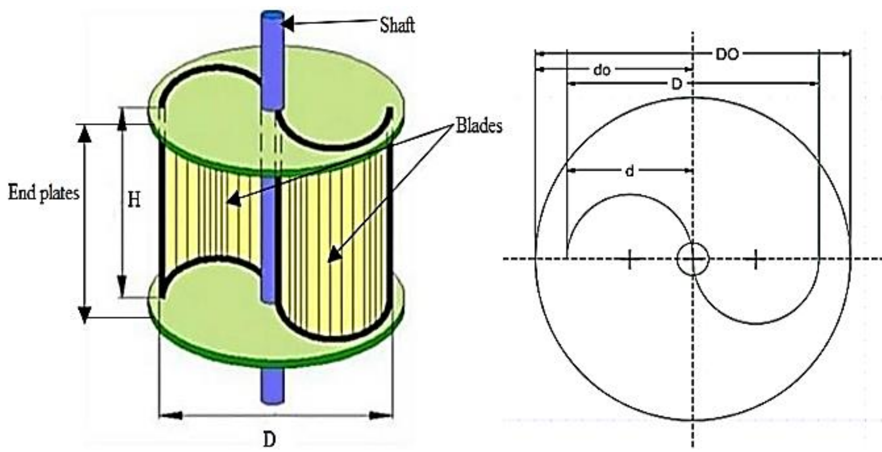

Figure 5.5. Schematic diagram of savonous rotor wind turbine (Ali, 2013).

II. Tip speed ratio (TSR)

The tip speed ratio is defined as the ratio of the peripheral velocity of the Savonius rotor to the free stream velocity of wind speed. The TSR of a turbine is expressed as in the equation 4.7 (Ali, M., 2013) and $\lambda = 0.8$ read from the performance curve from Figure 5.7.

$$\lambda = \frac{V_{rotor}}{V} \quad (5.7)$$

$$v_{rotor} = \omega \times d \quad (5.8)$$

Where: V_{rotor} =the peripheral velocity of Savonius rotor (m/sec)

V = the wind speed (m/sec)

ω = the angular velocity of Savonius rotor (rad/sec).

d = the diameter of the semi-cylindrical Savonius rotor (m).

III. Torque Coefficient (Ct)

The torque coefficient is the ratio between the torque developed by the rotor and the theoretical torque consequently available in the wind and is given by equation 5.9

$$C_t = \frac{T}{T_W} \quad (5.9)$$

Where: T = the rotor torque (N.m)

Tw = the wind available torque (N.m)

$$T_W=\frac{1}{4}\times\rho\times A_s\times d\times V^2 \tag{5.10}$$

Where: ρ = the air density (kg/m^3).

d= distance of rotor radius

The torque is defined as the force acting tangentially over the rotor blade, operating at a distance of rotor radius (d) from the center, it is given as in equation 5.11.

$$T=I\times\alpha \tag{5.11}$$

The moment of inertia tells us "how much energy is stored in a rotating shaft or about how much energy it will take to accelerate the shaft to a particular velocity.

Where: I= the rotor moment of inertia (kg.m^2)

m= total mass of the turbine

r =effective radius of turbine and α is Angular acceleration

The total moment of inertia for the savonius wind turbine is expressed in equation 5.12 (Ali, M., 2013).

$$I = I_b + I_s + I_p \tag{5.12}$$

Where: I_b = the moment of inertia for two blades of savonous rotor. (kg.m^2)

I_s = the shaft moment of inertia (kg.m^2) and I_p is the end plates moment of inertia (kg.m^2)

The moment of inertia for two blades of savonous rotor is given in equation 5.13

$$I_b = \frac{8}{3\pi}\times m\times d^2 \tag{5.13}$$

$$m = \frac{\rho\pi}{2} \times H \times t \times d \tag{5.14}$$

Where: m = mass of the two blades (kg)

The Moment inertia of the shaft is calculated in equation (5.15), the shaft used must meet the minimum weight requirement as far as possible and must be strong enough to withstand intermittent wind loads. The shaft moment of inertia is given in equation 5.15

$$I_s = \frac{1}{2}m({r_o}^2 + r^2) \tag{5.15}$$

$$m=\rho\times\pi\times({r_o}^2 - r^2)L \tag{5.16}$$

Where: m = mass of the shaft.

L=length of shaft and r_1 and r_2 are the outer and inner radius of the hollow shaft.

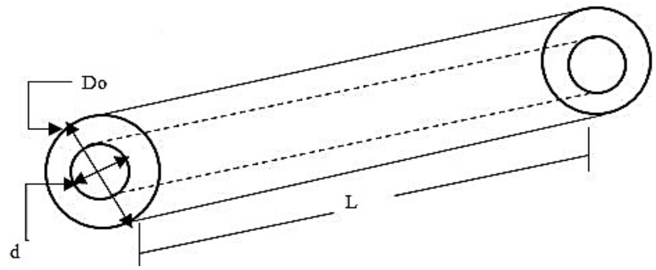

Figure 5.6. Wind turbine shaft

The the end plates moment of inertia is given based on equation 5.17

$$I_p = \frac{1}{2}\rho \times \pi \times t \times d^4 \quad (5.17)$$

The angular acceleration (α), is given as in equation 5.20:

From rotational of the turbine

$$\omega^2 - \omega_o^2 = 2\theta\alpha \quad (5.18)$$

Where the turbine start from zero

$$\omega_o^2 = 0 \quad (5.19)$$

$$\alpha = \frac{\omega^2}{2\theta} \quad (5.20)$$

Therefor for one cycle

$$\theta = 2\pi \text{ , } \alpha = \frac{\omega^2}{4\pi} \quad (5.21)$$

IV. Power and power coefficient

The output power from a wind turbine depends on the turbine's size and the wind's speed through the rotor are indicated in equation 5.22.

$$P_a = \frac{1}{2}\rho \times A_s \times V^3 \quad (5.22)$$

$$V_{rated} = 1.3 + (1 + V_{avr}) \quad (5.23)$$

The power transferred to a wind turbine or the rotor extracts from the wind is expressed in equation 5.23.

$$P_w = P_a \times C_P = \frac{1}{2}\rho \times A_s \times V^3 \times C_P \quad (5.24)$$

Where: P_w = the extracted power from the wind

P_a =the available power from the wind

The energy output from the AC-DC converter and charge controller is expressed in equations 5.25 and 5.26 (Oğuz & Özsoy, 2015).

$$P_{conv} = P_w \times \eta_{conv} \quad (5.25)$$

$$P_C = P_{conv} \times \eta_C \quad (5.26)$$

The energy output into the battery is expressed using equation (5.27) (Oğuz & Özsoy, 2015).

$$P_B = P_C \times \eta_B \quad (5.27)$$

The actual wind power to be converted to useful energy or the net wind power output to drive the boat is expressed in equation 5.28 (Oğuz & Özsoy, 2015)

$$P_{net\ w} = P_B \times \eta_M \quad (5.28)$$

Where: $P_{net\ w}$ = power from the wind

η_{Conv} = efficiency of the converter

η_C = efficiency of the generator

η_B = efficiency of the battery

The total hourly electrical load from wind energy is calculated using equation 5.29 (Oğuz & Özsoy, 2015)

$$P_{WE} = P_{net\ w} \times t \quad (5.29)$$

where: P_{wE} =hourly energy required from the wind turbine

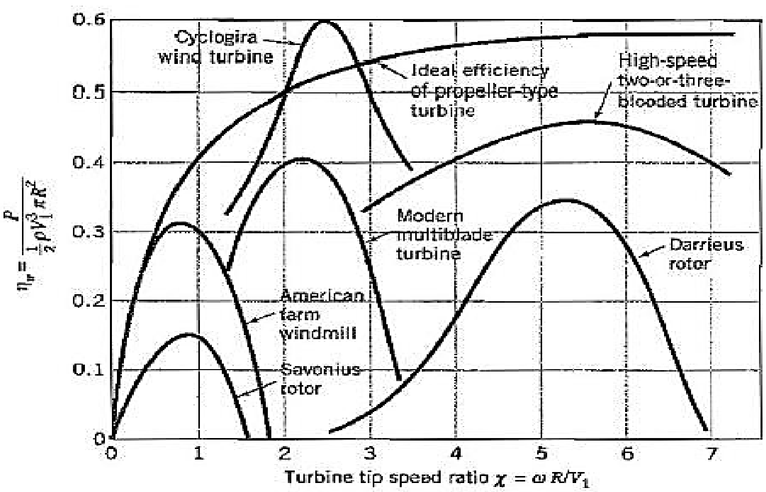

Figure 5.7. Efficiency plot of wind turbines

5.5 Battery Sizing for the System

To determine the number of batteries, the daily total electric energy requirement to propel the boat must be considered using equation 5.30.

$$E = P_{pro} \times t \quad (5.30)$$

Where: E = daily total electric energy requirement (Wh/day)

P_p= Propulsion power and t is operating work time

The role of battery in the system was used to store the energy. For the proposed project DC motor was selected. The motor voltage is used 48V.

$$Batt_{cap}=\frac{\text{Total energy}}{DOD\times\eta_B\times Sys_{Vol}} \tag{5.31}$$

The guidance system voltage

Where: DOD = maximum allowable depth of battery discharge

Sys_{Vol} = System voltage and

η_B = Efficiency of battery

The maximum DOD is 80% (Bow et al., 2021). The total number of batteries is obtained by dividing the capacity $Batt_{cap}$ of the battery bank in ampere-hours by the capacity of one of the battery Cb selected in ampere-hours using equation 5.32.

$$N_{batt}=\frac{Batt_{cap}}{C_b} \tag{5.32}$$

The number of batteries in series equals the DC voltage of the system divided by the voltage rating of one of the batteries selected.

$$N_{batt\ Series}=\frac{Sys_{Vol}}{V_b} \tag{5.33}$$

Then the number of parallel paths Np is obtained by dividing the total number of batteries by the number of batteries connected in series and expressed in equation 5.34:

$$N_{Par}=\frac{N_{batt}}{N_{Seri}} \tag{5.34}$$

Table 5.4. Battery Specification

Specifications of lithium Battery model	
Nominal Capacity	200 Ah
Nominal Voltage	12.8 V
Efficiency	99%
Self-Discharge	<3% per Month
Dimensions (L x W x H)	522 x 267 x 220 mm
weight	27.7 kg

CHAPTER SIX

NUMERICAL ANALYSIS OF ENERGY DEMAND AND STABILITY OF THE BOAT

6.1 Introduction

In this chapter, CATIAV521 was used for geometry modeling, and ANSYS 19 R3 CFD was used to simulate fluid-object flow interaction analyses. ANSYS Hydrodynamics was also used to check the stability of the boat. The simulations were based on the Reynolds mean-Navier-Stokes equations. Figure 6.1 shows the procedure used for the analysis.

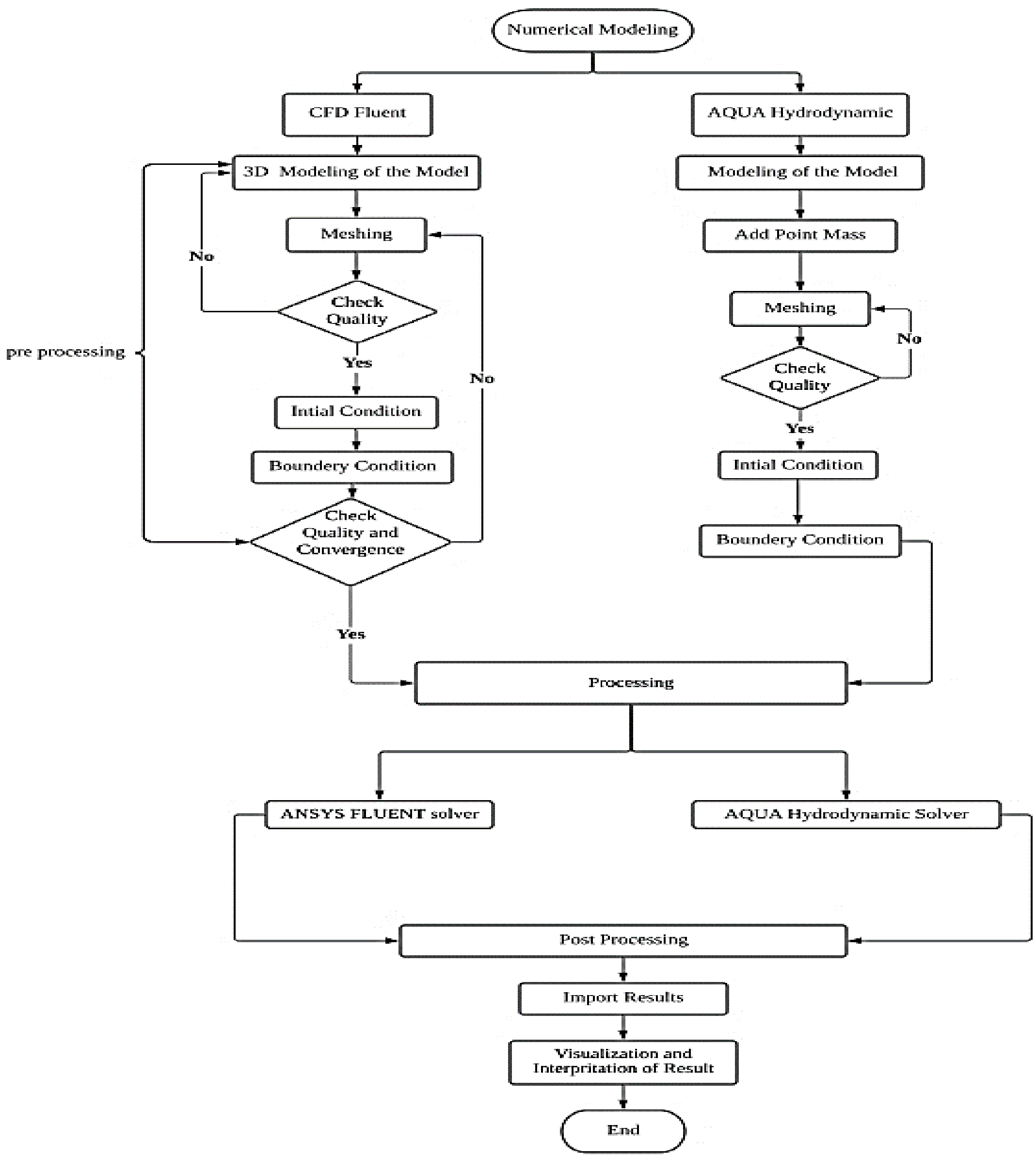

Figure 6.1. Flow chart of Numerical method

6.2 Governing Equations

The governing differential equations of fluid dynamics form the basis for modern computer modeling, known generically as computational fluid dynamics (CFD). The Navier–Stokes equations are the set of conservation laws used in CFD. In the early 1800s, G.G. Stokes in England and M. Navier in France independently derived the equations. The equations are extensions of the Euler Equations that take into account the flow's viscosity.

The Navier-Stokes equations are the governing equations for fluid flows consisting of the continuity, the momentum equations, and Energy (first law of thermodynamics. The equation of continuity implies a material balance over a stationary fluid element. The momentum equations, also called the equation of motion, describes the momentum balance which according to Newton's second law requires that the rate of change in momentum on the fluid particle is equal to the force acting on it. Laminar and turbulent flow can be described using the dimensionless coefficient known as the in honor of Sir Osborne Reynolds' (1883) contribution to the study of hydrodynamics. For a ship, the Reynolds Number is calculated using the equation 6.1.

$$R_n = \frac{LV}{\upsilon} \tag{6.1}$$

Where: Rn =the Reynolds number

L = length of the boat (ft.)

V = velocity (ft. /sec) and ν = kinematic viscosity of water (ft^2 /sec)

- The length of the boat is 19.685(ft.), the speed is 12.30315 (ft. /sec) and kinematic viscosity of water (ft^2 /sec) 9.1913031e-6 (ft^2 /sec) at average temperature on Lake Tana is 27.11.

  $R_n = 26.35 \times 10^6$ So, this flow is turbulent.

6.2.1 Conservation of Mass

The equation for conservation of mass, or continuity equation, is shown in equation 6.2. It is the general form of the mass conservation equation and is valid for incompressible as well as compressible flows (Versteeg, & Malalasekera, 2010).

$$\frac{\partial \bar{u}}{\partial x} + \frac{\partial u'}{\partial x} + \frac{\partial \bar{v}}{\partial y} + \frac{\partial v'}{\partial y} + \frac{\partial \bar{w}}{\partial z} + \frac{\partial w'}{\partial z} = 0 \tag{6.2}$$

6.2.2 Conservation of Momentum

The second equation comes from the conservation of momentum. The forces acting on the control volume are represented by equivalent stress. The normal stresses act perpendicular to the surface and shear stresses act on the plane of the surface. The equation for conservation is shown in Equations 6.3 - 6.5 (Versteeg, & Malalasekera, 2010).

$$\rho\frac{du}{dt}=\frac{\partial(-p+\tau_{xx})}{\partial x}+\frac{\partial\tau_{yx}}{\partial y}+\frac{\partial\tau_{zx}}{\partial z}+S_{Mx} \tag{6.3}$$

$$\rho\frac{dv}{dt}=\frac{\partial\tau_{xy}}{\partial x}+\frac{\partial(-p+\tau_{yy})}{\partial y}+\frac{\partial\tau_{zy}}{\partial z}+S_{My} \tag{6.4}$$

$$\rho\frac{dw}{dt}=+\frac{\partial\tau_{xz}}{\partial x}+\frac{\partial\tau_{yz}}{\partial y}+\frac{\partial(-p+\tau_{zz})}{\partial z}+S_{Mz} \tag{6.5}$$

6.3 Turbulence Modeling

Turbulent flow is characterized by the three-dimensional irregular flow. It is a random state of motion in which velocity and pressure change over time. The flow usually consists of rotational eddies that vary in three dimensions. Even inflows where the average velocity and pressure vary only in one or two dimensions, there are still turbulent fluctuations in three dimensions (Frisk & Tegehall, 2015) The most common turbulence models use the Reynolds expansion for instantaneous velocities and pressures. Reynolds equation averaged over Navier-Stokes (RANS) (Versteeg, & Malalasekera, 2010) and can be written as in equation 6.6.

$$\bar{U}\frac{\partial\bar{u}}{\partial x}+\bar{v}\frac{\partial\bar{v}}{\partial y}+\bar{w}\frac{\partial\bar{w}}{\partial z}=-\frac{1}{\rho}\frac{dp}{dx}+v\left(\frac{\partial^2\bar{u}}{\partial x^2}+\frac{\partial^2\bar{u}}{\partial y^2}+\frac{\partial^2\bar{u}}{\partial z^2}\right)-\left(\frac{\partial\overline{u'^2}}{\partial x}\right)+\left(\frac{\partial\overline{u'v'}}{\partial y}\right)+\left(\frac{\partial\overline{u'w'}}{\partial z}\right) \tag{6.6}$$

The turbulence modeling selected for this study is the SST k-ω model which is a combination of the standard k- and k-ω models. It is used for complex flows such as in flows with adverse pressure gradients, separating flows, and which has shown good performance for complex flows (Ahlstrand et al., 2020).

$$\rho\frac{\partial\omega}{\partial t}+\rho\bar{u}_j\frac{\partial\omega}{\partial t}=\alpha^{\omega\varepsilon}\frac{\omega}{k}\tau_{ij}\frac{\partial\bar{u}_i}{\partial y}-\beta^{\omega\varepsilon}{}_2\,\rho\varepsilon^2+\frac{\partial}{\partial x_j}\left[(\mu+\sigma^{\omega}{}_2\mu_T)\frac{\partial\omega}{\partial x_j}\right]+2\rho\sigma^{\omega\varepsilon}{}_2\frac{1}{\omega}\frac{\partial k}{\partial x_j}\frac{\partial\omega}{\partial x_j} \tag{6.7}$$

6.4 Multiphase Flow

To simulate a ship moving in the water, the model must incorporate both water, air, and the boundary between them. The proposed simulations contain two fluids, water, and air, which need to be simulated as two different phases. This can be done by using the multiphase method in ANSYS FLUENT. The multiphase method divides the computational domain into two different phases based on where the free surface is placed (Voxakis, 2012). In a multiphase flow, each fluid may possess its flow field or they share a common flow field (Andersson et al., 2018).

The VOF formulation enables the modeling of two immiscible fluids and is used to compute time-dependent solutions. However, it can also be used for steady-state calculations if the solution is independent of the initial conditions and there are distinct inflow boundaries for the two different phases (Ahlstrand et al., 2020).

6.5 ANSYS - Fluent

Modeling flow, turbulence, heat transfer, and reactions for industrial applications ranging from airflow over an aircraft wing to combustion in a furnace, from bubble columns to oil platforms, from blood flow to semiconductor manufacturing, and from cleanroom design to wastewater treatment plants are possible with ANSYS Fluent software. Special models have been added to the software to allow it to model in-cylinder combustion, aeroacoustics, turbomachinery, and multiphase systems.

6.5. 1 Geometry description

The geometry of the designed boat was created in CATIA V5R19. The model has been done by using the overall dimensions of the boat. Sketch tracer Generation is the initial stage of modeling in which the basic profile or part of the boat is formed by tracing from the image. After that, the surface was generated by using Surface Generation, and the corresponding extruding thickness was given and then its part was assembled. Figure 6.2 shows boat geometry at different views.

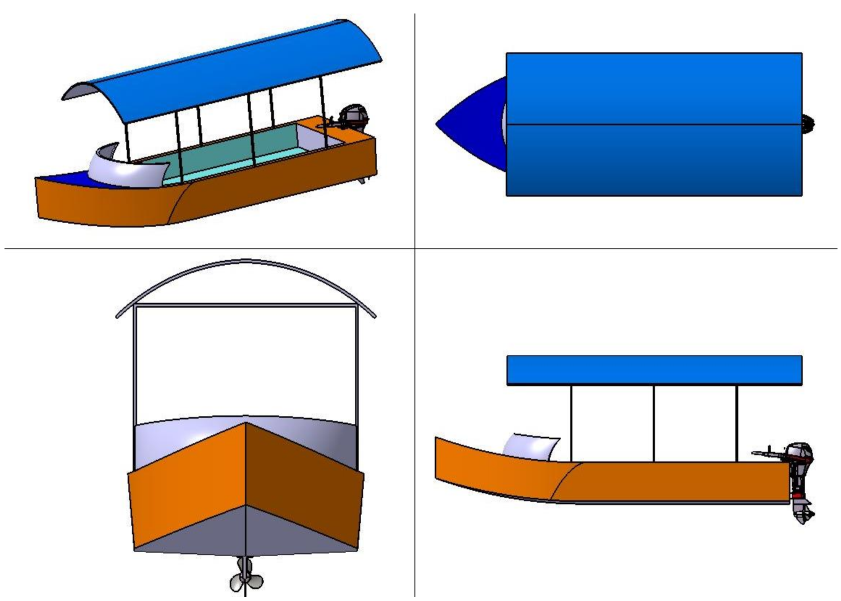

Figure 6.2. A different view of the boat created by using CATIA V5R19

The geometry was then exported into ANSYS 19 R3 Design-Modeler. Figure 6.3 shows the geometry after being imported to the ANSYS workbench in STP format.

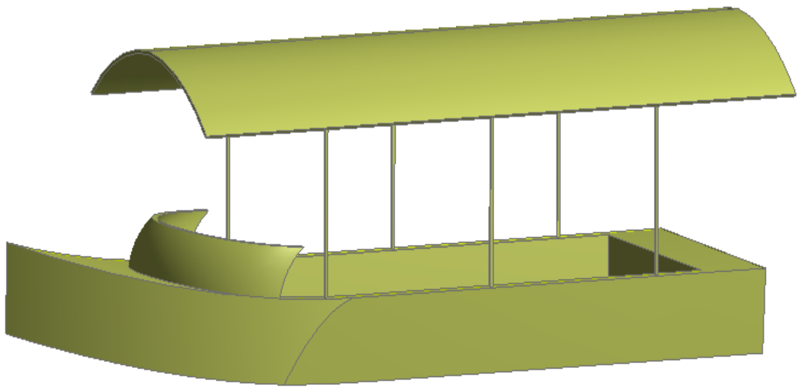

Figure 6.3. The Geometry of the boat after being imported to ANSYS

6.5.2 Computational domain definition

After the boat geometry was imported to the software, the domain was built as a rectangular block and a large domain was developed because it is very important to avoid effects from the domain boundaries to the hull (Frisk & Tegehall, 2015). The inlet and outlet were placed 1LO A and 3LOAforward and backward, respectively, the bottom, top, and the distance away from the boat set boundaries were placed 1LOA. A smaller rectangular block was built around the free surface area. To reduce the grid size, the body model is scaled down by five because it is more advantageous to reduce the computational cost. The computational domain and the named selection can be seen in Figure 6.4.

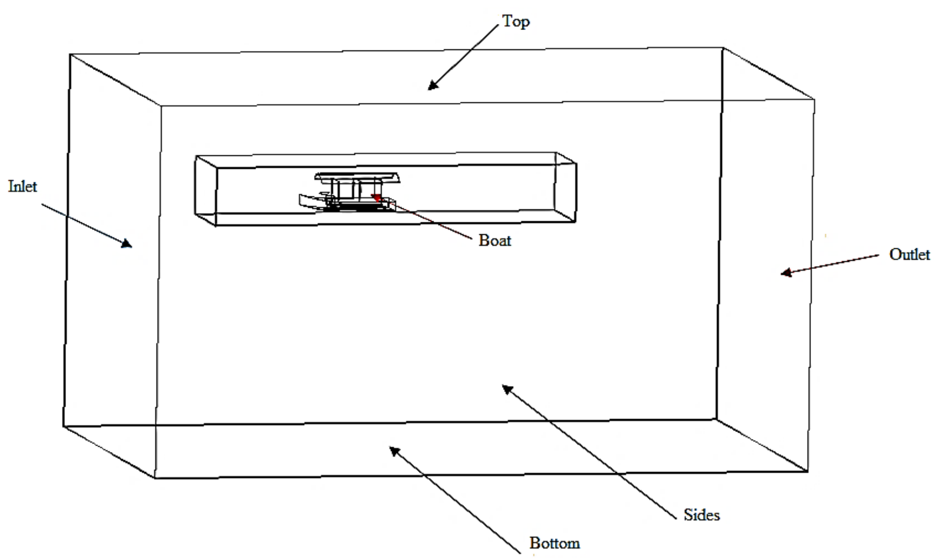

Figure 6.4. The computational domain for a boat

To control the mesh around the boat, a small box is created. The smallest inner box the boat model inside an enclosure for each case is shown in Figure 6.5.

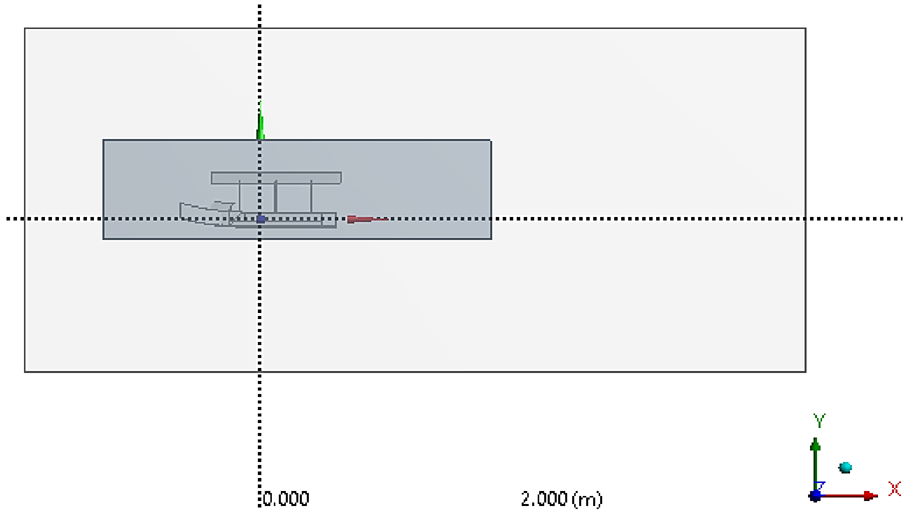

Figure 6.5. The geometry of the boat inside an enclosure and inner boxes

6.5.3 Mesh generation

After the domain is created the next step is meshing, for the use of numerical equations, the domain is divided into smaller cells, called a mesh. The mesh used in fluent was created using ANSYS Meshing. The domain was meshed using the function body of influence to achieve the refinements around the boat. The mesh density was focused on certain regions of the domain. It helps to reduce the amount of time and effort spent to get accurate results. (Frisk & Tegehall, 2015) .To focus on certain regions of the domain. A fine mesh was used o as shown in Figure 6.6 the mesh near the boat is very fine to get an accurate result. The outer volume has meshed with coarse elements fine around the boat surface.

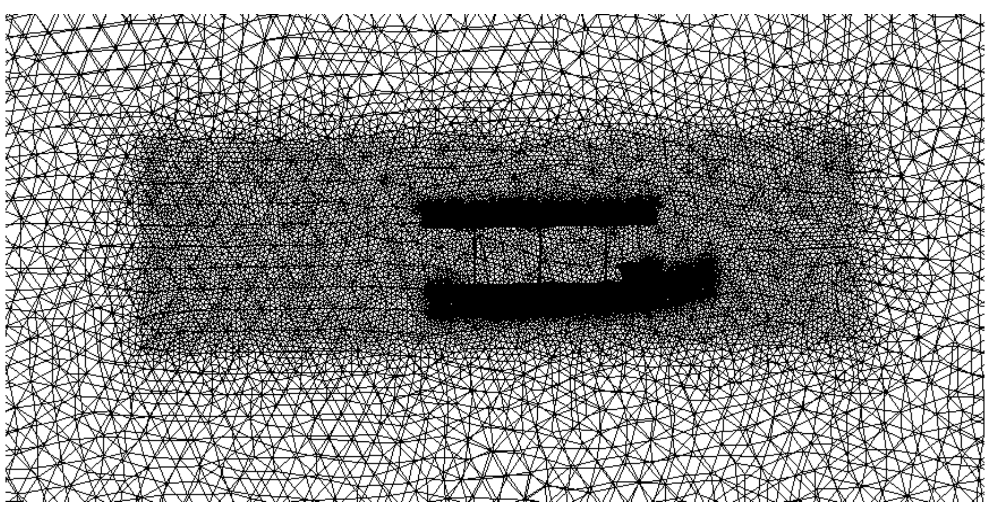

Figure 6.6. Fine mesh generated near the boat and on the boat

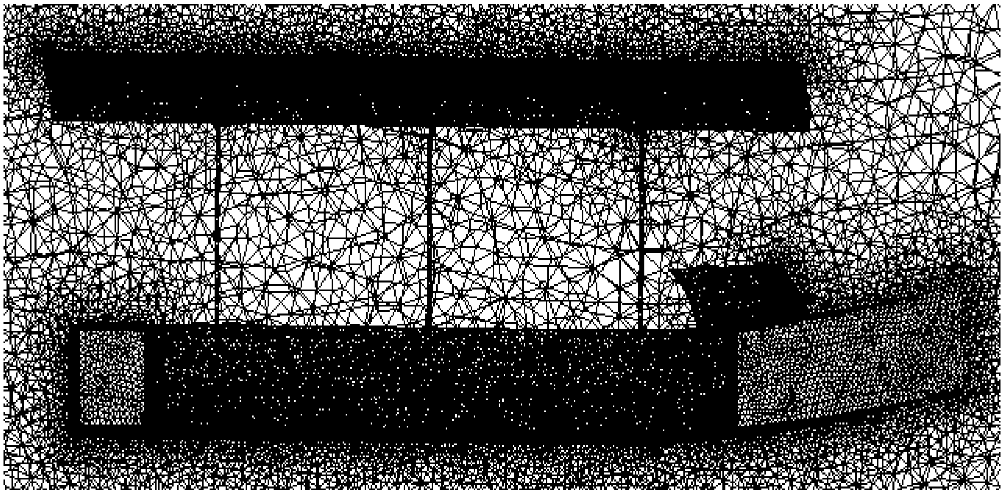

Figure 6.7. Fine mesh generated on the boat

According to the User's Guide for Fluent, Mesh quality is determined by the minimum orthogonal quality. Orthogonal quality ratings range from 0 to 1, with lower values signifying worse quality cells. The minimal orthogonal quality should not be less than 0.01, with the average value being much higher, as shown below in Figure 6.8 the mesh quality is greater than 0.01.

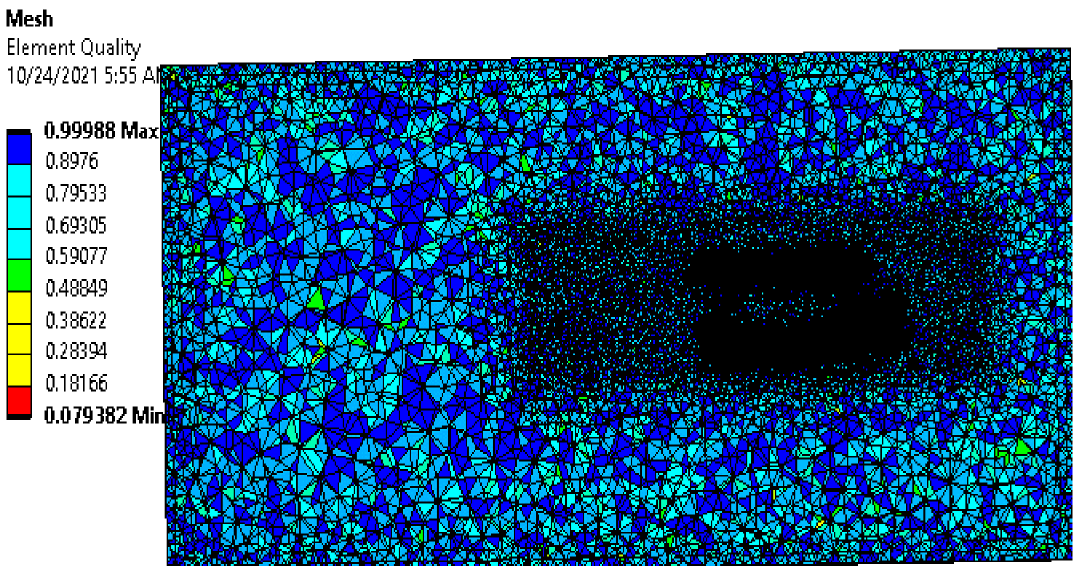

Figure 6.8. The quality of the mesh for the boat

6.5.4 Grid independence test

Grid independence should be checked through a mesh convergence study, meaning that the mesh is checked to be good enough to not affect the solution. A coarser mesh can be used to save computational cost, this mesh type is provided results with acceptable accuracy. Should be checked through a mesh convergence study, meaning that the mesh is checked to be good enough to not affect the solution. By repeating this procedure until the fluid property has converted to a certain value, it can be assured that the mesh is good enough to not affect the solution. Table 6.1 indicated the drag coefficient using the independence test.

Table 6.1. Grid independence test

Mesh	Nodes	Elements	Drag coefficient
1	137661	752007	0.281
2	202740	1,115294	0.277
3	316378	1,742360	0.271
4	523579	2,901238	0.269

6.5.5 Model setup

For the proposed simulation the mesh was converted to polyhedral cells in fluent, and the two models were applied thus are the viscous model and multiphase model. For the viscous model, the SST k-ω model was chosen and for the multiphase, the VOF was used as a model, open channel flow as VOF sub-model, implicit as volume fraction formulation, and the body force formulation was set as an implicit body force. The material for the two phases in the multiphase was defined as air and water. The gravity force was defined as 9.81 m/s^2 in the negative y-direction. The boundary condition for the inlet was set as a pressure inlet, this is because the open channel flow model is used. The outlet was set to a pressure outlet, the boat set to a wall, top, bottom, sides are set to symmetry, and for the inlet and outlet, the turbulence intensity and the turbulent viscosity ratio were set to default, i.e. 1 % and 10, 5 % and 10, respectively and the bottom level was set to 1.2 m. Since the VOF model is applied, the pressure-based solver is used and the solution is set to be steady-state. The solution method used is a coupled scheme and the second-order upwind scheme is chosen for all but the gradient, the pressure, and volume fraction discretization were least-square cells based PRESTO! , and compressive is used, respectively. The quality of the simulations was ensured by residual criteria of 10^{-5}.and a mesh convergence. The velocity used in the simulation is the maximum effective speed and it is scaled by using the Froude number. The Froude number is used to determine the speed at which the real boat scale model. Equation 6.11. Shows in the equation of Froude number. The boundary conditions used for the simulation are indicated in Table 6.2. (Ahlstrand, & Lindbergh, 2020) and (Frisk & Tegehall, 2015).

Table 6.2. Boundary Conditions

Surface/Part	**Type**	**Condition**
Inlet	Pressure Inlet	velocity: 1.8m/s, Turbulent intensity: 1% Viscosity ratio: 10
Outlet	Pressure Outlet	Gauge pressure = 0 Pa Turbulent intensity:5% Viscosity ratio:10
Sides	Symmetry	-
Atmosphere	Symmetry	-
Bottom Boat	Symmetry Walls (Stationary)	- No-slip

6.6 Total Resistance Prediction

The total ship resistance represents the total force exerted during the propulsion system. The total resistance and total coefficient are calculated using the given equation 6.8 (ITTC1957).

$$R_T=\frac{1}{2}C_T\times\rho\times S\times V^2 \tag{6.8}$$

Where: RT = Total hull resistance)

CT = Coefficient of total hull resistance

ρ = Density of fluid

S = wetted surface area of the hull and is the velocity of the model

The total coefficient is calculated using equation 6.9 (ITTC1957)

$$C_T=C_V+C_A+C_R \tag{6.9}$$

Where: C_V =viscous coefficient,

C_A= air resistance coefficient

C_R = residual resistance coefficient.

$$C_A=\frac{A_{VT}}{1025\times S} \tag{6.10}$$

Where: AVT = average frontal area of the vessels above water plane

S = wetted surface area

Figure 6.9 shows the wetted surface of the hull is determined to calculate the resistance force to get the propulsions power of the boat. The value of the wetted surface area of the boat is ($12m^2$) is determined using ANSYS software.

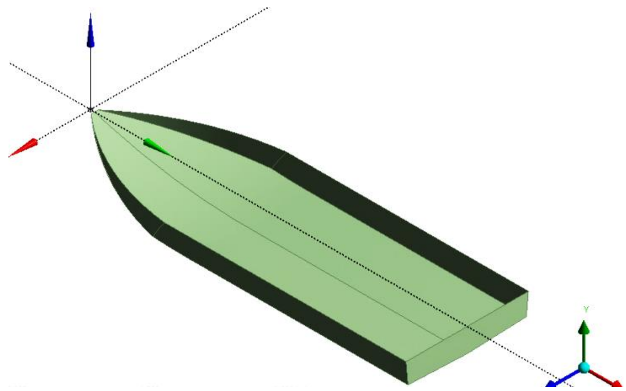

Figure 6.9. The wetted surface area of the hull

The viscous resistance coefficient (C_V) is proportional to the hull's surface roughness. However, the model's surface roughness will differ from that of the boat and can be determined by the value of viscous resistance from CFD. The residual resistance coefficient, C_R, is defined as the total model resistance coefficient minus the model friction resistance coefficient and the value of residual resistance using Froude no reading from Appendix C. The "Froude number" (F_n) is named after William Froude (1810-1878), one of the pioneers in ship model testing. It is a dimensionless metric of velocity used by naval architects and used in the indication of the influence of gravity on the motion of fluids. It is expressed as in Equation 6.11.

$$F_n = \frac{V}{\sqrt{g\,L}} \qquad (6.11)$$

Where: V = velocity

g = Acceleration of gravity

L = Length of boat or model (L_{PP}, LBP, or LWL)

6.6.1 Effective Power (P_E)

Effective power is the power needed to overcome the total resistance force and it is expressed using equation 6.12. (ITTC1957)

$$P_E = R_T \times V \qquad (6.12)$$

6.6.2 Service allowance

The service allowance is used to determine the installed main engine power, which means it must be calculated depending on the predicted service area. The size of the Boat must also be considered, as the service limit for small boats will be larger than larger boats. In addition, the Hull shape will have an impact on the required service allowance. According to Harvland, the percentage ranges from 15 to 40% depending on the locality.

$$P_E = R_T \times V \frac{1 + \text{service\_allowance\%}}{100} \tag{6.13}$$

6.6.3 Propulsion Power (P_P)

Propulsion power is the total power needed for propulsion or overall power and it is the ratio of effective power to the overall efficiency and expressed using equation 6.14. (ITTC1957)

Where: P_P = Propulsive Power

ηT = Total efficiency

$$P_P = \frac{P_E}{\eta_T} \tag{6.14}$$

The Total efficiency of the boat is expressed in equation 6.15.

$$\eta_T = \eta_H \times \eta_O \times \eta_R \times \eta_S \tag{6.15}$$

Where: η_H = Hull efficiency

η_O = Propeller in open water condition

η_R = Relative efficiency and η_S -Transmission efficiency (shaft line and gearbox)

I. Hull efficiency (η_H)

The hull efficiency is a function of the wake fraction, w, and the thrust deduction fraction, t, [Harward 1983].

$$\eta_H = \frac{1 - t}{1 - w} \tag{6.16}$$

The form in the aft body (Fa) can be described by factors: [-2, 0, +2], negative values for U shape, positive for V-shape, and zero for N-shaped hull form. Wake fraction determined as ITTC57 and thrust deduction is obtained using Equations 6.17 and 6.18.

$$w = \frac{0.1 \times B}{L_{WL}} + 0.149 + \frac{\frac{0.05 \times B}{L_{WL}} + 0.449}{585 - \frac{5027 \times B}{L_{WL}} + 11700 \times \left(\frac{B}{L_{WL}}\right)^2 \times (0.98 - C_B)^3 + 1} + \frac{0.025x\ F_a}{100 \times (C_B - 0.7)^2 + 1} - 0.18 + \frac{0.00756 \times F_a}{\left(\frac{D_{prop}}{L_{WL}} + 0.002\right)^2 + 1} \tag{6.17}$$

Where: w =wake fraction and t is thrust deduction fraction

D_{prop}= propeller diameter which is 0.713x max_ draught −0.08

C_B= block Coefficient

L_W = water line length

$$t=\frac{0.625\times B}{L_{WL}}+0.08+\frac{0.165-\frac{0.25\times B}{L_{WL}}}{525-\frac{8060\times B}{L_{WL}}+20300\times\left(\frac{B}{L_{WL}}\right)^{2}\times(0.98-C_B)^3+1}$$

$$-0.01\times F_a+2\times\left(\frac{D_{prop}}{L_{WL}}-0.04\right) \quad (6.18)$$

II. Relative rotated efficiency and shaft efficiency:

According to ITTC, behind propeller efficiency, as the relative rotated efficiency in average is close to one (it normally varies between 0.95 and 1.05) the size of this value depends on propeller shaft length, the number of bearings, and the gearbox. A shaft line with a directly mounted propeller is approximately 0.98, while it is 0.96 – 0.97 for a shaft system including a gearbox solution.

6.7 Stability Test Using ANSYS AQWA

In this thesis work, to perform stability of the existing and the new design of boat, ANSYS AQWA software, is selected from among the available different software's used in marine engineering. It can be used to examine the effects of the wave and wind on floating systems.

6.7.1 AQWA Boundary Condition

The boundary conditions used in ANSYS AQWA are listed as follows:

I. Model description

The 3D geometry of the boat is created on CATIA V5R19 and imported to ANSYS R19.3, AQWA Hydrodynamics. The draught or height from the surface to the underside of the boat was labeled by using a cut water plane area. On hydrodynamic analysis, a solid model is not considered. The software only accepts surface model which is massless, therefore the structural load and other additional loads must be input by using the point mass (kg) tool.

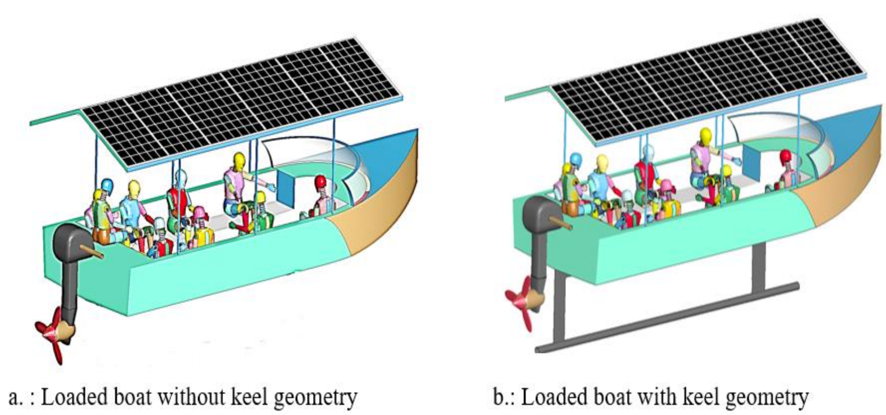

Figure 6.10. The Geometry of the new designed boat

The depth of water was set according to the global coordinate systems. The maximum depth of Lake Tana was estimated as 14m depth.

II. Mass moment of inertia

It is one input data to set the AQWA boundary condition. The mass of inertia was taken from CATIA V5 then, the radius of gyration was done by using a manual system. If the whole mass of the body is supposed to be concentrated at a distance k from the axis of rotation then,

$$I = mk^2 \tag{6.18}$$

The radius of gyration for boat

$$k_{xx} = \sqrt{\frac{I_{xx}}{m}} = \sqrt{\frac{2672.7}{3654.511}} = 0.85$$

$$k_{yy} = \sqrt{\frac{I_{yy}}{m}} = \sqrt{\frac{13677.28}{3654.511}} = 1.93$$

$$k_{zz} = \sqrt{\frac{I_{zz}}{m}} = \sqrt{\frac{13677.44}{3654.511}} = 1.93$$

Where: k=called the radius of gyration

m = mass

I_{xx} = Mass moment of inertia about the x-axis.

I_{yy}=Mass moment of inertia about the y-axis and,

I_{zz}=Mass moment of inertia about the z-axis.

Figure 6.11 shows the point of mass according to the center of gravity (coordinate of point mass).

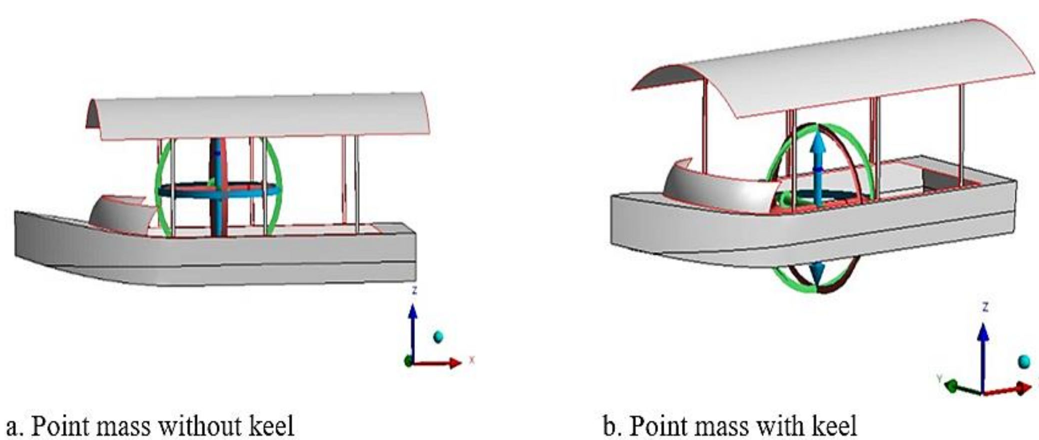

Figure 6.11. Center of the position of the point mass

III. Mesh generation

The Mesh generation tools were set, According to the ANSYS AQUA R19.3 manual**,** the mesh used on this boat shape was Global Basic mesh type. The maximum number of elements should not be greater than 40,000. If Global Controls is set to Basic, a limited number of meshing options are available in the Details panel. The mesh is automatically generated on the bodies in the model; its density is based on the diffeaturing tolerance and maximum element size.

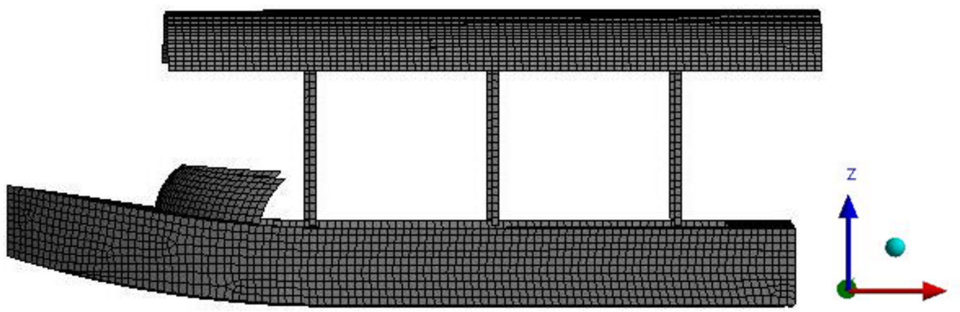

Figure 6.12. Mesh Generated on the Geometry

- ❖ The wind load coefficient is worked under hydrodynamic response only. Their value was set according to data by a read from Appendix D. The value of wind load coefficient is shown in Table 6.3.

Table 6.3. Boat input data wind force coefficient

Degree	Moment of (yaw) coefficient of wind	Drag force coefficient (C_D) of wind	Side force coefficient (C_S) of wind
0	0	0.25	0
75	0.35	1.75	1.6
100	-0.18	-0.25	0.85
180	0.01	-0.2	0.2

This result can be imported into the ANSYS for Hydrodynamic response Analysis and Stability. The result will be inserted as Newton per (meter/sec)^2 Therefore rearranged formula was written as,using equation 6.13 (Aqua Theory Manual, 2013) .

$$\frac{F}{V^2} = C\frac{1}{2}\rho A \quad (6.13)$$

Where: A=Average Projected area from which the wind applied or current applied,

C = Current or wind coefficient in dimensionless from the above table,

ρ = Density of water or wind

The standard value of air and water density are indicated in Table 6.4.and value from the model are indicated in Table 6.5.

Table 6.4. The standard value of air and water density

The standard density of air	1.225 kg/m^3
The standard density of water	1025 kg/m^3

Table 6.5. Estimated value from the model

Frontal Area above the water surface	1.573m^2
Side Area above the water surface	4.7067m^2
Frontal Area bellow water surface	0.683m^2
Side Area below the water surface	1.9vm^2

The converted input data using equation 6.13 for crosswind force are indicated in Table 6.6

Table 6.6. Converted input data for crosswind force coefficient

Degree	Moment of (yaw) coefficient of wind	Drag force coefficient (C_D) of wind	Side force coefficient (C_S) of wind
0	0	0.24	0
75	0.72	1.686	4.61
100	-0.52	-0.24	2.45
180	0.029	-0.193	0.576

VI. Hydrodynamic Pressures and Motions

The Pressures and Motions results object enables the visualization and display of several results generated from AQWA once a hydrodynamic solve has been performed. The Incident Wave Amplitude can be modified to provide results that are factored from the unit 1m wave that is the default; extreme modification may extend results beyond the capabilities of linear analysis.

V. Hydrodynamic response Analysis

Dynamic Stability Test When we apply the Dynamic Stability test wind force coefficient must be considered to the system in addition to wave loading.

- The number of intermediate frequencies is set to 20.
- The number of the intermediate directions is set to 7.
- Wave direction interval is set to standard 45degree.
- The wave grid size was set to 10.

❖ The Wave Directions tree object enables the definition of a range or single wave direction to use in the analysis. In this case, only a single wave direction can be analyzed. Waves are automatically created in -180 and +180 directions, and either the Interval or the number of intermediate directions (No of Intermediate Directions) can be specified. If a direction range of particular interest, additional ranges or specific directions can be added. The wave directions of motion for different wind direction are shown in Figure 6.13.

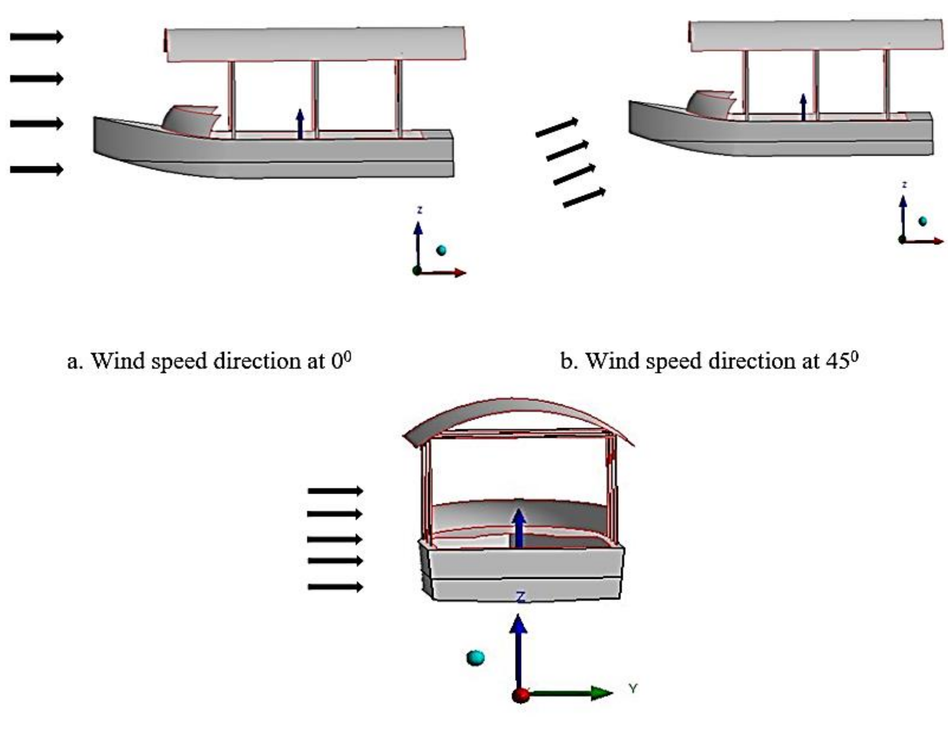

a. Wind speed direction at 0^0

b. Wind speed direction at 45^0

c. Wind speed direction at 90^0

Figure 6.13. The Wave Directions of motion at the different direction

CHAPTER SEVEN

RESULTS AND DISCUSSIONS

7.1 Introduction

In this chapter, the results of the simulation of the boat CFD analysis, the feasibility study for implementing wind and solar hybrid power system for boats are shown. In addition stability test and the sizing and selection of the system, the battery is reported and discussed in detail.

7.2 CFD Analysis Results and Discussions

In this section, the CFD analysis of the boat is used to determine the resistance power and the interaction of the fluid motion on the boat. The analysis of CFD results is examined in this study utilizing commercial software ANSYS-Fluent. The volume of fluid technique is utilized in conjunction with the Reynolds averaged Navier-Stokes equations and two models are applied to the simulations was SST k-ω turbulence for viscous and multiphase model VOF model are used to describe the two-phase flow of water and air around the boat.

7.2.1 CFD Results of Boat

To ensure numerical stability and accuracy, the numerical calculation was performed using second-order discretization for 3500 iterations, since in this case, the residual and drag coefficient converged. The graph of the residual history is shown in Figure 7.1.

I. Residual history

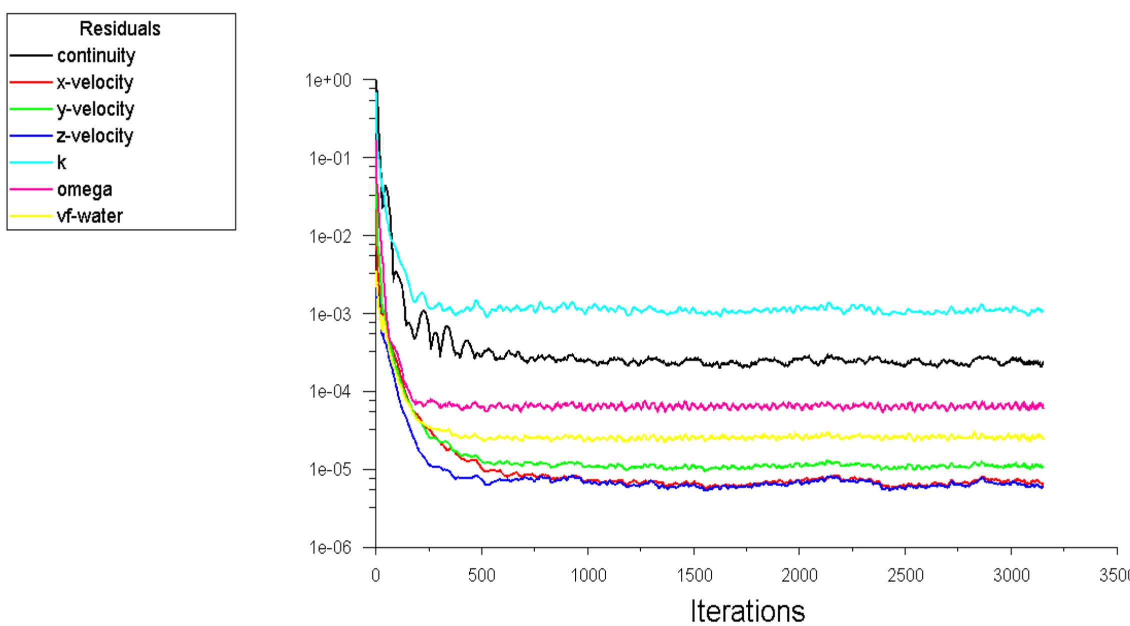

Figure 7.1. Residual history of the boat

II. Drag Coefficient

As it is shown in Figure 7.2 the drag coefficient converges after 400th iteration from the study of these CFD results, the drag coefficient is 0.27 at the speed of 1.8 m/s and this is used to determine the viscous resistance coefficients. A lower drag coefficient means that the object will have less aerodynamic or hydrodynamic drag and it required less propulsion power. A specific surface area is always related to the drag coefficient.

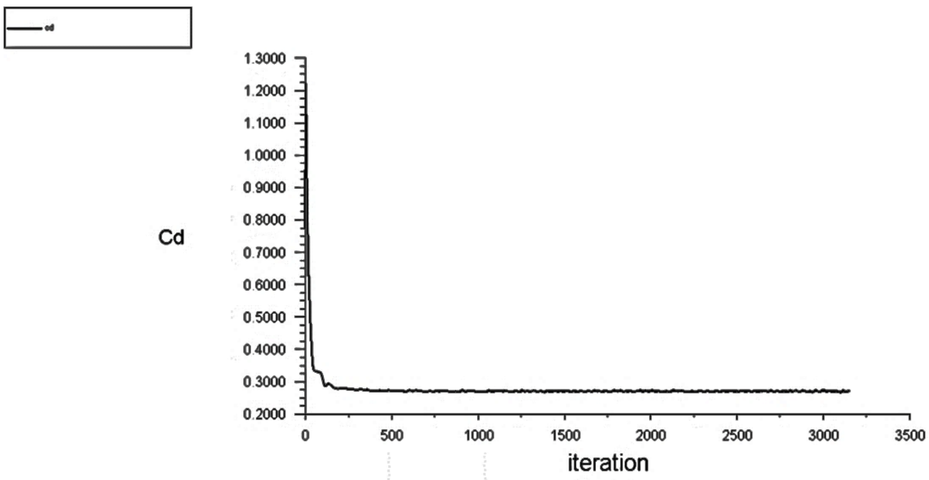

Figure 7.2. Drag coefficient of the boat

III. Volume fraction of water at the boat

Figure 7.3 shows the contour plots of the volume fraction of water on the boat at the initial stage or when the boat is not moving. The volume fraction is a measure of the phase present on the surface of the boat, where 1 represents only water, represented by red color, while 0 represents only air, represented by blue color. Values between 0 and 1 represent the proportion of water to the total volume.

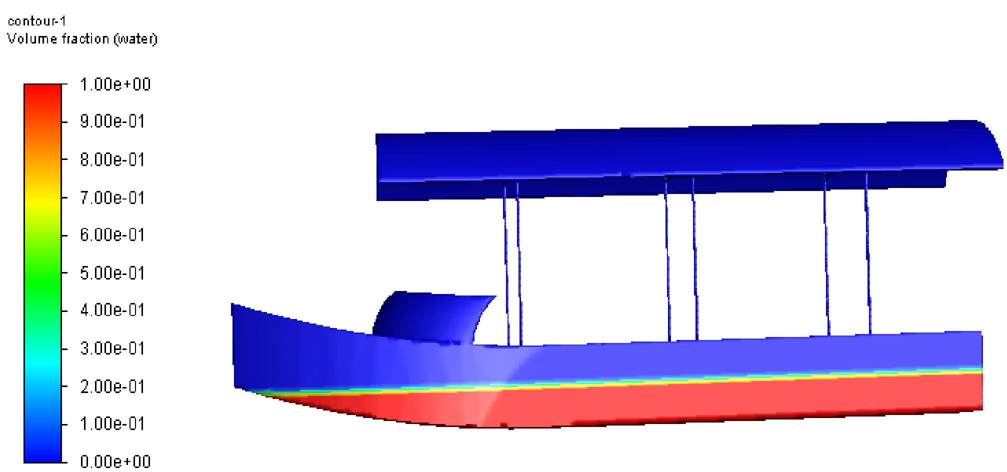

Figure 7.3. The volume fraction of water when the boat is at an initial stage

Figure 7.4 shows the contour plots of the volume fraction of water on the boat when the boat is in a moving condition.

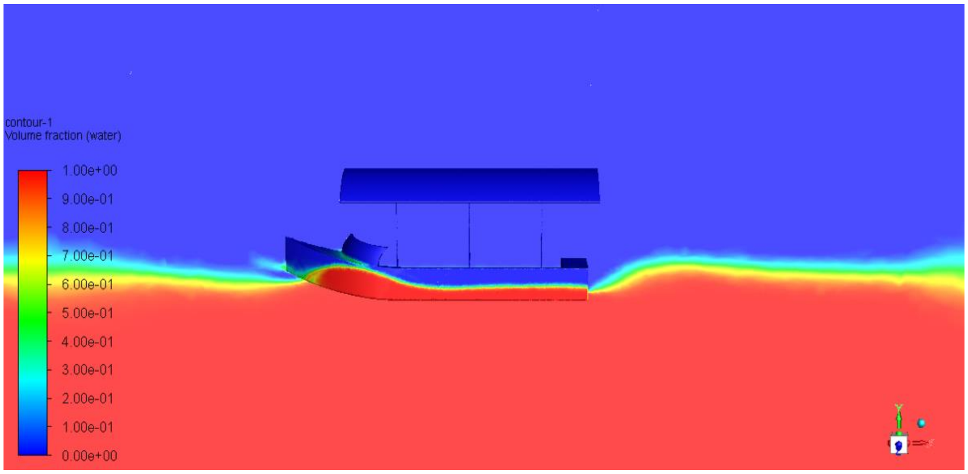

Figure 7.4. The volume fraction of water at the symmetry plane of the boat

The free surface is defined as the interface between water and air where the volume fractions are 0.5. Figure 7.5 shows the fluid motion around the boat.

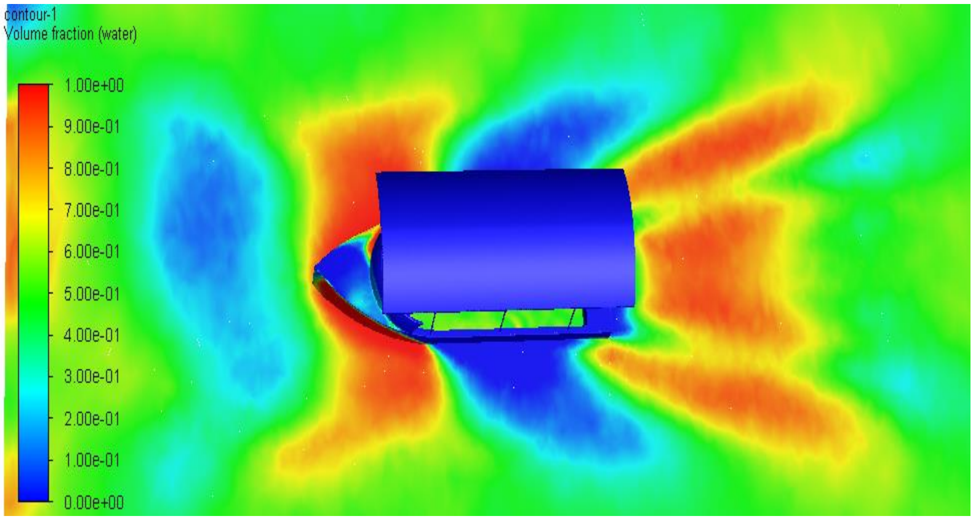

Figure 7.5. Flow condition for the volume fraction of water at the plane surface

IV. Pressure Contour

As illustrated in Figure 7.6 the expected overall pressure distribution are shown, and provides a flow around the boat. The pressure is extremely high on the roof and a portion of the wetted surface or (draught) component. Because of the high pressure, the velocity is low at that point. The pressure in the back is less than in the front. As a result, there is a drag force-directed backward. The pressure intensity is indicated by the colors on the pressure contour. The highest pressure is indicated by the red color, while the minimum pressure is indicated by the blue color.

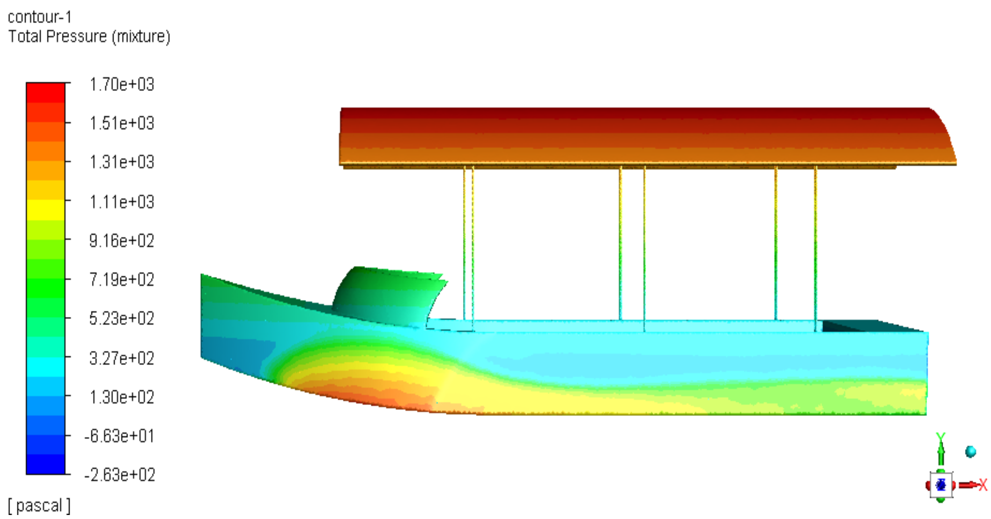

Figure 7.6. Contour plots of total pressure on the boat

V. Velocity Contour

The velocity and pressure attain their lowest and maximum values near the stagnation point, as shown in Figure 7.7. The turbulence kinetic energy is considerable at the front and the rear of the boat and when compared to the front part of the boat the turbulence kinetic energy is higher at the rear of the boat, due to this there is a drag at the rear. The airflow pressure in front of the boat is higher than atmospheric pressure.

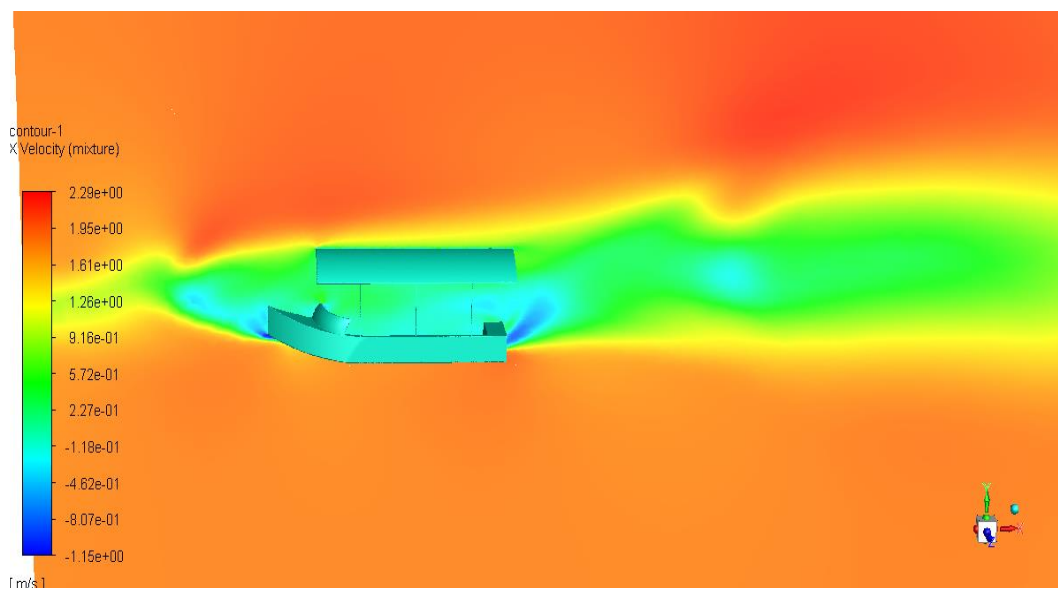

Figure 7.7. Velocity Contour of the boat

Once the drag coefficient is obtained from the CFD result. The next step is to determine the total resistance of the boat.

7.3 Results of total boat Resistance

The total resistance of the boat is computed using a total coefficient of resistance, wetted surface area, and velocity of a boat at full load. Where the velocity of the boat at full load is 1.86 m/s and total coefficient resistance is the sum of viscous resistance (obtained from CFD result which is 0.03379), air resistance (obtained by using equation 6.10), and residual resistance (obtained from Appendix C using Froude no. is 0.012). The total boat resistance is obtained using equation 6.8.

Effective Power

It is obtained by using total resistance force and considering service allowance as it is indicated in equation 6.12.

Propulsion Power

The propulsion power is expressed using 6.14 and the overall efficiency of the system is obtained using equation 6.15 and its value is 0.57. The results of the above three parameters (The boat total resistance and power) were summarized in Table 7.1.

Table 7.1. Results of the boat total resistance and power

Total resistance (R_T) (N)	976.4
Effective power (P_E) (W)	2179.3
Propulsion Power (P_P)(W)	3823.4

7.4 The solar and wind energy results

To determine the available energy from the wind and the solar system, a feasibility study is required. The results obtained under the two power units were discussed as follows.

7.4.1 Solar energy

Here the solar energy was obtained after determining the solar power which is obtained by calculating the average hourly and monthly solar power generated by the panels and then transferred to the batteries.

I. Power from solar panel

Based on Equation 5.1, the energy produced by solar panels varies during the day. As shown in Figure 7.8. The maximum mean daily power produced by solar panels is 1080.32W in the winter season and minimum power generation 631W in the summer season. The spring and autumn (fall) seasons are almost produced the same power.

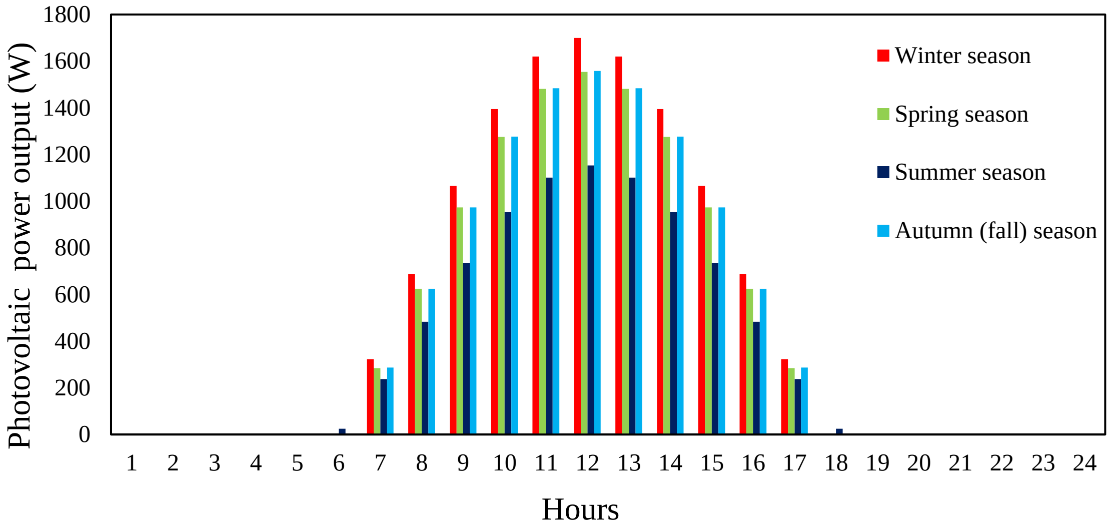

Figure 7.8. PV power output on different weather conditions

As shown in Figure 7.9 the maximum hourly power produced by solar panels for February 16 from 2011-2019 is 1746.7 W and the daily average power was 1111.51 W between 10:00 AM to 15:00 this is due to the high availability of sunlight during the afternoon. The PV power output for all months is listed in Appendix -A Figure A-13.

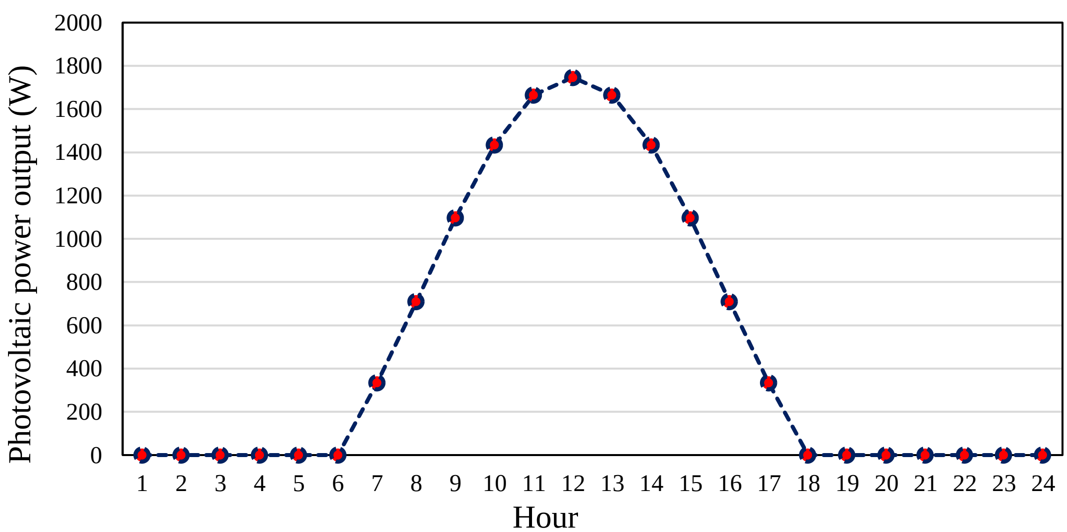

Figure 7.9. Power output from solar panel

In addition, the power generated by solar panels within 12 months is shown in Figure 7.10 as it is indicated the maximum solar power produced by the solar panel was 1111.51 Watts in February and the minimum was 689.93 Watts in august month.

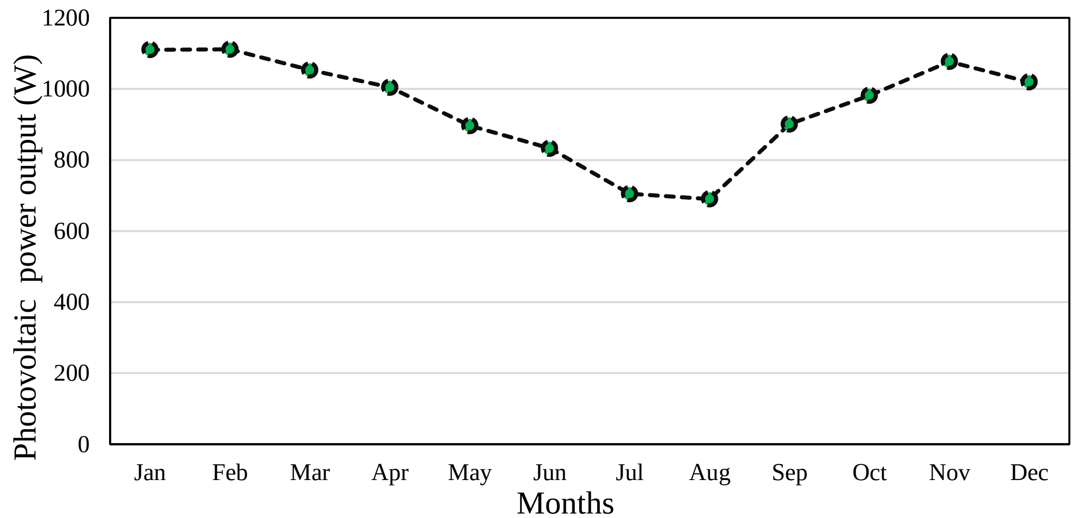

Figure 7.10 . Monthly average solar panel power

II. Total solar energy stored and discharged during the charging and discharging process

After the solar panels produce electricity, the system goes into the battery, taking into account the total losses the system produces. At the beginning of the process, energy gets stored and discharges when the boats start to move. The output power after entering the battery is obtained using Equation 5.4. As shown in Figure 7.11, the maximum amount of energy stored during the charging process per hour is 5.67 MJ an average of 3.9 MJ in February. The consumption power is high and not perfectly suited to PV production so, it needs an additional source of energy.

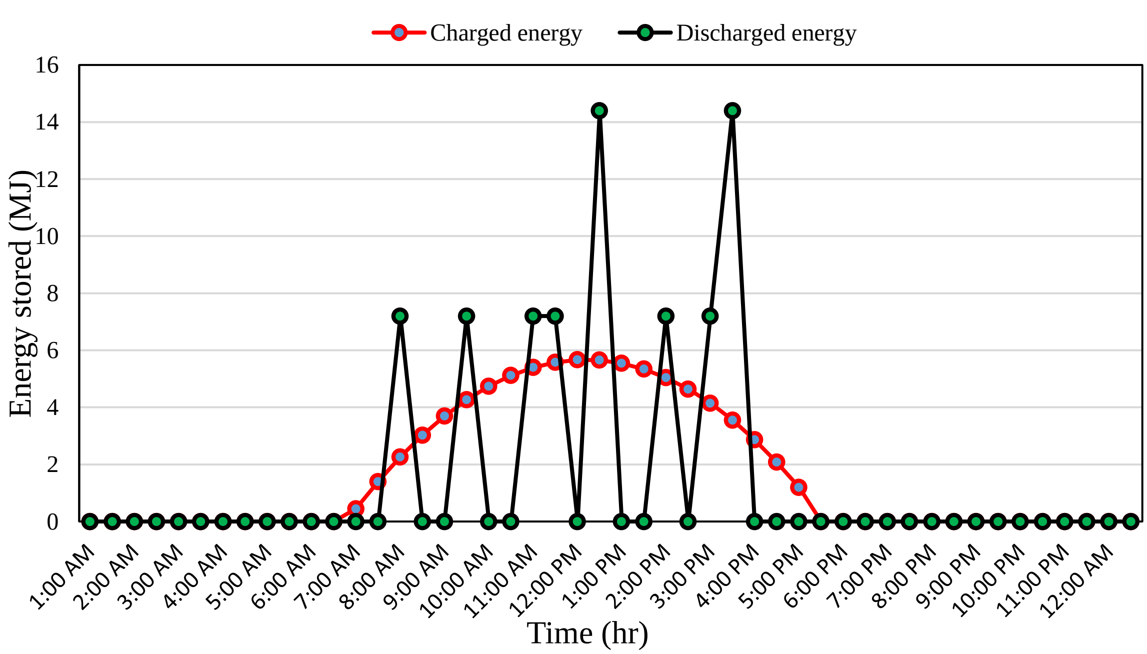

Figure 7.11. Energy balance in charging and discharging on February 16

7.4.2 Wind energy

This section presents the results of a numerical study on the assessment of wind energy potential obtained by determining wind energy and is discussed step-by-step as follows.

I. The size of wind turbine

Here Study was done using the mean annually effective wind speed to determine the cut-in speed, turbine speed, torque, etc. The basic formulas and equations used to calculate the output of the wind turbine is given expressed in equations 5.6, 5.10, and 5.11. The results of wind turbine design were tabulated in Table 7.2.by using average effective wind speed.

Table 7.2. Summary of wind turbine design parameters

V(m/s)	A_S (m^2)	TW(N/m)	I($kg.m^2$)	T (N/m)	Pa (W)	P (W)	n(rpm)
3.04	1.44	2.44	1.55	2.02	24.7	3.72	38.7

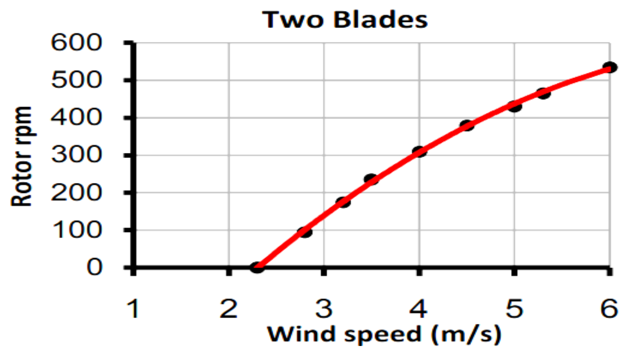

Figure 7.12. Rotor rpm versus wind speed for two blades (Ali, M., 2013)

The curve of wind speed and rotor speed (rpm) is shown in Figure 7.12. As the wind speed increases from [(0 m / s) to (3 m / s), the Savonius wind turbine begins to move. The speed at which the wind turbine begins to move, the wind speed is called the cut-in speed, and the low cut-in speed for this type of wind turbine is about (2.7 m / s). The summery of wind speed indicated in Table 7.3

Table 7.3. Summary of wind speed parameters

Cut-in wind speed	2.7
Rated wind speed	4.5
Rated power	11.8

Figure 7.13 shows the power curve of a wind turbine for May 15. The turbine starts operating at cut-in speed, and then the power output increases in a cubic curve with wind speed until the wind speed reaches rated speed, at which point the turbine starts to operate at rated power.

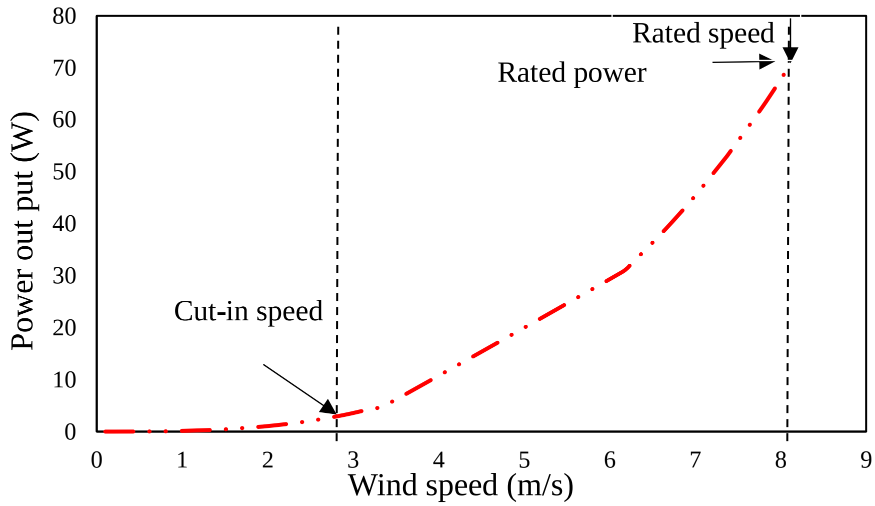

Figure 7. 13. Wind turbine power curve

II. Power generated by wind turbines

Equation 5.22 was used to obtain the power extracted from the wind turbine since the wind speed in the study area was lower so that the effective wind speed is used to determine the wind power. As indicated in Figure 7.14, the maximum mean daily power produced by a wind turbine is 18.005 Watts in the spring season, and the minimum power generation is 13.31 Watts in the autumn (fall) season.

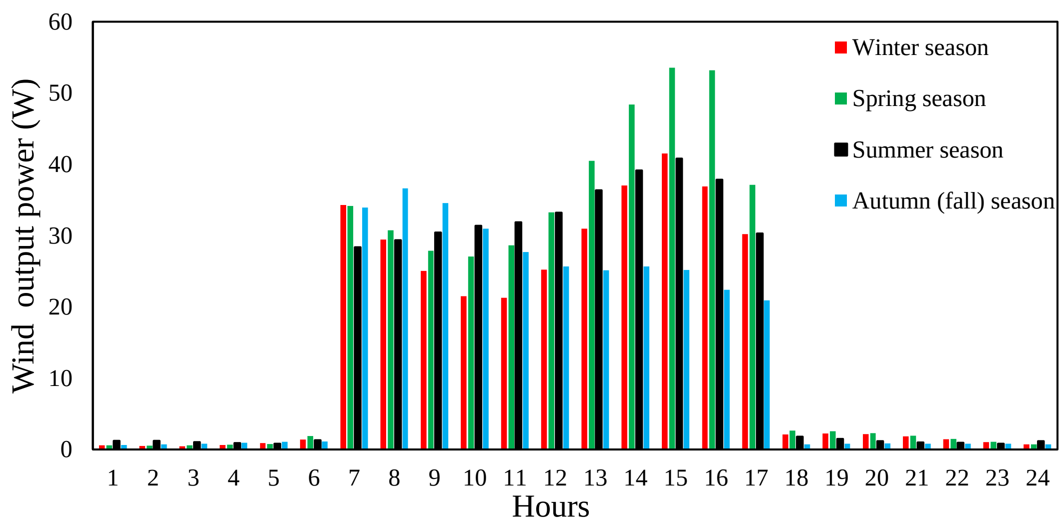

Figure 7.14. Wind turbine power output on different weather conditions

As shown in Figure 7.15, the wind is minimal until the time reaches 8:00 AM. The maximum power output generated by a wind turbine for May 15 from 2011- 2019 is 70.6 watts and the average daily power is 22.7 watts. From this point onwards, the power decreases significantly as the wind speed decreases. Winds at night and in the morning are much lower.

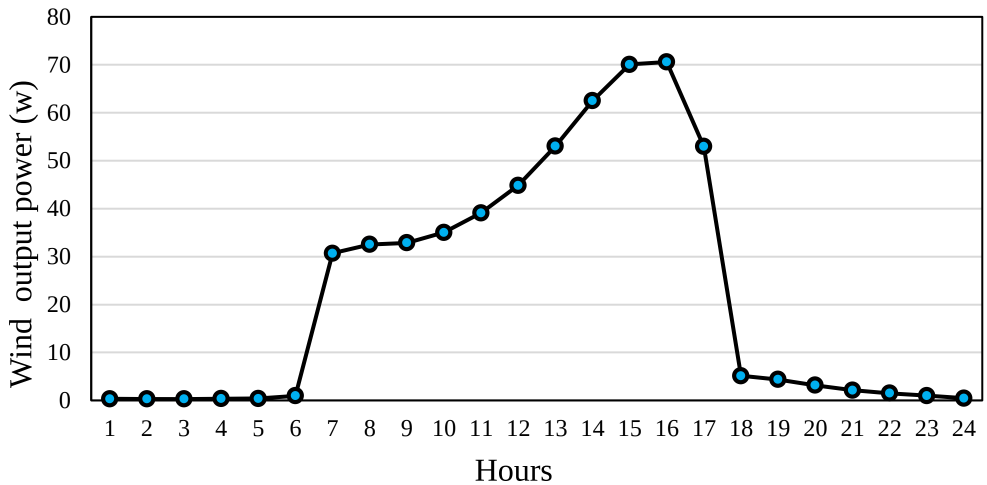

Figure 7.15. Hourly Power from a wind turbine (May

Figure 7.16 shows the monthly average wind power generated by a wind turbine that has been used for 12 months. The maximum power is generated by the wind turbine on May 15 with 22.7 W, the minimum power generated is 11.7 in December and the annual average value is 15.5W.

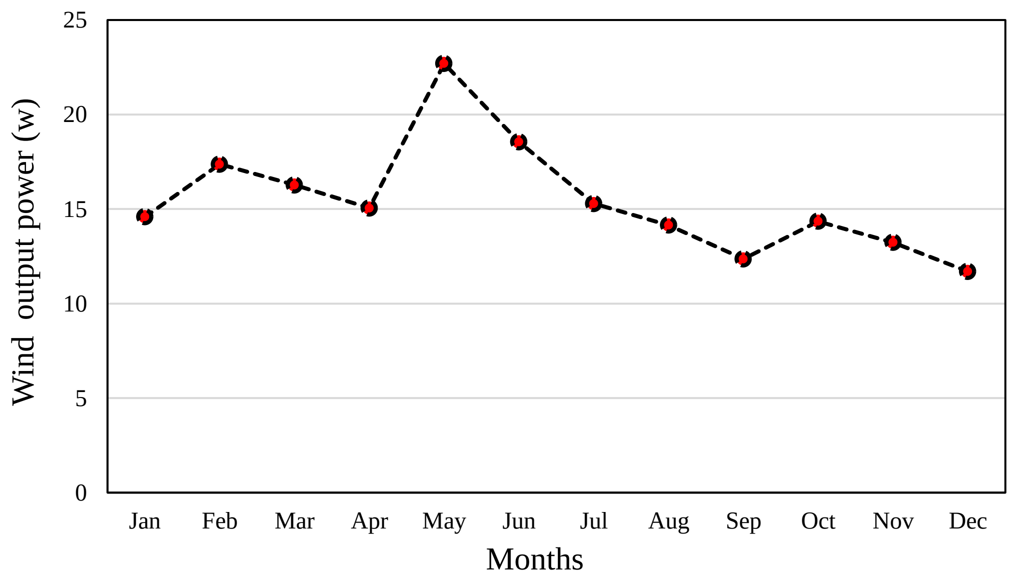

Figure 7.16. Monthly average power from wind turbine

III. Total wind energy stored and discharged during the charging and discharging process

After the power is transferred from the wind turbine to the battery, it is converted to actual wind power using Equation 5.26 and this can be indicated graphically in Figure 7.17, the maximum amount of energy stored during the charging process per hour is 0.6 MJ and averagely 0.195 MJ on May 15.

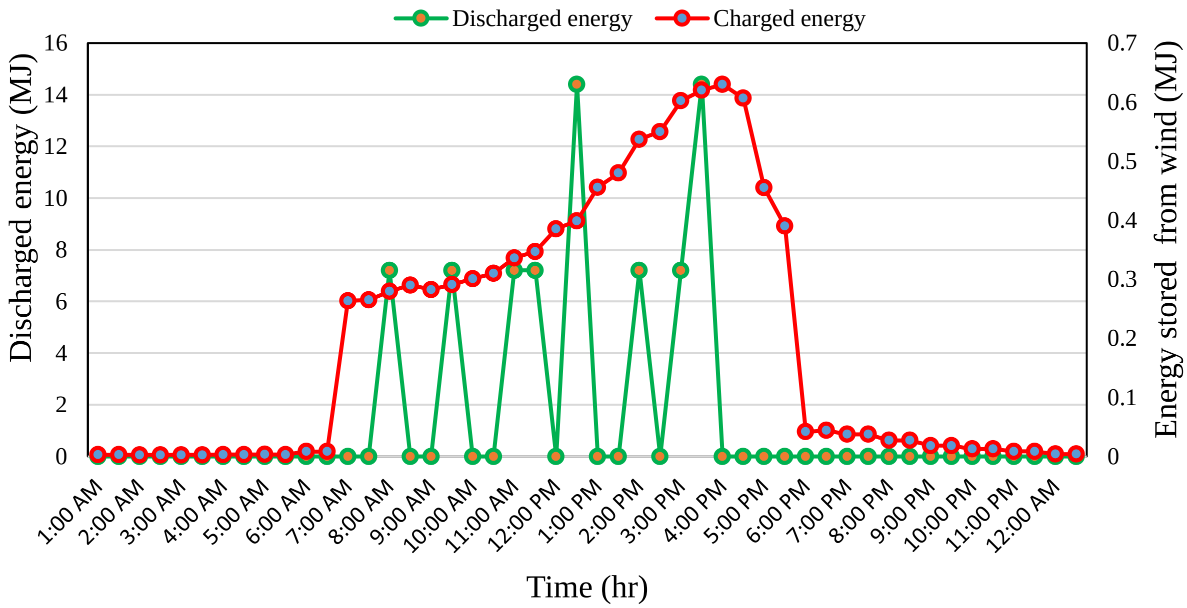

Figure 7.17.Wind power output from the battery

Figure 7.18 shows the hybrid energy output from solar and wind energy. The total maximum energy harvested is 1478 Wh, by solar panel, and from the wind turbine is 168 Wh.

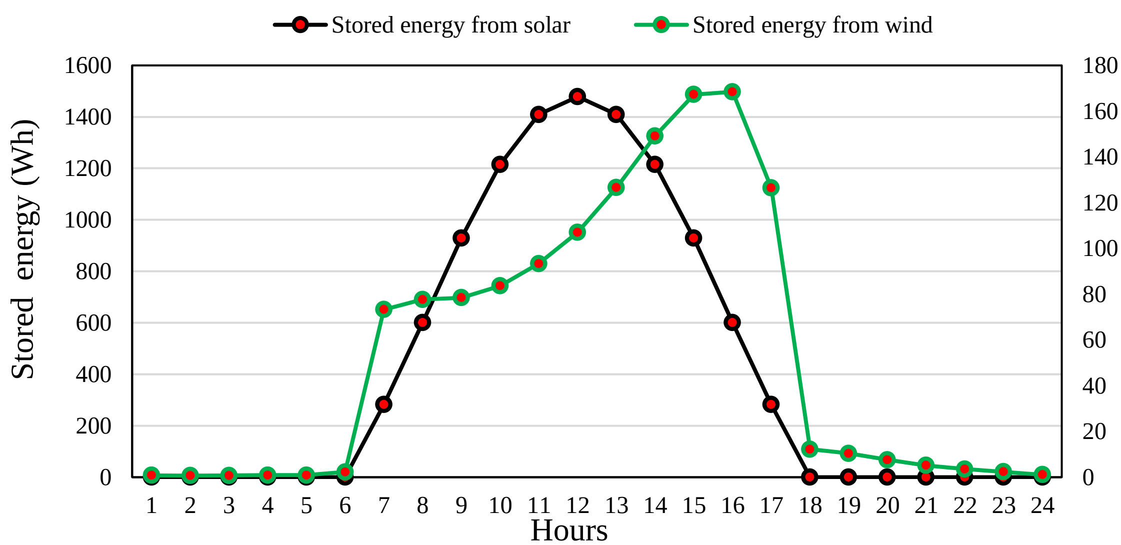

Figure 7.18. Output Power from the hybrid System

- The solar energy value is calculated by multiplying the expected net power output by 7 hours of bright sunlight using Equation 5.5. From Table A-1 in Appendix A, the maximum energy produced from solar energy was 10.35 kWh, and an average of 6.66 kWh per day for February 16. The minimum amount of solar energy is produced when the sun begins to rise and when it sets.

- ❖ Wind energy is calculated using equation 5.26 and the wind blows for 24 hours a day, so the wind turbine can operate 24 hours a day. From Appendix a Table A-2, the maximum energy produced from four turbines is 4.04 kWh and the average daily energy is 1.3 kWh.

7.5 Feasibility Study for Implementing Wind and Solar Hybrid Power System

From the study or determination of the wind energy and solar energy values discussed in section 7.4, the following points were noted:

- By taking average energy output from the solar system is 6.66 kWh which is feasible to integrate with other energy sources.
- The average energy obtained from the wind turbines was 1.3 kWh which is the minimum to implement on boats.
- From the result shown in section 7.3 the required power to propel the boat is around 4 kWh.

From these points, it can be concluded that the energy from the wind turbine is minimum, and the energy produced by the solar system is enough to derive the boat almost for 1:30 hour, however as stated by the boat owners around Bahirdar city, the boat works an average of 5 hours a day so it is minimum to integrate the wind turbine with a solar system to propel the boat. Implementing the wind turbines on the boat with less energy out will result in;

- High cost with minimum energy output.
- Increase the weight of the boat with less energy output.

Thus it has been preferable to propel the boat by integrating solar energy with an electric grid system that uses energy stored in the battery.

7.6 Sizing and Selecting the System Battery

The required power to propel the boat is around 4000 W per hour. So the daily electric energy requirement to propel the boat is obtained by multiplying the propulsion power with the working hours. Based on the electrical load calculation, it should provide a maximum power of 20 kWh for 5 hours. To achieve the required performance, the depth of discharge (about 80%) of the battery system must be considered. The voltage required is 48V, according to the selected DC motor specification from Appendix E. The battery system consists of 3 (parallel) battery banks with each bank consisting of 4 battery packs connected in series and another detail of the sizing battery is summarized In Table 7.4, and the schematic diagram of the battery is shown in Figure 7.19.

Table 7.4. Battery System Calculation

E (daily energy consumption)	20kWh
Battery capacity	578.74 Ah
Number of a battery connected by parallel	3 battery
Number of a battery connected by series	4 battery
Total battery requirement	12 battery

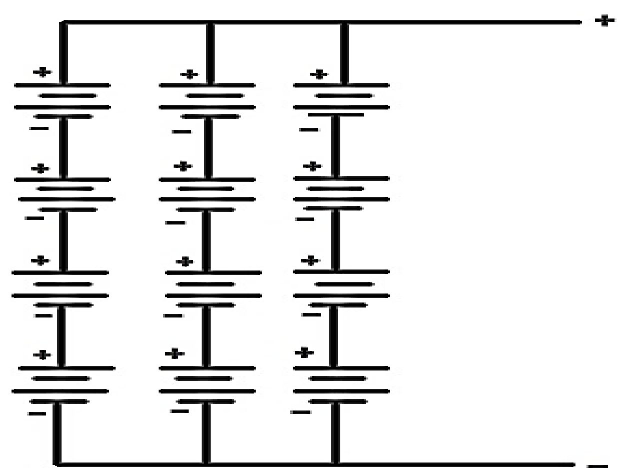

Figure 7.19. Schematic diagram of series-parallel battery connection

7.7 ANSYS AQWA Simulation Results and Discussion

The AQWA hydrodynamic analysis software was used to analyze the motion response and the time-frequency characteristics of the boat during the interaction of wind and waves. When dealing with stability the first thing to keep in mind is the weight. In this study, the weight of existing and modified boats is considered in various aspects to test the stability.

- First, an 800 kg unloaded exiting boat is considered, then the boat is loaded with an additional mass of 1400 kg.
- Second, modified boats with and without load are considered. The modified boat weighs 1400kg with no load, which is heavier than the existing model. This is due to additional components such as batteries, solar panels, and other accessories. When the modified model is fully loaded, the total mass will be 2800 kg. The detail of the mass of each component of the existing and modified model is shown in Appendix Table B-1

7.7.1 Hydrostatic static results

The hydrostatic stability results are indicated in Table 7.5 at different mass of the boat.

Table 7.5. Hydrostatic static results

PARAMETER / MASS	800 kg)	(1400kg)	(2300 kg)	(2800 kg) (with keel)
Vertical CG (m)	0.5	0.5	0.5	0.5
Actual Volumetric Displacement:	1.36	1.36	2.46	2.46
Equivalent Volumetric Displacement:	0.78	0.78	2.24	2.73
Centre of Buoyancy (CoB) Position (x, y, z) (m)	(3.72,-1.99, -0.07)	(3.72,-1.99, -0.07)	(3.59,1.46, -0.12)	(3.59,1.46, -0.12)
Cut Water Plane Area (m^2)	9.46	9.46	9.99	9.99
Metacentric height (m)	1.43	1.43	0.53	0.93
Restoring moments/degree rotation(MX/MY) Nm/°(x,y)	(342.73,3322.79)	(342.73, 3322.79)	(229,3833)	(334.14, 3928.62)

The metacentric height (GM) is an indicator to measure the initial static stability of a floating body. It is calculated as the distance between the center of gravity of the container and its metacenter. In the experimental case, when the container is tilted to one side, this is considered an imaginary point. The GM cases are explained as follows:

- ✓ If the GM value is less than zero, the boat becomes unstable (GM < 0).In this case, the uprighting moment is less than zero. The ship does not have initial stability and after environmental influence, the ship will be inclined an equilibrium position will be not be achieved.
- ✓ When the GM value is zero (GM = 0), the boat begins its initial stability and uprighting moment zero. In this case, after external loads, the ship does not return to the starting position because the new position is in equilibrium.
- ✓ When the GM value is greater than zero, the boat becomes stable (GM > 0), uprighting the ship will return to its initial position, a larger metacentric height implies greater initial stability against turnover.

Figure 7.20 shows the vessel stability diagram of the center of gravity (G), a center of buoyancy (B), and metacenter (M) with the vessel upright and fixed over near one side.

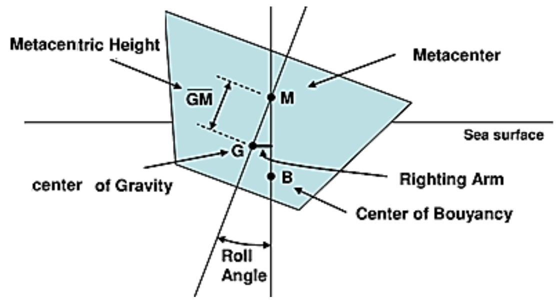

Figure 7.20. The vessel stability

As long as a load of a vessel remains stable, the centre of gravity is fixed (relative to the vessel). For small angles, the metacentre can also be fixed, while the centre of buoyancy moves as the vessel's heels. For vessels design, it is recommended to consider adjusting the centre of gravity to keep the metacentre height. According to the marine structural designer, the metacentric height of large vessels should not be less than 0.15 m. But for a small size or scaled one that has a length from 1-16m GM should have above 0.75m. From the simulated results of boat design of hydrostatic stability testing all outcomes of metacentres at the different vertical centre of gravity positions from the centre of buoyance are well agreed with technical data. As the centre of gravity moves downward length of the righting arm increases thereby providing a better righting moment.

Figure 7.21 shows that as the centre of gravity increases, the metacentric height decreases linearly for the mass of (800 kg), but the variation of the structural load has no effect on small-angle hydrostatic stability analysis except that it has a greater impact on wave loading character. Therefore according to the design, there must be recommended structural weight that have also a greater contribution for balancing the system from wave impact load.

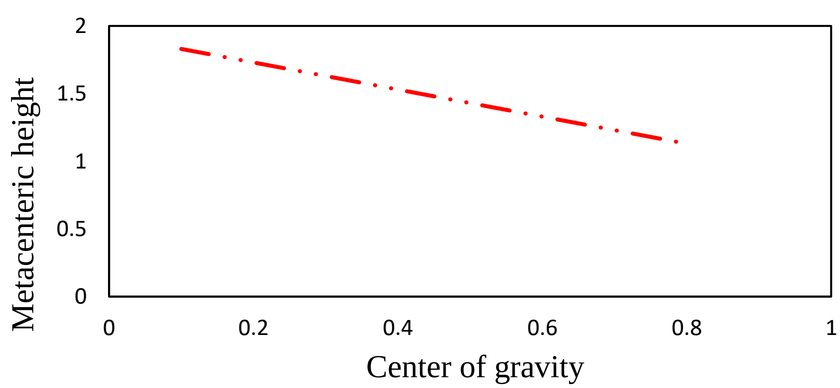

Figure 7.21. Relationship between vertical centers of gravity with metacentric

Figure 7.22 shows the graphical plot of wave impact analysis of boats that depends on out balances ratio. As the weight of the structure increases the out of balance ratio or behaviour of structural disturbance under given wave loading become decreases.

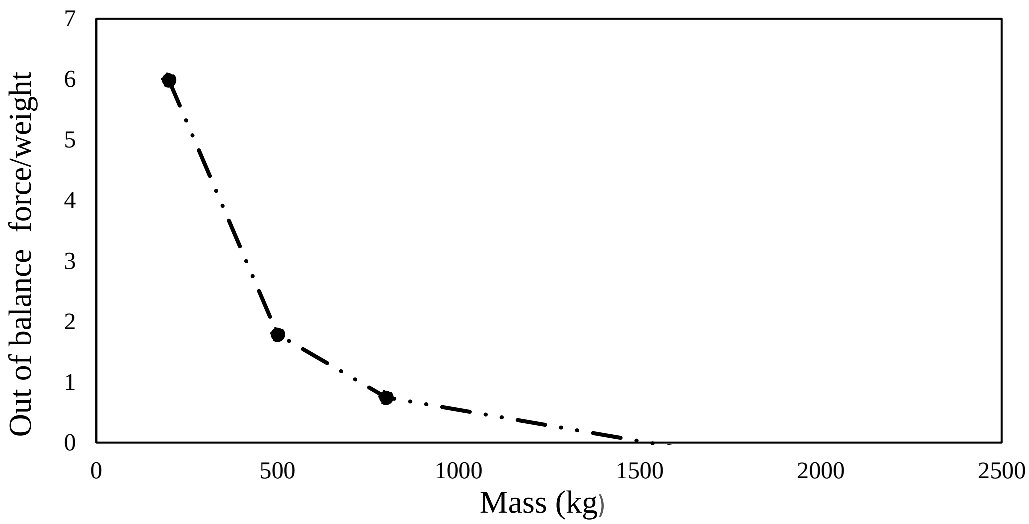

Figure 7.22. Out of balance at different mass

Figure 7.23 shows the Pressures and Motions distribution on the surface of a boat at a direction of 90 degrees. The maximum pressure value is 7.19 N/m^2 which is indicated by red color and the minimum value is indicated by blue color which is 1.112 N/m^2. The pressure is extremely high on the portion of the wetted surface area or at the draught part of the boat. The other pressures and motions distribution of boat about an angle of 0 degrees and 45 degrees can be found in Appendix B in Figure B-1 and Figure B-2.

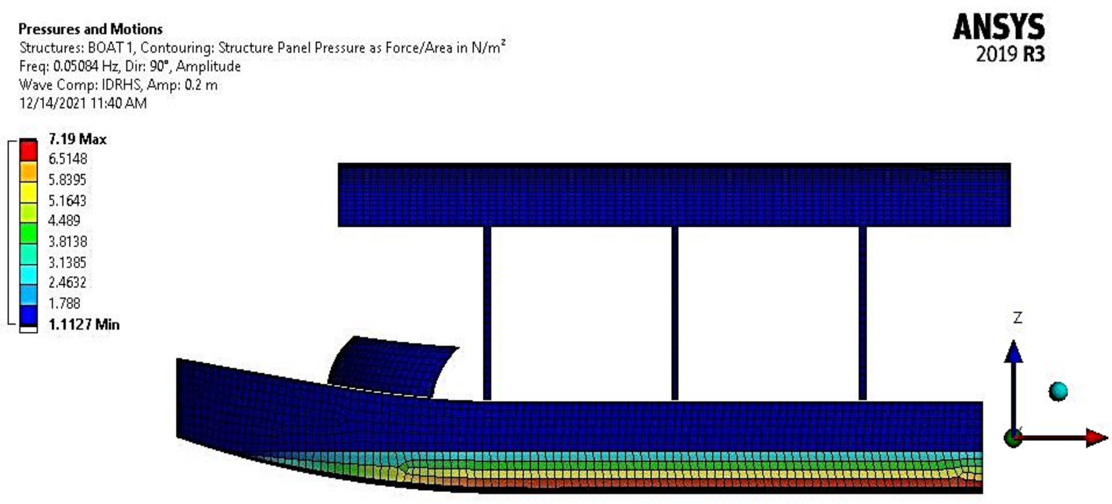

Figure 7.23. Hydrodynamic Pressures and Motions

7.7.2 Hydrodynamic response analysis results

The hydrodynamic responses of a moving boat were studied under regular waves through ANSYS hydrodynamic response. For ANSYS AQWA calculation, no forward speed effect is taken into consideration, the waves considered to compute the RAOs are in the range of periods [1s to 40 s].

I. Response amplitude operators (RAOs)

RAOs show the behavior of the boat in different waves angel's with periods. The RAO depends on the size (draft and area of waterline) and the mass properties of the boat, wave RAOs could be separated into two parts: rotation and translation, the most dangerous motion is heave -translation and roll rotational (Ozorishin, 2012).

The hydrodynamic simulation software AQWA uses a series of regular wave simulations to obtain the RAO value of the overall motion response of the boat. Figure 7.24 shows the degrees of freedom for the motion of the boat.

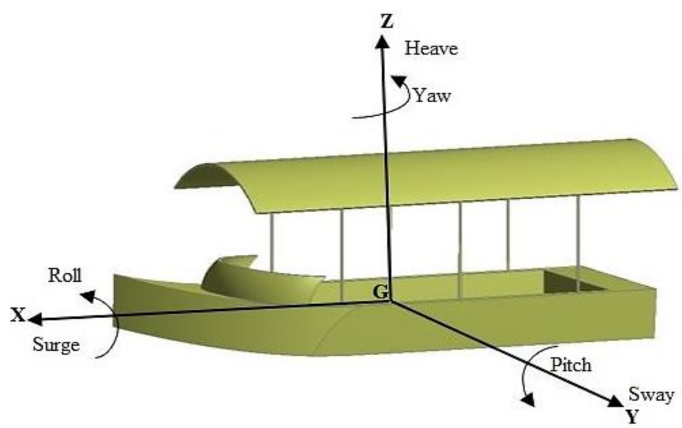

Figure 7.24. Six-degrees-of-freedom for boat motion

- ❖ Three wave's directions are analyzed: at 0 degrees (head seas), 90 degrees (beam seas), and 45 degrees, (Quartering Seas).

By varying the crosswind speed and wave direction. Thus, the response of the boat is tested under three conditions.

1) The wave direction is set to 0 degrees or parallel to the movement of the boat, and the relative wind speed is calculated by adding the speed of the boat and the actual wind speed of the area of the study at 3.84 m/s.
2) The wave direction was the same as the above condition (condition one) except that the value of the relative wind speed is the difference between the speed of the boat and the actual wind speed of the area of the study at speed of 1.63m/s.

3) Lastly the direction was defined at 45 and 90 degrees to the movement of the boat and the wind speed is equal to the actual wind speed of the study area which is 2.2 m/s.

a) RAO for Roll Motion

As shown in Figure 7.25, the roll and yaw RAO values are close to zero when the wave angle is 0 °. The yaw angle of rotation is close to zero and is not taken into consideration, because it is nearly close to zero. The maximum rolling angle at head seas (0 degrees) is 0.000578 for the mass of 2800kg at the abscissa position of 31 sec for speed 1.63 m/s and 0.000581 for speed of 3.84 m/s. However, the RAO value at pitching degree of freedom is high.

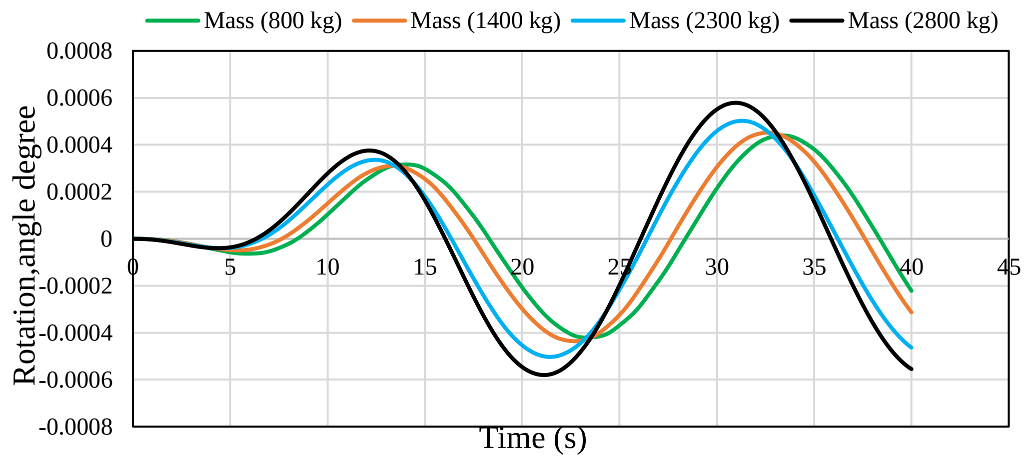

a) At speed of 1.63 m/s

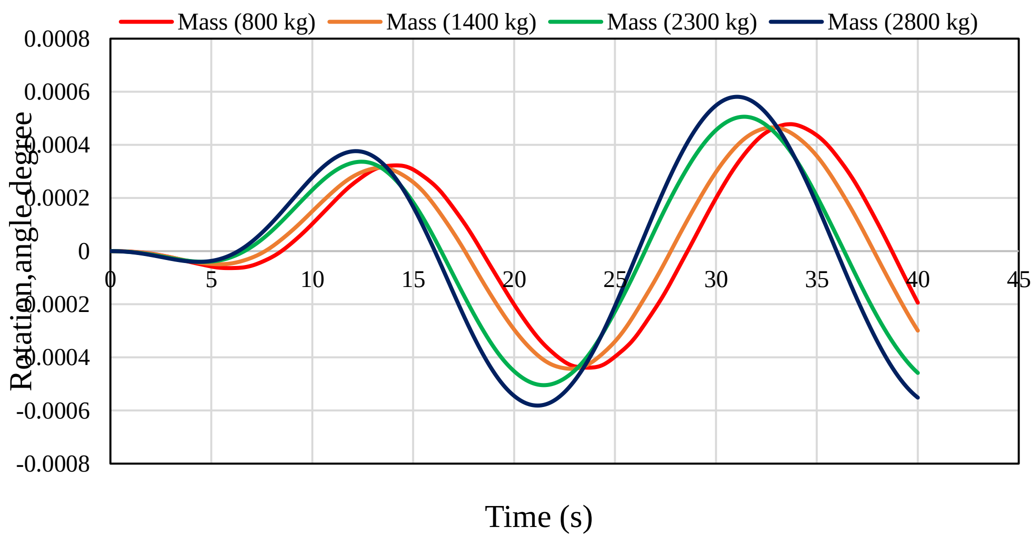

a) At speed of 3.84 m/s

Figure 7.25. Roll in Head Seas

The most dangerous motion in the quartering wave direction is the rolling rotation angel. Figure 7.26 shows the effect of rolling in quartering seas. The maximum rolling angle at quartering seas (45 degrees) is 0.34 degrees for a mass of 2800 kg at a position along the abscissa axis of 25 s at a wind speed of 2.2 m/s.

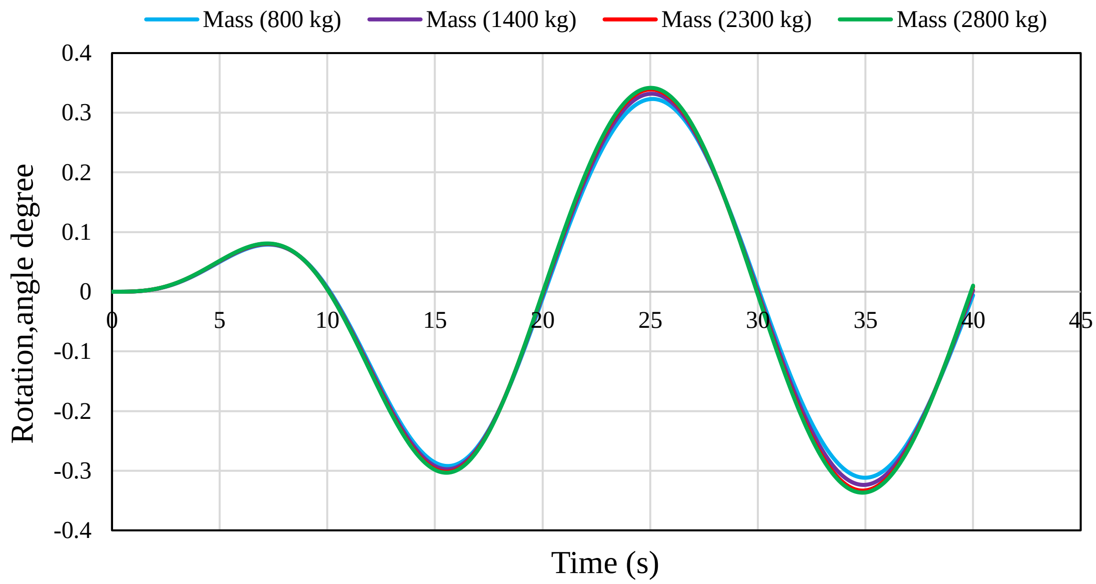

Figure 7.26. Roll in Quartering Seas

The roll, heave, and sway of the motions are considered at the beam seas. As shown in Figure 7.27, the rolling motion of the Beam Sea is the most dangerous inclination. The maximum rolling angle at the beam seas (90 degrees) is 0.485 for a mass of 2800 kg at the coordinate position of 24.8 seconds for the average wind speed value is 2.2 m/s.

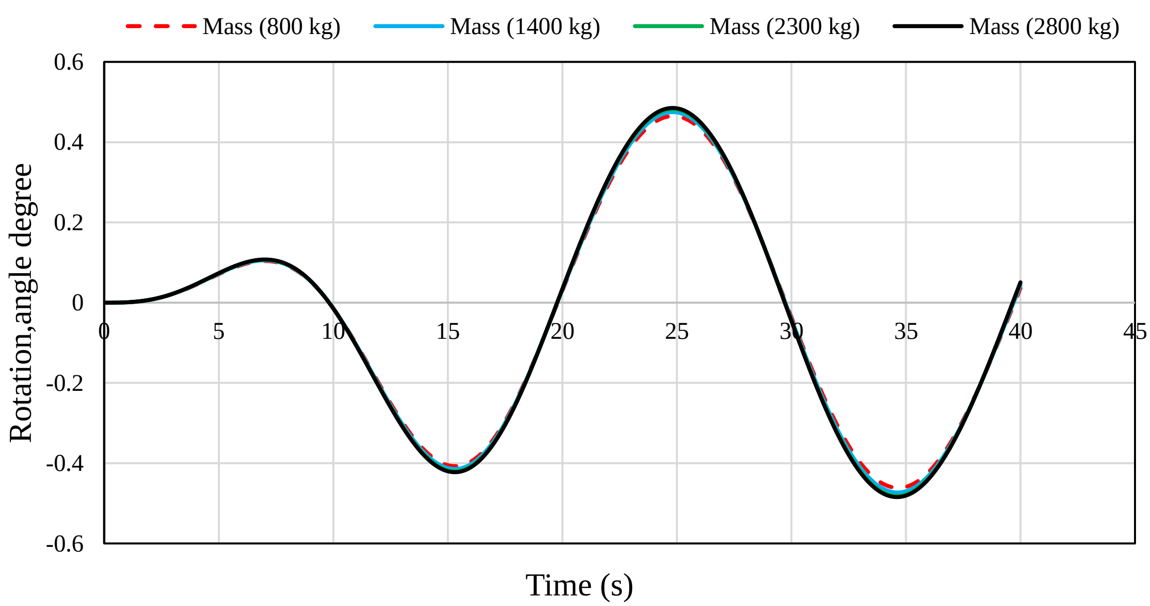

Figure 7.27. Roll in Beam Seas

b) RAO for Pitch Motion

As shown in Figure 7.28, the maximum pitch rotation at 0 degrees is 0.45 for the mass of 800kg for both speed conditions. The pitch response amplitude operator also shows a significant increase in head seas. The pitch period for beam and quartering Seas will not be taken into consideration, because it is less than in the head sea.

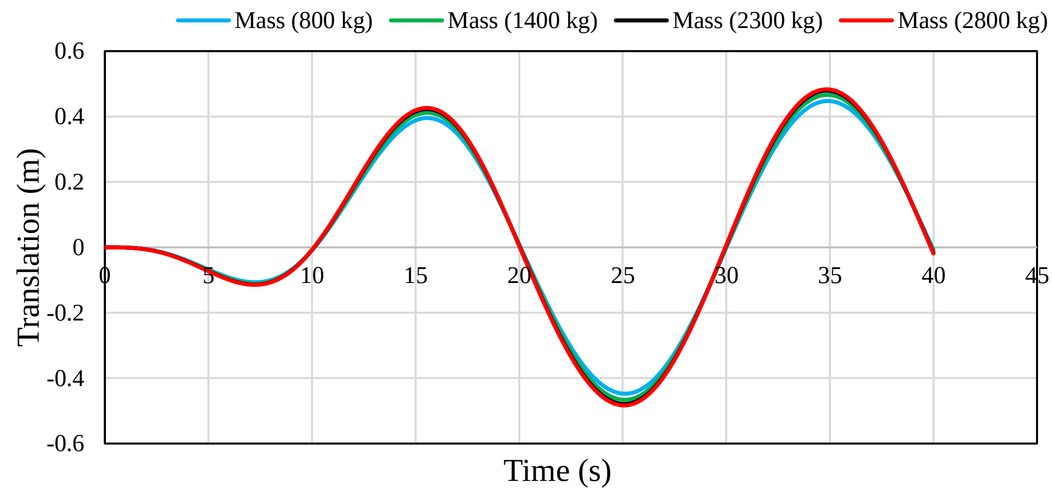

a) At speed of 1.63 m/s

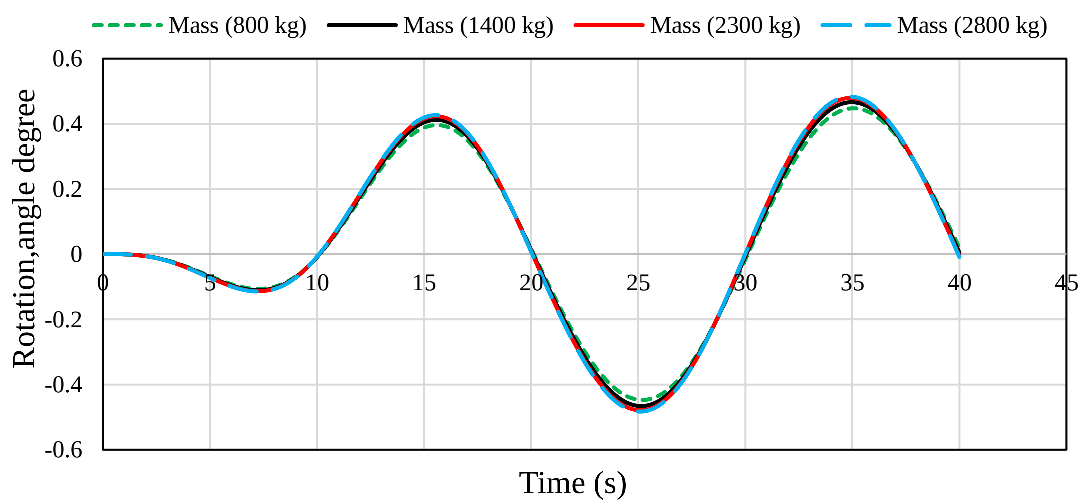

b) At speed of 3.84 m/s

Figure 7. 28. Pitch in Head Seas

c) RAO for Heave Motion

Figures 7.29 and 7.30 show the RAO of the heave concerning the head sea and beam sea angles. The heave is practically well behaved and increases from zero in a short period. The Heave translation value is 0.3m in both wave conditions.

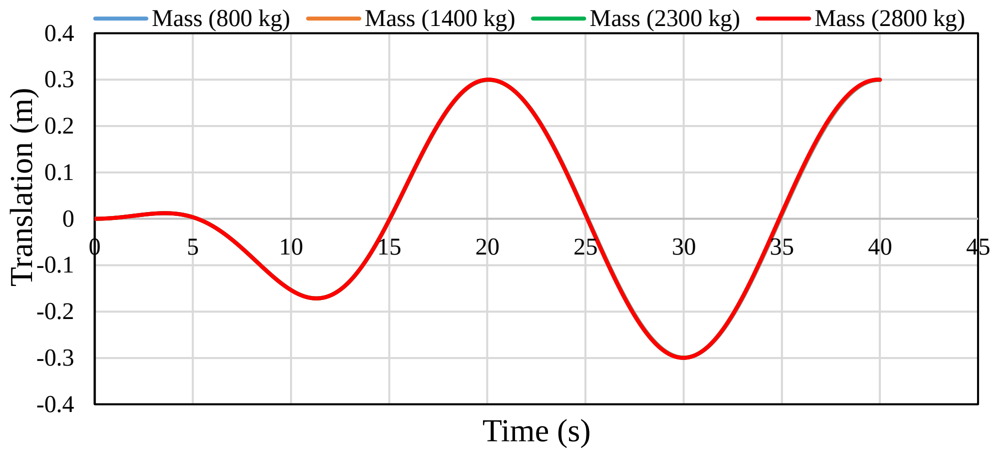

a) At speed of 1.63 m/s

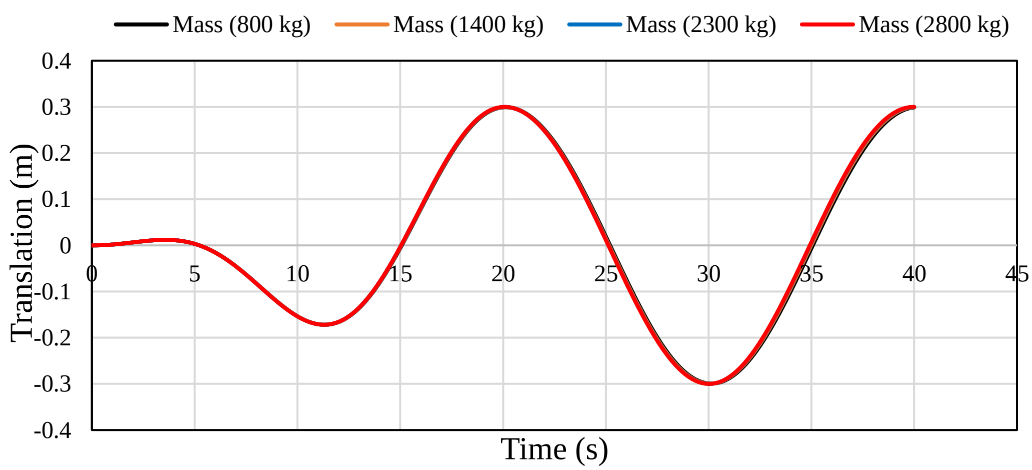

b) At speed of 3.84 m/s

Figure 7.29. Heave in Head Seas

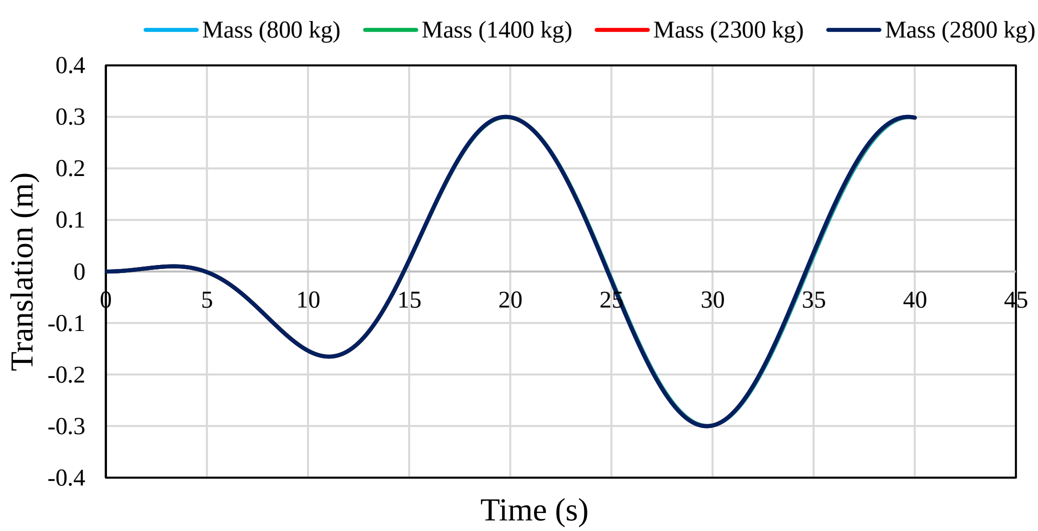

Figure 7.30. Heave in Beam Seas

d) RAO for Sway Motion

Figure 7.31 shows the RAO value for the swaying motion of a boat. The Rao value of the swaying motion at a 90-degree angle is higher than that of other wave angles. The swaying motion of the minimum mass is also large. The RAO value increases, indicating that the swaying and heaving are more significant under the transverse wave state. The movement of the sway has a greater impact on the handling quality of the ship than the stability, but the value of the sway is not great, adding a small keel on the boat reduces sway a little bit.

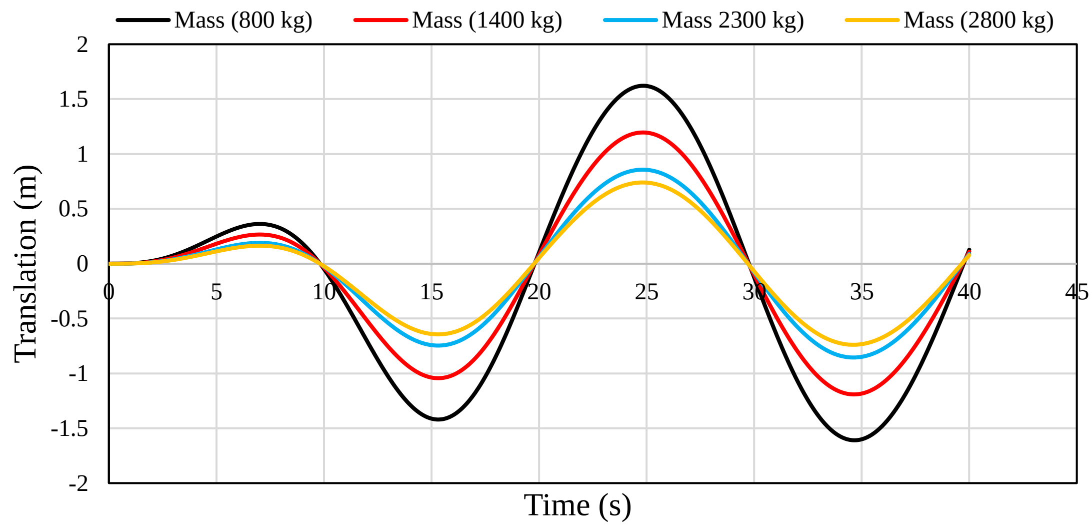

Figure 7.31.Sway in Beam Seas

Figure 7.32 shows the roll graphs for different wave directions for a boat weighing 2800 kg since this option has the worst stability.

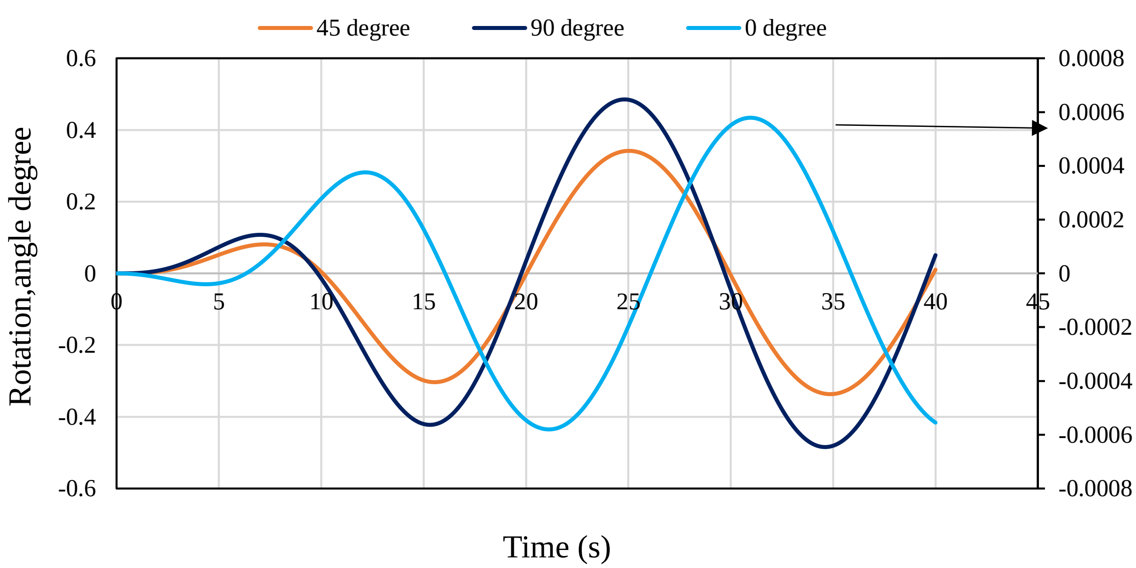

Figure 7.32. Roll in different wave directions for 2800 kg

The value of RAO rolling at a 90-degree angle is much higher than other wave angles. This is because the length of the vessel is relatively large. In the case of a transverse wave, the wave force affects the length of the structure, and the moment of the structure receiving the wave force increases. The value of roll for different wave directions for mass 800kg and 2300 kg is found in Appendix B in Figure B-9 and Figure B-10.

7.8 Verification

CFD validation is intended to test the extent to which the model accurately represents reality, to achieve that there are two alternative methods. The primary one is through comparing the results of the CFD with experimental results and another one through cross-checking with preceding CFD studies which undertake validation from experimental findings.

In this study the boat model taken is the local recreational boat which is manufactured locally, hence it is cumbersome to validate it with previous studies carried out at the international level. In addition to that validation of numerical results is limited to the previous researchers' works because the experimental budget allocated for this study is a barrier against conducting the new experimental setup and study.

As a result that the validation of the CFD model (SST k-ω) is carried through merely referring to the suitability of the aforementioned turbulence model for Boat performance analysis. In numerous boat design analysis or performance study, the SST k-ω model is utilized and have shown a very good correlation with the experimental findings (Frisk, D & Tegehall, 2015) .

(D. Purnamasari et al., 2017). Based on that the finding of this study is well constructed and verified. The propulsion power for the same length of the boat was 5hp this was done by written Java code (Garbe, 2017). The stability analysis of the boat was also verified based on the metacentric height (ITTC1957). According to the towing tank commit agreement, the height of the metacenter for small vessels is more than 0.75 m. This is a decent agreement that the designed boat is 0.93m for a full load on the numerical technique of stability analysis.

7.9 Preparation of model

A small boat was built for demonstration purposes. The scale used in the development of the prototype was 1:12. For the manufacture of the boat, light and inexpensive materials were chosen. Figure 7.33 and Table. 7.6 shows the materials and equipment used in the development of the prototype. For the manufacture of the hull of a small boat, aluminum 0.8 mm thick was used.

Table 7.6. Materials used for the proposed project

No	Components	Value	Unit
1	Solar panel	3.5	W
2	Aluminum sheet	2	m
3	Lead acid Battery	6	V
4	DC-generator	11	V

Figure 7.33. Materials used to develop the prototype

The charging circuit diagram and propulsion system used in the prototype are shown in Figure 7.34.

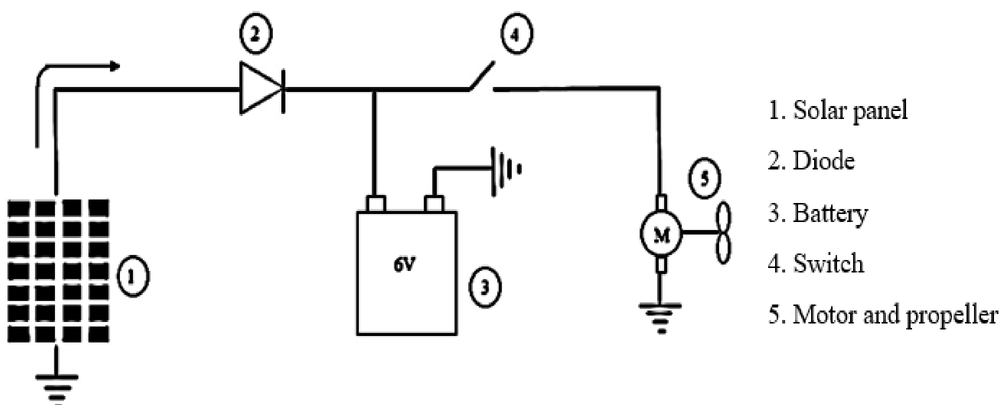

Figure 7.34. Charging circuit diagram and propulsion system

Finally, the model was constructed as shown in Figure 7.35. When testing the boat without the application of keel it tends to swing whereas when the keel is installed it maintain the required stability. The movement of the sway has a greater impact on the handling quality of the boat. Adding a keel on a hull increases the transverse stability, directional stability generally reduces sway thus built model is fully functional.

Figure 7.35. Boat model

7.10 Cost Feasibility Analysis of Solar System

The methods used to study the economic viability of investment projects are life cycle cost (LCC), net present value (NPV), internal rate of return (IRR), and payback period (PP). In this study, a life cycle cost (LCC) was used to evaluate the economic analysis of the proposed solar photovoltaic system and grid.

7.10.1 Cost analysis of solar photovoltaic system

Life cycle costs are tools for estimating the total cost of the project, including start-up costs, fuel costs, operating and maintenance costs, replacement costs. The life cycle cost (LCC) of the photovoltaic solar power system and electric motor can be determined as in the following equation (Muslim et al., 2018).

$$LCC=C_o+ O+ M+R \quad (7.1)$$

Where: C_o = initial capital cost

O = operating cost and M is maintenance cost

R =total replacement cost

- The initial cost is the total cost of each part of the PV system and electric system, i.e. PV array, charge controller, battery, cable, and electric motor. The total initial cost (Co) of the system can be estimated using equation (7.2) (Hossain et al., 2019)

$$C_o=C_{PV}+C_{bat}+C_{ctrl}+C_wC_{E_M} \quad (7.2)$$

Where: C_{PV} =cost of solar panel

C_{bat}= cost of battery

C_{ctrl}=cost of a charge controller

C_w= cost of electric wires and C_{E_M} is the cost of an electric motor

The cost of solar panel can be calculated using equation (7.3) (Kelley et al., 2010):

$$C_{PV} = W_P \times U_{PV} \tag{7.3}$$

Where: W_P = power of each arrangement (W)

U_{PV}= cost of per watt unit

The cost of electric wires is assumed by considering 6% of the PV array price

- ❖ To calculate the operating cost, we need to consider the unit price of electricity in Ethiopia, which is 2.019 ET. Birr / kWh, the total daily energy required to drive a boat is 20 kW. The boat runs for 5 hours and it covers 72km a day for 345 days.20 days for maintenance and rest, so the operating cost of the proposed system will be calculated in 20 years.

The total cost of the utility power from the grid (C_{Grid}) can be calculated using equation (7.4) (Hossain et al., 2019).

$$C_{Grid}=345 \times E_d \times C_{unit} \times L \tag{7.4}$$

Where: C_{Grid} = cost of the utility power from the grid

E_d = daily energy requirement

C_{unit} = the cost of per unit energy and L is the project lifetime

- ❖ To calculate the maintenance cost of the system assume 2% of the initial cost (Co) of the system.
- ❖ To calculate the replacement cost of the system assume that the only replacement component is Battery. The life span of a lithium-ion battery is >10 years.
- ❖ The total initial capital cost is 369,710.45 Birr and the total electricity bill for 20 years is 278622 Birr.
- ❖ The cost analysis of grid-connected and solar connections is performed using an equation. (7.1) to (7.4) and presented in Table 7.7.

Table 7.7. Total cost of each components

Item	Quantity	Unite price (ET. birr)	Total cost (Birr)
Solar panel (1W)	872.64W	35	30,542
Battery 1 (2.4kWh)	12pc	16,000	192,000
Electric motor	1pc	141,806	141,806
Charge controller	1pc	3,862.35	3,862.35
Electric wire	-	1500.10	1500.10
Total initial capital cost			369,710.45
Operating cost	20kW	2.019	278622
Maintenance cost	-	-	7394.20
Replacement cost	12pc	16,000	192,000
Life-cycle cost (LCC)			847726.65

7.10.2 Cost analysis of fuel

- To calculate the operating cost of gasoline, the unit cost of 1 liter of gasoline is 31 birr and can travel 5 kilometers with 1 liter of gasoline. The operating cost of fuel is calculated on a 20-year cycle the calculation of fuel cost is based on equation 7.5 (Setiawan et al., 2015).

$$C_{Fuel} = U_{NPV,fuel} \times N_L \times D \times Y \quad (7.5)$$

Where: U_{NPV} = the price of fuel (Birr)

N = the number of litters of fuel needed in a day (L),

D = the number of days in a year in which diesel operated and Y is years

- To calculate the maintenance Yamaha motor cost of the system assume that 10% of the initial cost (Co) and the replacement cost is considered only the motor cost after 10 years.

Table 7.8. The total cost of each component for gasoline

Item	Quantity	Unite price (ET. birr)	Total cost (Birr)
Yamaha motor	1pc	200,000	200,000
Total initial capital cost			200,000
Operating cost (72 Km)		576	3,080160
Maintenance cost	-	-	20,000
Replacement cost	-	-	200.000
Life-cycle cost (LCC)			3,500160

From the above data, it can be concluded that building a gasoline fuel system is still more expensive than building a photovoltaic system and energy from the electric grid. Energy from PV and electric grid systems has a high initial cost, but very low operating cost, maintenance cost, low fuel costs, and therefore low replacement costs. On the other hand, energy from gasoline is characterized by very high operating costs which are represented by fuel with operation and maintenance costs. Based on these data, Figure. 7.36 shows the compression of both technologies over 20 years of operation.

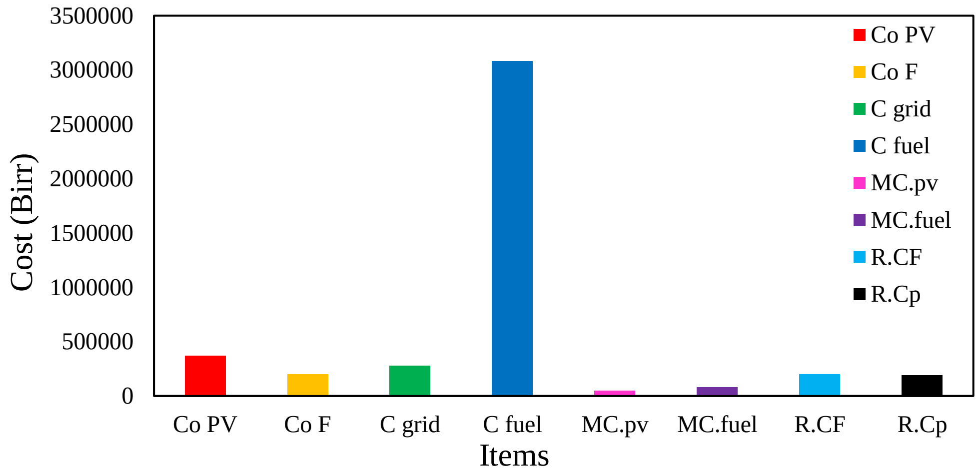

Figure 7.36. The compression cost of both technologies over 20 years of operation

The life cycle cost of the gasoline generator is very high. This is due to the high cost of fuel consumed by gasoline generators, the high cost of maintenance, and the high operating costs. Figure 7.37 shows the life cycle cost of the proposed system and gasoline engine.

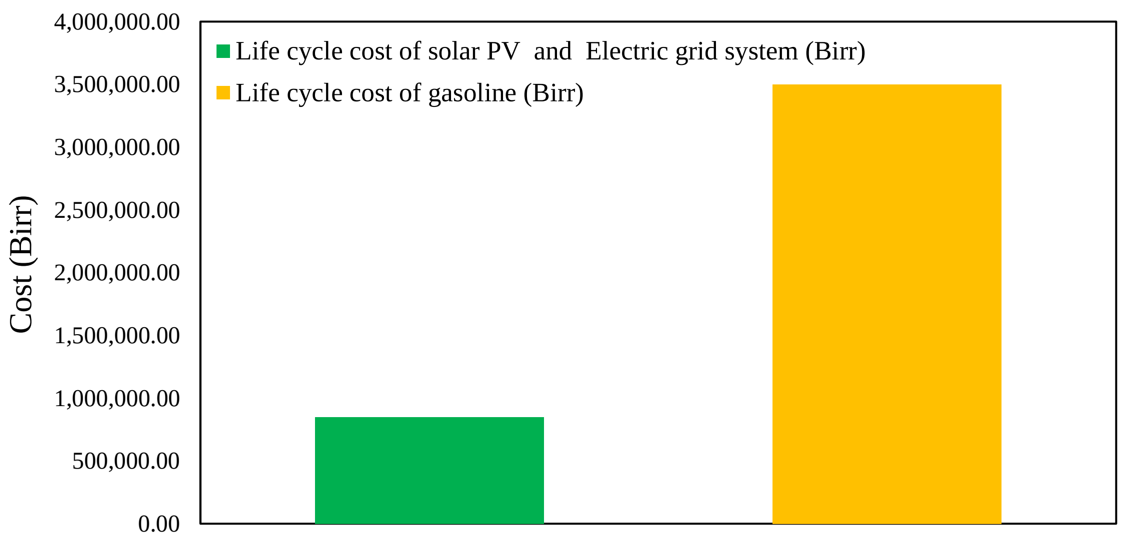

Figure 7.37. The life cycle cost of the proposed system and gasoline engine

CHAPTE R EIGHT

CONCLUSIONS AND RECOMMENDATIONS

8.1 Conclusions

This study aims to investigate the possible use of renewable energy; solar and wind as a power source for a recreational boat. In addition, this study clearly illustrates the problems of our country's existing gasoline engines boats and designs alternative power sources to address them. As a solution, the integration of solar and wind energy as a power unit was first attempted to drive the boat, and later another solution was adopted after studying the feasibility of the integration. Finally, it is concluded to propel the boat by integrating solar energy with a grid system by using energy stored in batteries. Modeling, stability analysis, propulsion power, and cost estimates of the boat model are presented. As a result, the modified boat reduces costs and environmental pollution. From cost analysis, it concludes that a gasoline fuel system is even more expensive than a PV system and energy from the power grid. Energy from PV and grid systems has high initial costs, but very low operating, maintenance, and fuel costs, and therefore low replacement costs. The main findings are summarized as follows:

- ✓ The drag coefficient is obtained from the CFD program and used to determine the viscous resistance coefficients.
- ✓ The propulsion power to propel the boat is 3823.4 W
- ✓ The maximum mean daily power produced by solar panels is 1080.32W in the winter season and minimum power generation 631W in the summer season.
- ✓ The maximum power generated by solar panels is 1746.7 Watts in February and the minimum is 1111.51 Watts in August month.
- ✓ The wind turbine begins to move at a minimum speed of 2.7 m/s speed.
- ✓ The maximum mean daily power produced by a wind turbine is 18.005 Watts in the spring season, and the minimum power generation is 13.31 Watts in the autumn (fall) season.
- ✓ The maximum power is generated by the wind turbine in May with 22.69 W and the minimum power generated is 11.7 W in December.
- ✓ The maximum energy harvested by solar panels is 1478 Wh, and 168 Wh from the wind turbines.

- ✓ The average energy produced from solar is 6.66 kWh and from wind 1.3 kWh.
- ✓ The daily electric energy requirement to propel the boat is 20 kWh for 5 hours. The battery system consists of 3 (parallel) batteries and 4 battery packs connected in series.
- ✓ The stability analysis of the boat is determined based on the metacentric height. From the simulated results of boat design of hydrostatic stability testing, the height of the metacentre is more than the recommended 0.75m.
- ✓ A small boat is built for demonstration purposes. 1:12 ratio scale is used in the development of the model which is constructed by light and inexpensive 0.8 mm thick aluminum materials. When testing the boat without the application of keel it tends to swing whereas when the keel is installed it maintained the required stability.
- ✓ The life cycle cost of the proposed PV solar system and electric grid system is 847,726.65 birr which is low compared to gasoline, which its life cycle cost is 3,500,160 birr.

8.2 Recommendations

- ✓ The designed boat has the capacity of carrying up to four people and it can be used in natural lakes as well as man-made lakes which are planned to be constructed in near future in the country. The newly designed boat is powered by energy processed from solar is minimizes environmental pollution and fuel cost. From the results of the cost analysis of the proposed system, it is recommended to use the PV solar system and electric utility for generating electricity instead of gasoline or diesel to propelled boats.

8.3 Recommendations for Future Work

- ✓ The recommended system is more beneficial as it is fully automated with a visual display system. For improved performance, it is recommended to substitute the charge controller with Arduino.
- ✓ In this study the wind load of the coefficient is calculated using a mathematical method, however, using CFD in the future to find this value can bring a better result.
- ✓ The total weight of the modified model is 2800 kg, this can be further reduced to a minimum as more weight consumes more power.
- ✓ The cost of fuel is analyzed based on the current market price, but it is more accurate to estimate the cost using data from previous years and also further study needs on the salvage cost and payback period.

Research Fund Acknowledgment

I would like to sincerely thank ASTU for the opportunity it has given me to complete my masters study. This research project is funded by Adama Science and Technology University under the grant Number ASTU/SM-R/322/21, Adama, Ethiopia.

REFERENCES

Adejumobi, I. A., Oyagbinrin, S. G., Akinboro, F. G., & Olajide, M. B. (2011). Hybrid solar and wind power: an essential for information communication technology infrastructure and people in rural communities. IJRRAS, 9(1), 130-138.

Adissu Bekele, Demiss Alemu and Manish Mishra (2013), Large Scale Solar Water Heating Systems Analysis in Ethiopia: A Case Study, International Journal of Sustainable Energy, 32 (4), 207-228.

Ahlstrand, F., & Lindbergh, E. (2020). Methods to Predict Hull Resistance in the Process of Designing Electric Boats.

Ali, M. H. (2013). Experimental comparison study for Savonius wind turbine of two & three blades at low wind speed. International Journal of Modern Engineering Research (IJMER), 3(5), 2978-2986Aymane,

Al-Kayiem, H. H., Bhayo, B. A., & Assadi, M. (2016). Comparative critique on the design parameters and their effect on the performance of S-rotors. Renewable Energy, 99, 1306-1317. https://doi.org/10.1016/j.renene.2016.07.015

A. Khaware, K. Gupta, H. Punekar and P. Sharkey (2019), "Numerical Simulation of Ship Motion and Life Boat Launch using Overset Mesh", International Workshop on Ship and Marine Hydrodynamics

Andersson, J., & Englund, M. (2018). Study of a Body Subjected to a Vertical Drop into Water–Experiment and Simulations

Asadi, F. (2018). Comparison of Different DC Motor Modeling Techniques. Journal of Electronic Research and Application, 2(2).

Aqwa Theory Manual, Ansys Inc., November, (2013).

Barrass, B., & Derrett, C. D. (2011). Ship stability for masters and mates. Elsevier.

Banjarnahor, D. A., Hanifan, M., & Budi, E. M. (2017, July). Design of hybrid solar and wind energy harvester for fishing boat. In IOP Conference Series: Earth and Environmental Science (Vol. 75, p. 012007).

Bañuelos-Ruedas, F., Camacho, C. Á. & Rios-Marcuello, S. (2011). Methodologies used in the extrapolation of wind speed data at different heights and its impact in the wind energy resource assessment in a region. Wind farm-technical regulations, potential estimation and siting assessment, 97-114.

Barelli, L., Bidini, G., Gallorini, F., Iantorno, F., Pane, N., Ottaviano, P. A., & Trombetti, L. (2018). Dynamic Modeling of a Hybrid Propulsion System for Tourist Boat. Energies, 11(10), 2592.

Bhatt, P., Mehar, H., & Sahajwani, M. (2019). Electrical Motors for Electric Vehicle A Comparative Study. Proceedings of Recent Advances in Interdisciplinary Trends in Engineering & Applications (RAITEA).

Bin Shamsuddin, M. Z., & Ragnarsson, E. (2003). A conceptual design of a fiber-reinforced plastic fishing boat for traditional fisheries in Malaysia. Development Division Fisheries, Malaysia.

Bow, M. A. T. Y. (2021). Monitoring Depth of Discharge of a Valve Regulated Lead Acid Battery in a Standalone PV System

Brusca, S., Lanzafame, R., & Messina, M. (2014). Design of a vertical-axis wind turbine: how the aspect ratio affects the turbine's performance. International Journal of Energy and Environmental Engineering, 5(4), 333-340.

Cancela, A, Lastra, R., Suárez, V., & Sánchez, Á. (2016). Design and Simulation of a Sustainable Photovoltaic Electric Plug-In Boat. European Journal of Sustainable Development, 5(3), 325-325

Çakıcı, F., Sukas, Ö. F., Usta, O., & Alkan, A. D. (2015). A computational investigation of a planning hull in calm water by u-ranse approach. In International conference on advances in applied and computational mechanics, Izmir, Turkey.

Chiroșcă, A. M., & Rusu, L. (2021). Comparison between Model Test and Three CFD Studies for a Benchmark Container Ship. Journal of Marine Science and Engineering, 9(1), 62

Chun, S. C. (2015). Development of a hybrid solar-wind turbine for sustainable energy storage. Kuala Lumpur.14.

D. Aldas, J. Constante, M, Gomez and G. Tapia (2019), "Monohull ship hydrodynamic simulation using CFD", International Journal of Mathematics in Operational Research, Vol: 15, No: 4.

Duffie, J. A., Beckman, W. A., & Blair, N. (2020). Solar engineering of thermal processes, photovoltaics, and wind. John Wiley & Sons.

Dunn, B., Kamath, H., & Tarascon, J. M. (2011). Electrical energy storage for the grid: a battery of choices. Science, 334(6058), 928-935.

D. Purnamasari, P. Utama and K. Suastika (2017), “CFD Simulations to Calculate the Resistance of A 17.500-DWT Tanker”, The 3rd International Seminar on Science and Technology.

E., Darhmaoui, H., & Sheikh, N. (2017). Savonius Vertical Wind Turbine: Design, Simulation, and Physical Testing. School of Sci. & Eng. Univ. Program.

Faber, J., Hanayama, S., Zhang, S., Pereda, P., Comer, B., Hauerhof, E., & Kosaka, H. (2020). Reduction of GHG Emissions from Ships—Fourth IMO GHG Study 2020, Final Report. IMO MEPC, 75(7), 15.

Franklin, E. (2017). Types of Solar Photovoltaic Systems.

Freire, S., & Pruna, M. R. (2009). Designing and Building a Solar Powered Model Boat. International Baccalaureate Organization, Geneva.

Frisk, D., & Tegehall, L. (2015). Prediction of high-speed planning hull resistance and running attitude. A numerical study using computational fluid dynamics.

Garbe, C. (2017). Design and Analysis of Wind Turbine Integrated Propelled Boat. (MSVED, ASTU).

Gale, P. A. (2003). The ship design process. Chapter, 5, 5-1.

G. Elkafas, M. Elgohary and E. Zeid (2019), “Numerical study on the hydrodynamic drag force of a container ship model”, Alexandria Engineering Journal, doi.org/10.1016.

Grm, A. (2017). Mathematical Model for Riverboat Dynamics. Brodogradnja: Teorija i praksa brodogradnje i pomorske tehnike, 68(3), 25-35.

Gürsu, H. (2014). Solar and wind-powered concept boats: The example of Volitant.

Hemez, C., Chiu, J., Ryan, E. C., Sun, J., Dubrow, R., & Pascucilla, M. (2020). Environmental and health impacts of electric service vessels in the recreational boating industry. Water Practice and Technology, 15(3), 781-796.

Hossain, C. A., Chowdhury, N., Longo, M., & Yaïci, W. (2019). System and cost analysis of stand-alone solar home system applied to a developing country. Sustainability, 11(5), 1403.

Keawsang K., Ratjiranukool, S., & Ratjiranukool, P. (2018, December). Estimation of solar radiation using Angstrom-Prescott model and interpolation of empirical coefficients in Thailand. In Journal of Physics: Conference Series (Vol. 1144, No. 1, p. 012049). IOP Publishing.

Kelley, L. C., Gilbertson, E., Sheikh, A., Eppinger, S. D., & Dubowsky, S. (2010). On the feasibility of solar-powered irrigation. Renewable and Sustainable Energy Reviews, 14(9), 2669-2682.

Krieger, E. M., Cannarella, J., & Arnold, C. B. (2013). A comparison of lead-acid and lithium-based battery behavior and capacity fade in off-grid renewable charging applications. Energy, 60, 492-500.

Lee, D. K., Jeong, Y. K., Shin, J. G., & Oh, D. K. (2014). Optimized design of electric propulsion system for small crafts using the differential evolution algorithm. International Journal of Precision Engineering and Manufacturing-Green Technology, 1(3), 229-240.

Maisuria, M. S., Patel, D. R., Parmar, K. P., & Patel, U. R. (2016, April). Experimental analysis of combined darrieus and savonius wind turbine.

Martí Bigorra, E. (2018). Design of a boat electric propulsion system based on solar energy (Bachelor's thesis, Universitat Politècnica de Catalunya).

Mengi, O. O., & Altas, I. H. (2015). A new energy management technique for PV/wind/grid renewable energy system. International Journal of Photo energy, 2015.

Meshesha, D. T., Tsunekawa, A., & Haregeweyn, N. (2019). Influence of raindrop size on rainfall intensity, kinetic energy, and erosivity in a sub-humid tropical area: a case study in the northern highlands of Ethiopia. Theoretical and Applied Climatology, 136(3), 1221-1231.

Muslim, H. N., Alkhazraji, A., & Salih, M. A. (2018). Feasibility study of using 2kWp residential PV system comparing with 2.5 kVA gasoline generator (Case study: Baghdad city). International Journal of Energy and Environment, 9(1), 57-62.

Nasirudin, A., Chao, R. M., & Utama, I. K. A. P. (2017). Solar-powered boat design optimization. Procedia Engineering, 194, 260-267.

Nema, P., Nema, R. K., & Rangnekar, S. (2009). A current and future state of art development of hybrid energy system using wind and PV-solar: A review. Renewable and Sustainable Energy Reviews, 13(8), 2096-2103.

Niu, H. C., Zhao, M. L., & Qin, F. Z. (2017, May). Study on the Ship Electric Propulsion System and Its Development. In 2017 7th International Conference on Applied Science, Engineering and Technology (ICASET 2017) (pp. 212-216). Atlantis Press.

Nurachman, D. (2018). Propulsion System Analysis for Solar-Powered Electric Water Recreational. In E3S Web of Conferences (Vol. 67, p. 04010). EDP Sciences.

Nyanya, M. N., & Vu, H. B. (2019). Wind propulsion optimization and its integration with solar power.

Oğuz, Y., & Özsoy, M. F. (2015). Sizing, design, and installation of an isolated wind-photovoltaic hybrid power system with battery storage for laboratory general illumination in Afyonkarahisar, Turkey. Journal of Energy in Southern Africa, 26(4), 70-80.

Osaretin, C. A., & Edeko, F. O. (2015). Design and implementation of a solar charge controller with variable output. Electrical and electronic engineering, 12(2), 40-50.

Pandey, C. K., & Katiyar, A. K. (2013). Solar radiation: Models and measurement techniques. Journal of Energy, 2013.

Postiglione, C. S., Collier, D. A., Dupczak, B. S., Heldwein, M. L., & Perin, A. J. (2012, October). The propulsion system for an all-electric passenger boat employing permanent magnet synchronous motors and modern power electronics. In 2012 Electrical Systems for Aircraft, Railway and Ship Propulsion (pp. 1-6). IEEE.

Reabroy, R., Tiaple, Y., Pongduang, S., Nantawong, T., & Iamraksa, P. (2015). The Possibility of using Electrical Motor for Boat Propulsion System. Energy Procedia, 79, 1008-1014.

Samaei, S. R., Azarsina, F., & Ghahferokhi, M. A. (2016). Numerical simulation of floating pontoon breakwater with ANSYS AQWA software and validation of the results with laboratory data. Bulletin de la Société Royale des Sciences de Liège, 85, 1487-1499.

Schultz, J. W., & Huard, S. (2013). Comparing AC Induction with Permanent Magnet motors in hybrid vehicles and the impact on the value proposition. Parker Hannifin Corporation.

Scurtu, I. C., Poenaru, V., & Tsarev, R. (2020, September). Analysis of stability characteristics for modern passenger multirole boat. In IOP Conference Series: Materials Science and Engineering (Vol. 916, No. 1, p. 012103). IOP Publishing.

Setiawan, A. A., Ramadhan, S. A., Wahyuni, N. S., Hidayah, A. N., Arifin, M. L. N. R., & Suyatna, H. (2015). Economic analysis comparison between solar photovoltaic and diesel generator for water pumping system in an Indonesia rural Karsts Area. KnE Energy, 8-15.

Shah, M. H., & Alsibiani, S. A. (2020). Design and construction of Savonius rotor.

Shirsath, P. P., Pise, A., & Shinde, A. (2016). Solar-wind hybrid energy generation system. International Journal of Engineering Research and General Science, 4(2), 546-550.

Skupień, E., & Prokopowicz, J. (2014). Methods of calculating ship resistance on limited waterways. Polish Maritime Research, (4), 12-17.

Ssenyimba, S., Kiggundu, N., & Banadda, N. (2020). Designing a solar and wind hybrid system for small-scale irrigation: a case study for Kalangala district in Uganda. Energy, Sustainability and Society, 10(1), 1-18.

Sui, C., de Vos, P., Stapersma, D., Visser, K., & Ding, Y. (2020). Fuel consumption and emissions of an ocean-going cargo ships with hybrid propulsion and different fuels over the voyage. Journal of Marine Science and Engineering, 8(8), 588.

Sunaryo, S., & Ramadhani, A. W. (2018). Electrical system design of solar-powered electrical recreational boat for Indonesian waters. In E3S Web of Conferences (Vol. 67, p. 04011). EDP Sciences.

Tamunodukobipi, D., Samson, N., & Sidum, A. (2018). Design Analysis of a Lightweight Solar Powered System for Recreational Marine Craft. World Journal of Engineering and Technology, 6(02), 441.

Tong, W. (2010). Fundamentals of wind energy. In Wind power generation and wind turbine design (p. 23). Southampton, UK: WIT Press.

Toptas, E., Bayrak, M. A., & Boz, T. (2020). Vertical axis hybrid wind turbine design. Journal of Mechatronics and Artificial Intelligence in Engineering, 1(1), 33-40.

Utama, I. K. A. P., Santosa, P. I., Chao, R. M., & Nasiruddin, A. (2013, September). New concept of solar-powered catamaran fishing vessel. In Proceeding of the 7th International Conference on Asian and Pasific Coasts (pp. 903-909).

Versteeg, H. K., & Malalasekera, W. (2007). An introduction to computational fluid dynamics: the finite volume method. Pearson education.

Vidal, J., (2007) CO2 Output from Shipping Twice As Much As Airlines, retrieved fromhttp://www.theguardian.com/environment/2007/mar/03/travelsenvironmentalimpact.transportintheuk

Vijverberg, J., Sibbing, F. A., & Dejen, E. (2009). Lake Tana: Source of the Blue Nile. In The Nile (pp. 163-192). Springer, Dordrecht.

Voxakis, P. (2012). Ship hull resistance calculations using CFD methods (Doctoral dissertation, Massachusetts Institute of Technology.

Walker, T. R., Adebambo, O., Feijoo, M. C. D. A., Elhaimer, E., Hossain, T., Edwards, S. J., & Zomorodi, S. (2019). Environmental effects of marine transportation. In World Seas: an environmental evaluation (pp. 505-530). Academic Press.

Winslow, A. R. (2017). Urban Wind Generation: Comparing Horizontal and Vertical Axis Wind Turbines at Clark University in Worcester, Massachusetts

W. Obaid, A. Hamid and C. Ghenai, "Wind-Fuel-Cell-Solar Hybrid Electric Boat Power Design with MPPT System," 2019 8th International Conference on Modeling Simulation and Applied Optimization (ICMSAO), Manama, Bahrain, 2019, pp. 1-5, doi: 10.1109/ICMSAO.2019.8880330

Woldegiyorgis, T. A. (2019). Estimation of Global Solar Radiation on Horizontal Surface from Sun Shine Hours and Temperature at Kombolcha, Amhara Region, Ethiopia. Journal of Energy, Environmental & Chemical Engineering, 4(3), 39.

Zefreh, M. A. (2016). Design and CFD Analysis of Airborne Wind Turbine for Boats and Ships. Int. J. Aerosp. Sci, 4(1), 14-24.

Zhang, H., & Xu, X. (2020). Research and Design of Wind and Solar Complementary Electric Sightseeing Boat. In E3S Web of Conferences (Vol. 145, p. 02056). EDP Sciences.

Zhang, Z. R., Hui, L., Zhu, S. P., & Feng, Z. H. A. O. (2006). Application of CFD in ship engineering design practice and ship hydrodynamics. Journal of Hydrodynamics, Ser. B, 18(3), 315-322.

Zhao, F., Yang, W., Tan, W. W., Chou, S. K., & Yu, W. (2015). An overall ship propulsion model for fuel efficiency study. Energy Procedia, 75, 813-818.

Zur Heide, F. (2012). Feasibility study for a potential biosphere reserve Lake Tana. Michael Succow Foundation.

https://www.usna.edu/NAOE/_files/documents/Courses/EN400/02.07%20Chapter%207.pdf

https://batteryuniversity.com

APPENDICES

Appendix A: Sunshine hour result

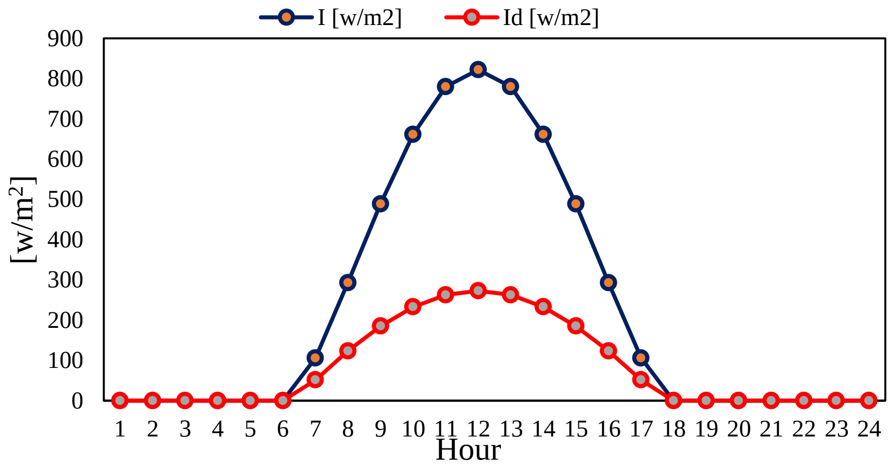

Figure A-1. Mean monthly global hourly and diffuse radiation for winter season [Dec - Feb]

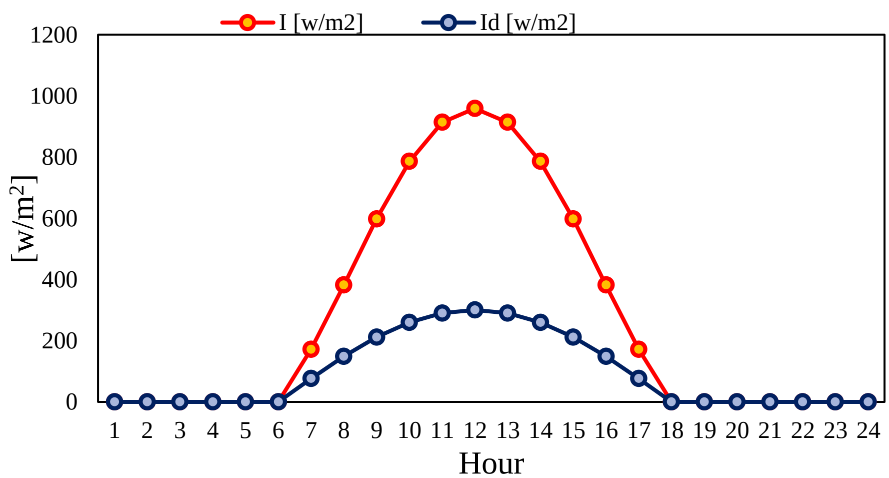

Figure A-2. Mean monthly global hourly and diffuse radiation for the spring season [Mar - May]

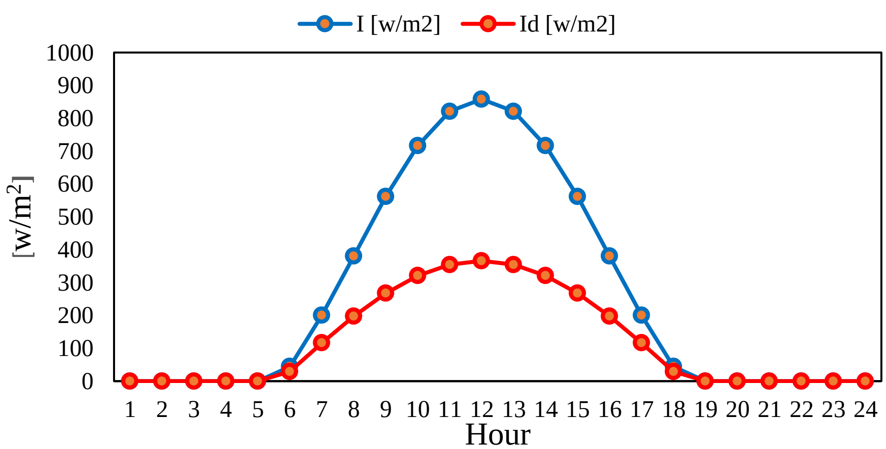

Figure A-3. Mean monthly global hourly and diffuse radiation for the summer season [Jun - Aug]

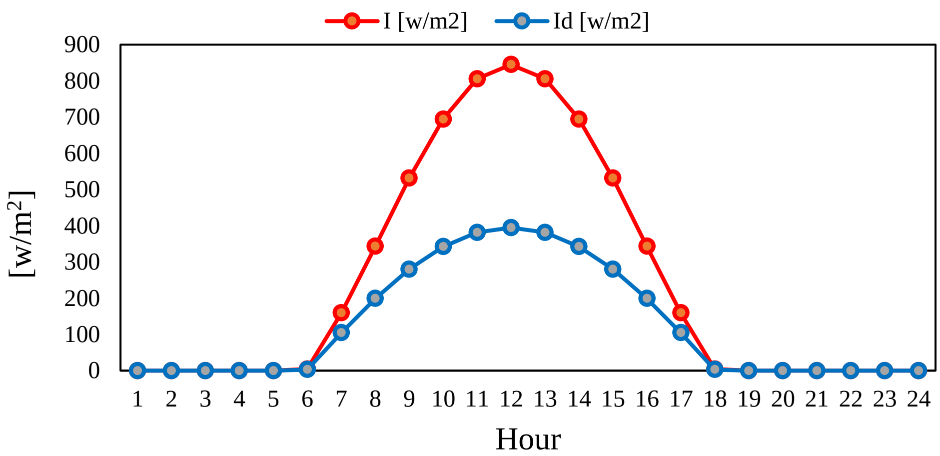

Figure A-4. Mean monthly global hourly and diffuse radiation for the autumn season [Sep - Nov]

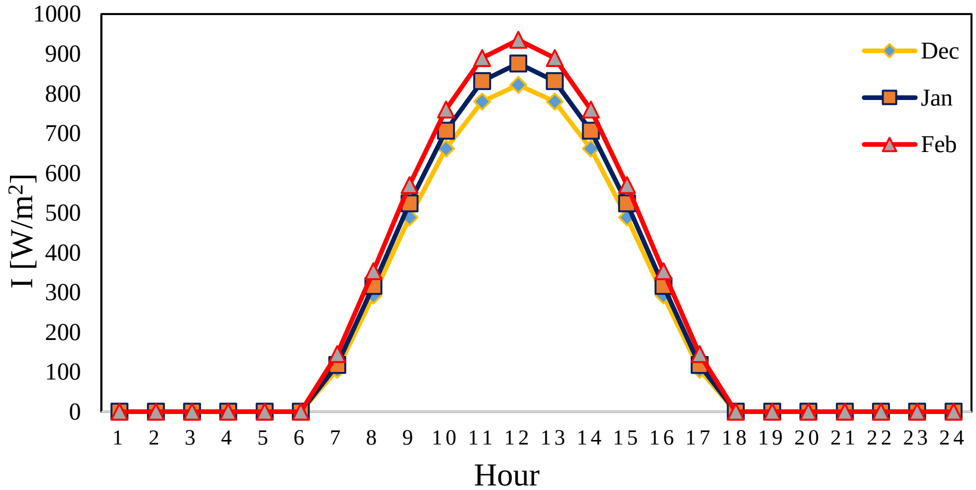

Figure A-5. Monthly average global hourly radiation for the winter season

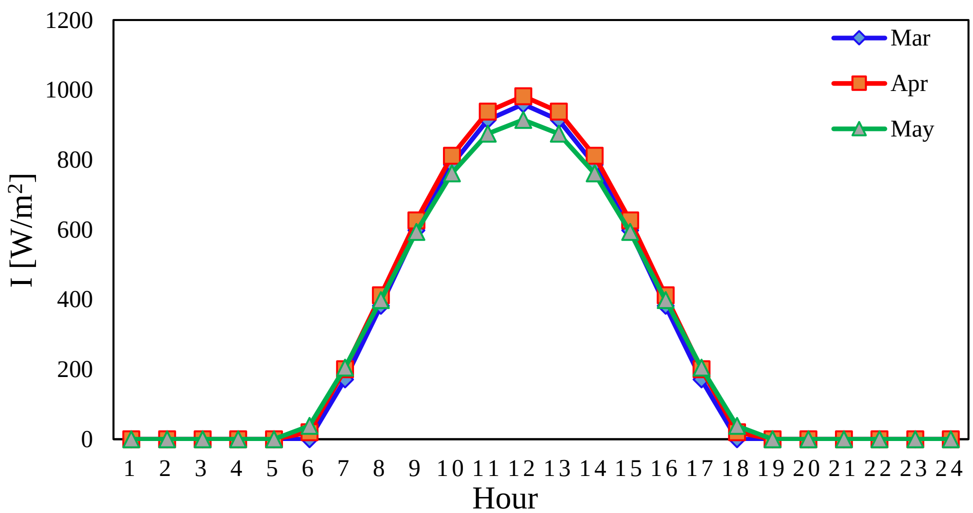

Figure A-6. Monthly average global hourly radiation for spring season

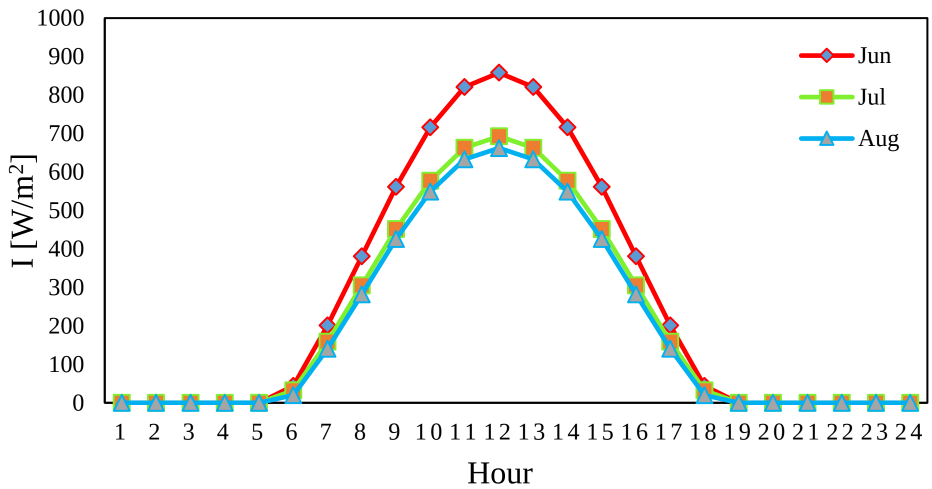

Figure A-7. Monthly average global hourly radiation for the summer season

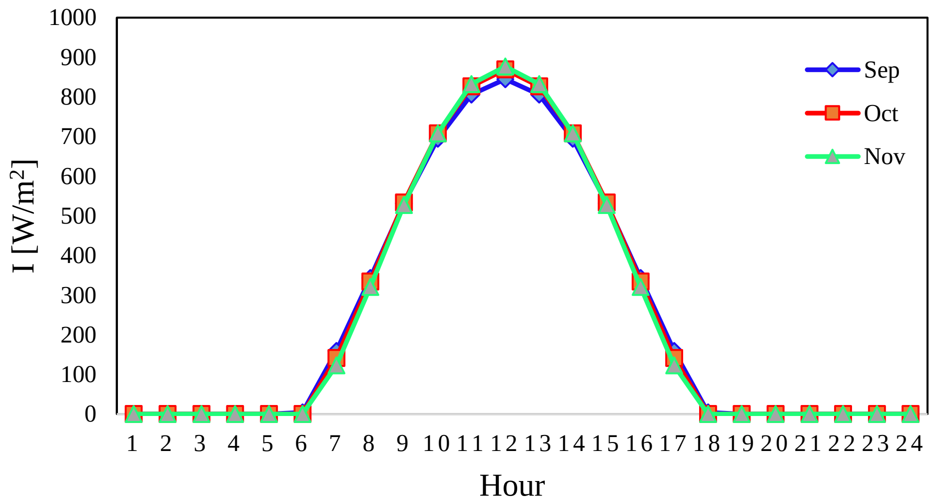

Figure A-8. Monthly average global hourly radiation for the autumn (fall) season

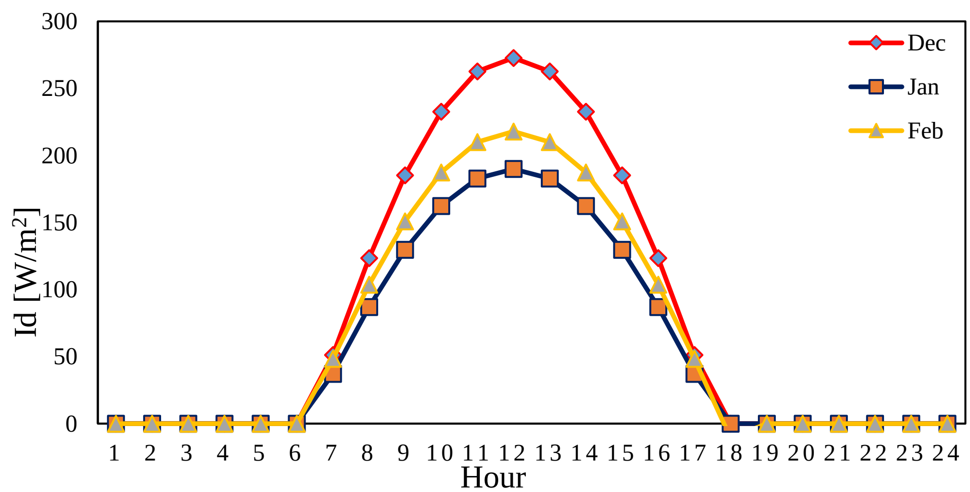

Figure A-9. Monthly average hourly diffuse radiation for the winter season

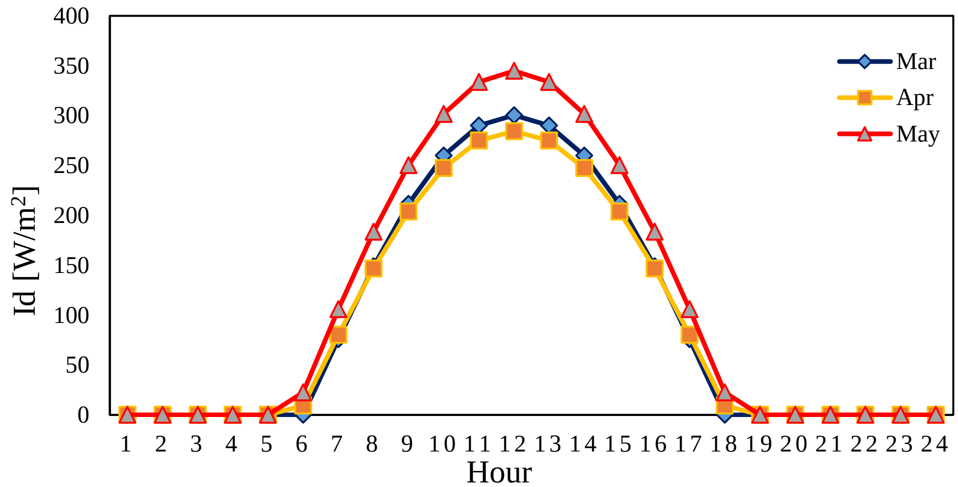

Figure A-10. Monthly average hourly diffuse radiation for spring season

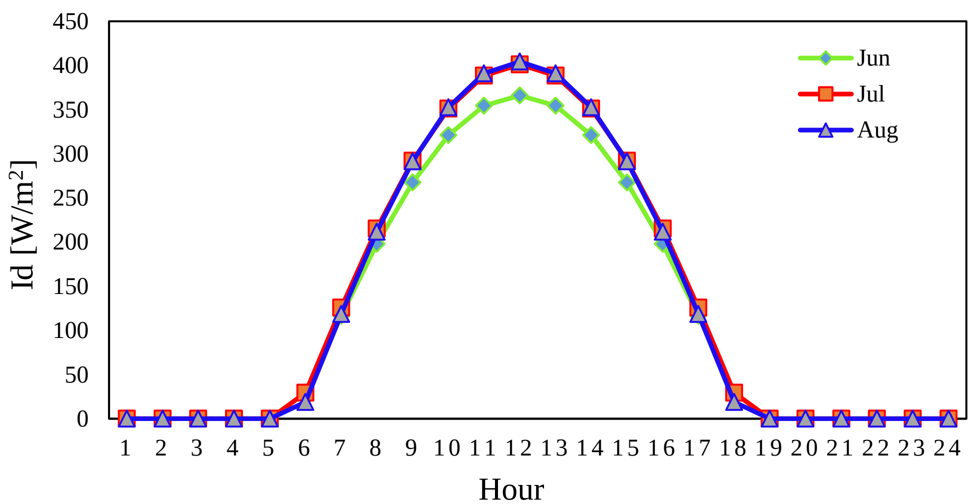

Figure A-11. Monthly average hourly diffuse radiation for the summer season

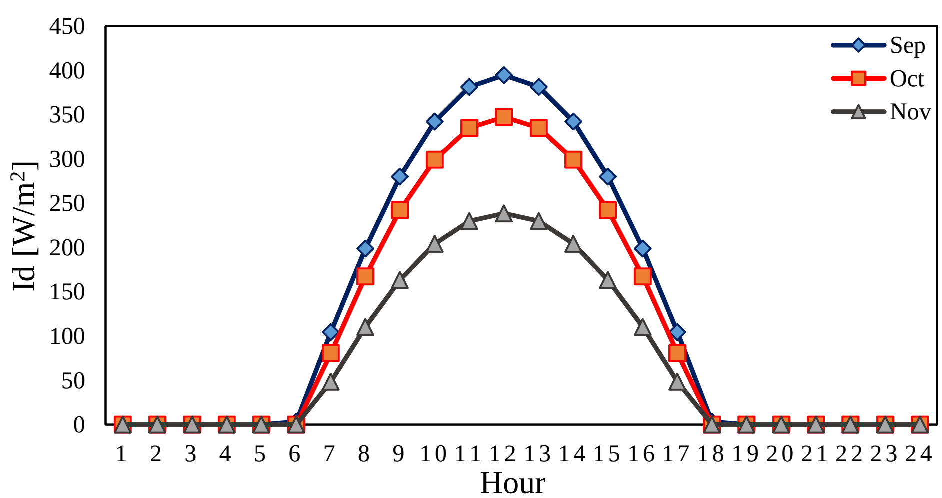

Figure A-12. Monthly average hourly diffuse radiation for the autumn (fall) season

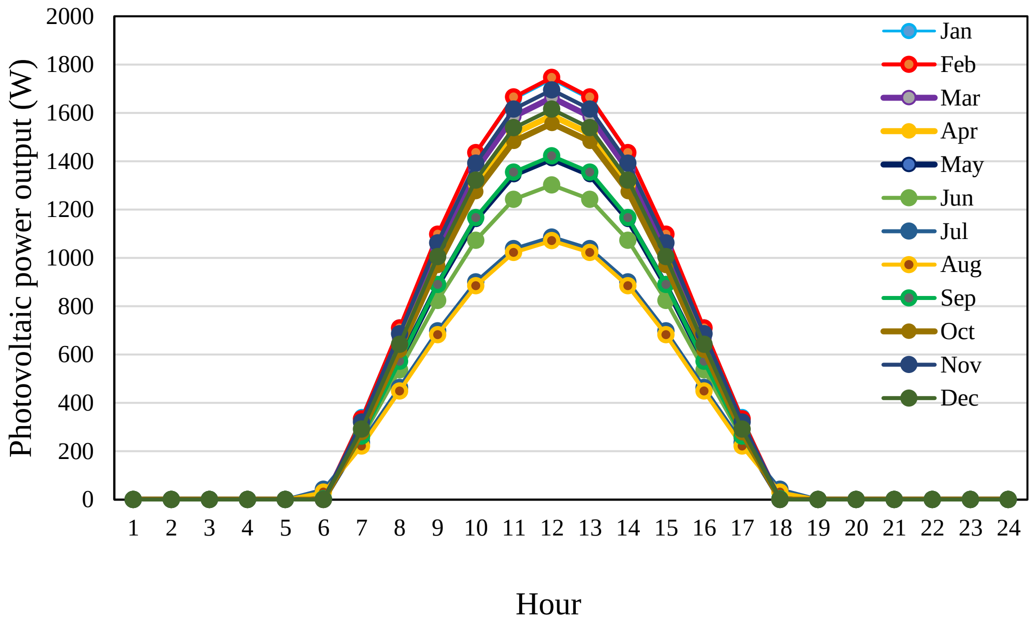

Figure A-13. Monthly Power output from solar panel

Table A-1.Total hourly energy generation from solar energy for February 16

Hour	Pv power (W)	Stord energy (Wh)	Hourly energy (Wh)
7	333.58	282.4	1976.523587
8	709.62	600	4204.624569
9	1097.04	928.6	6500.148927
10	1434.73	1214.4	8501.029295
11	1664.98	1409.32	9865.277806
12	1746.68	1478.48	10349.39071
13	1664.98	1409.32	9865.277806
14	1434.74	1214.4	8501.029295
15	1097.04	1214.4	6500.148927
16	709.62	600	4204.624569
17	333.58	282.4	1976.523587

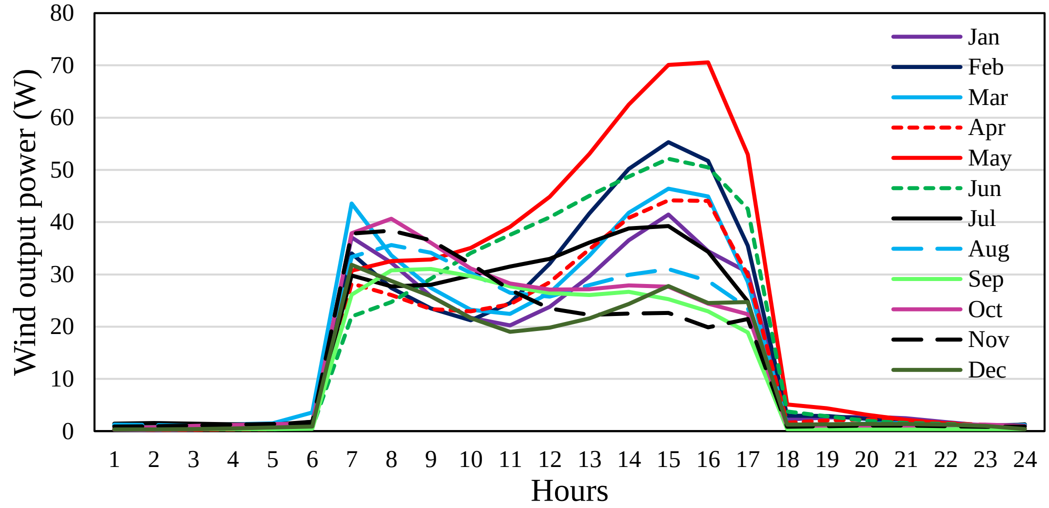

Figure A-14. Monthly Power output from wind turbine

Table A-2.Total hourly energy generation from wind energy for May 15

Time	Wind speed (m/s)	Stored power from wind (Wh)	Hourly energy (Wh)
1	1.41	0.800350335	19.20840803
2	1.4	0.695973352	16.70336044
3	1.4	0.727813459	17.46752301
4	1.45	0.861732512	20.68158029
5	1.45	0.917950214	22.03080513
6	1.55	2.289581624	54.94995898
7	2.1	73.25335138	1758.080433
8	2.42	77.65572664	1863.737439
9	2.42	78.4804286	1883.530286
10	2.34	83.617934	2006.830416
11	2.21	93.37150702	2240.916168
12	2.11	107.0726619	2569.743886
13	2.08	126.5941525	3038.25966
14	2.13	149.18376	3580.410239
15	2.03	167.2571373	4014.171294
16	1.84	168.4725119	4043.340286
17	1.5	126.4191091	3034.058618
18	1.4	12.23611561	293.6667747
19	1.425	10.40007895	249.6018948
20	1.452	7.575627605	181.8150625
21	1.43	5.127179813	123.0523155
22	1.46	3.544168415	85.06004195
23	1.41	2.359666066	56.63198558
24	1.41	1.071800169	25.72320405

Appendix B: ANSYS Hydrodynamic Results

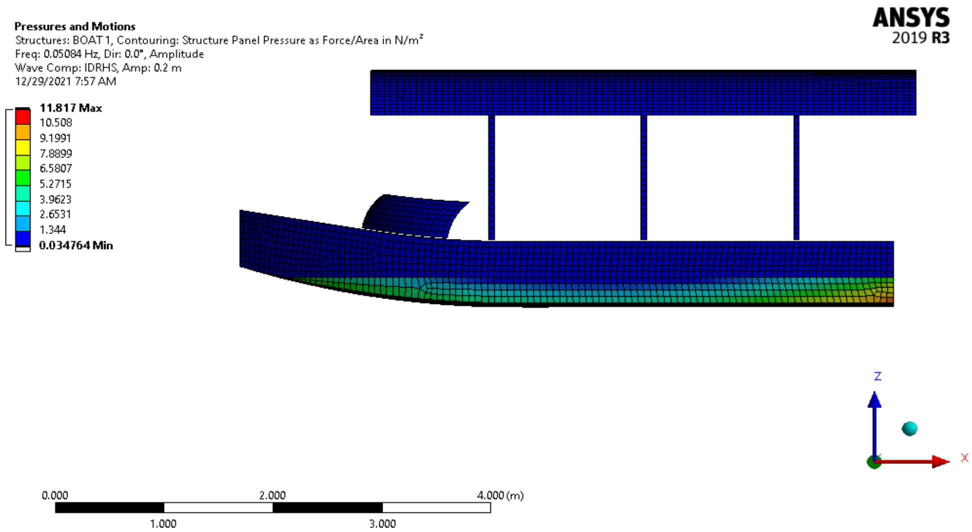

Figure B- 1. Hydrodynamic Pressures and Motions 0 degree

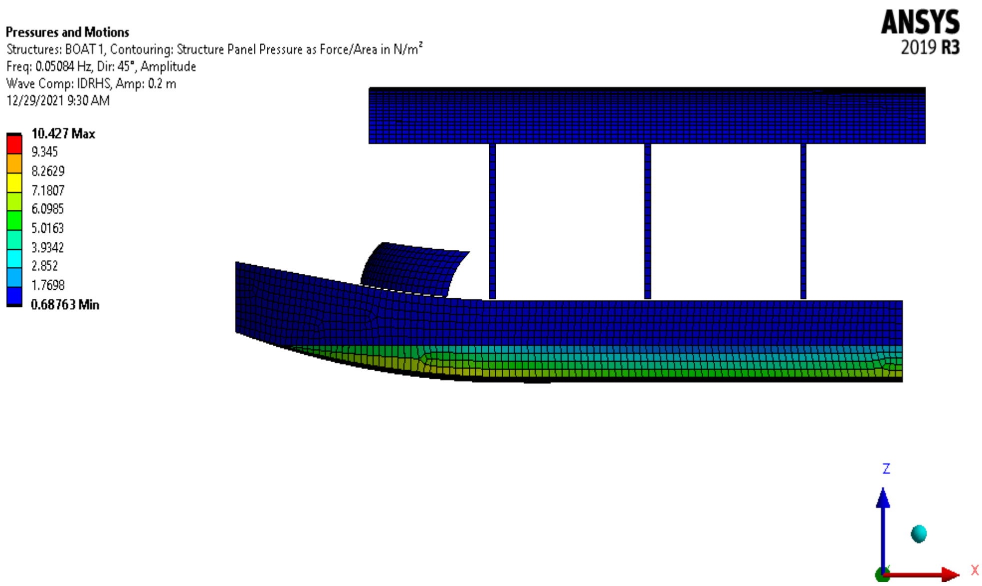

Figure B- 2. Hydrodynamic Pressures and Motions 45 degree

Table B-1. Wight of components

No	Components	Mass (kg)
1	Battery	324
2	Solar panel	150
3	Motor	29.5
4	Keel	200

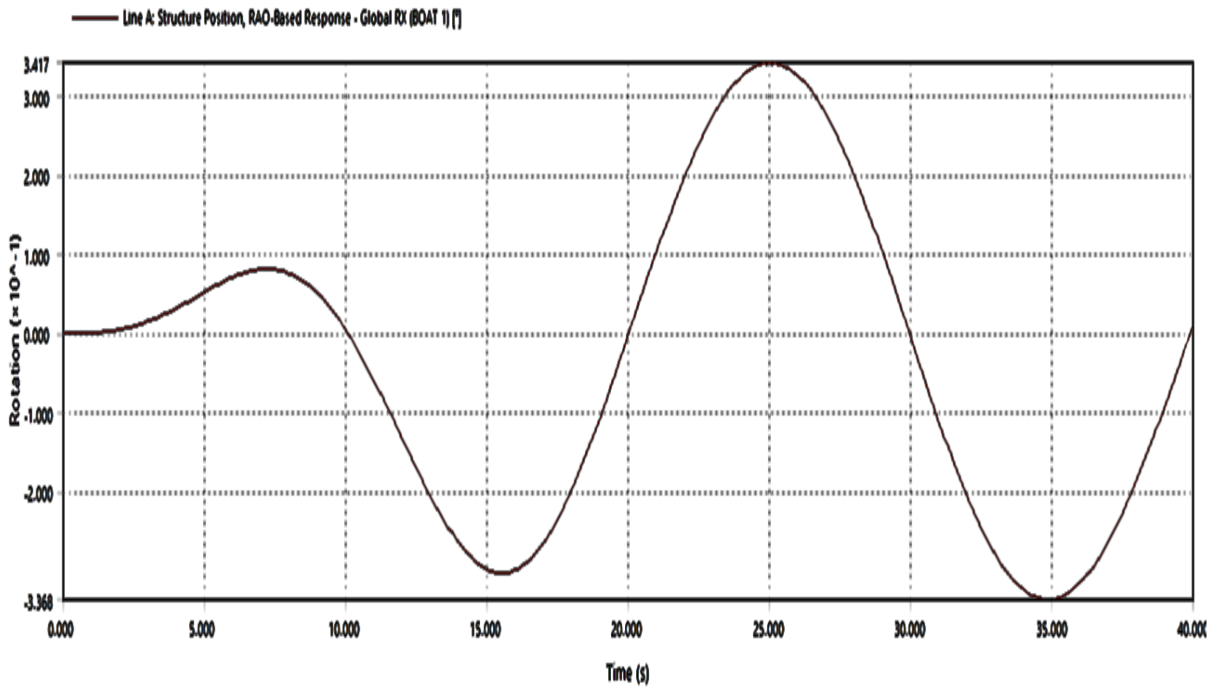

Figure B- 3. Roll in quartering Seas for the mass of 2800kg

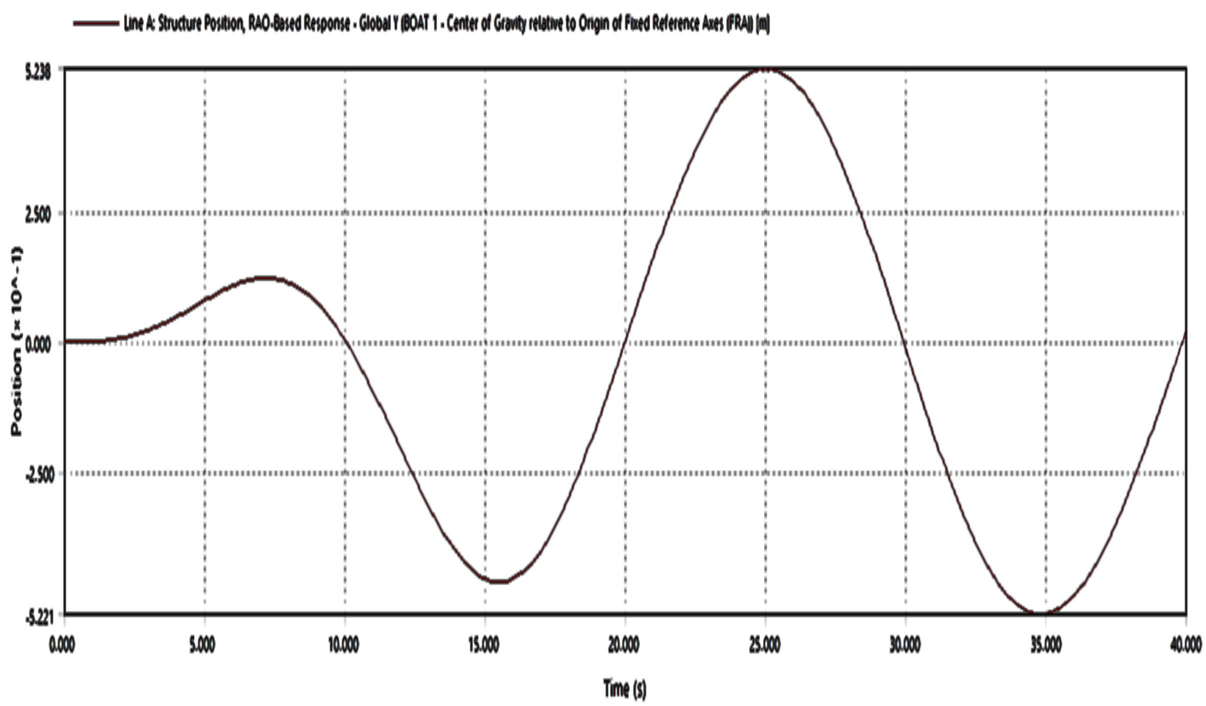

Figure B- 4. Sway in quartering Seas for the mass of 2800kg

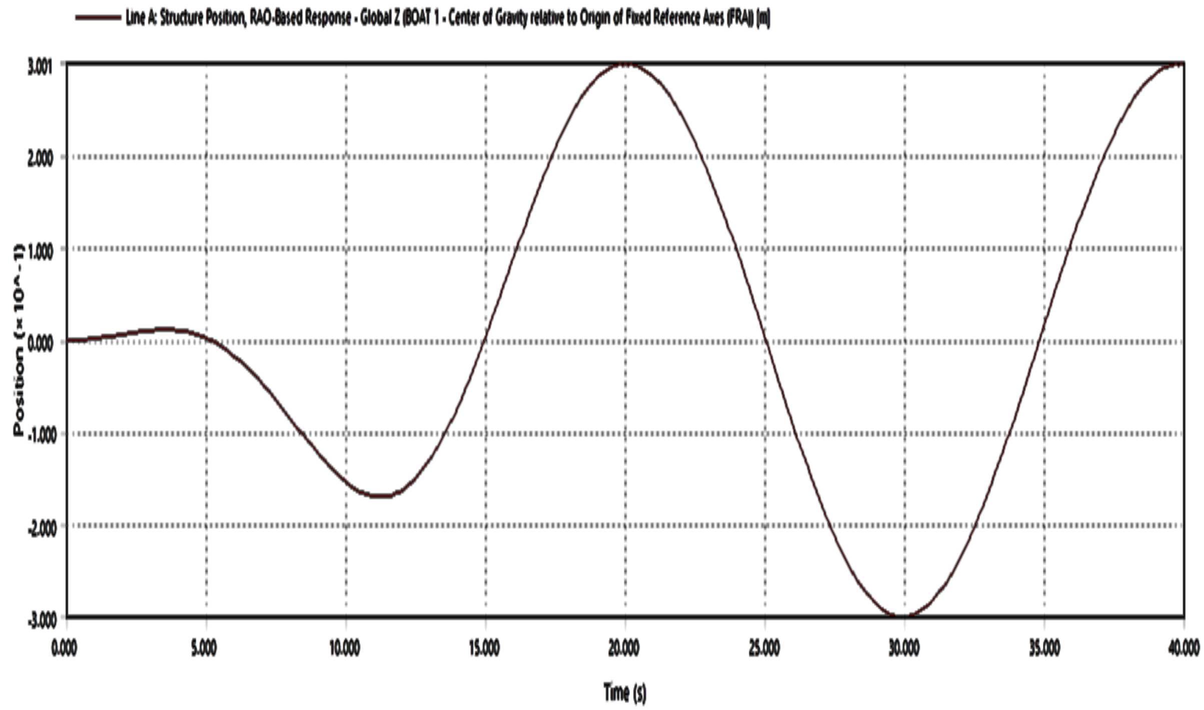

Figure B- 5. Heave in quartering Seas for the mass of 2800kg

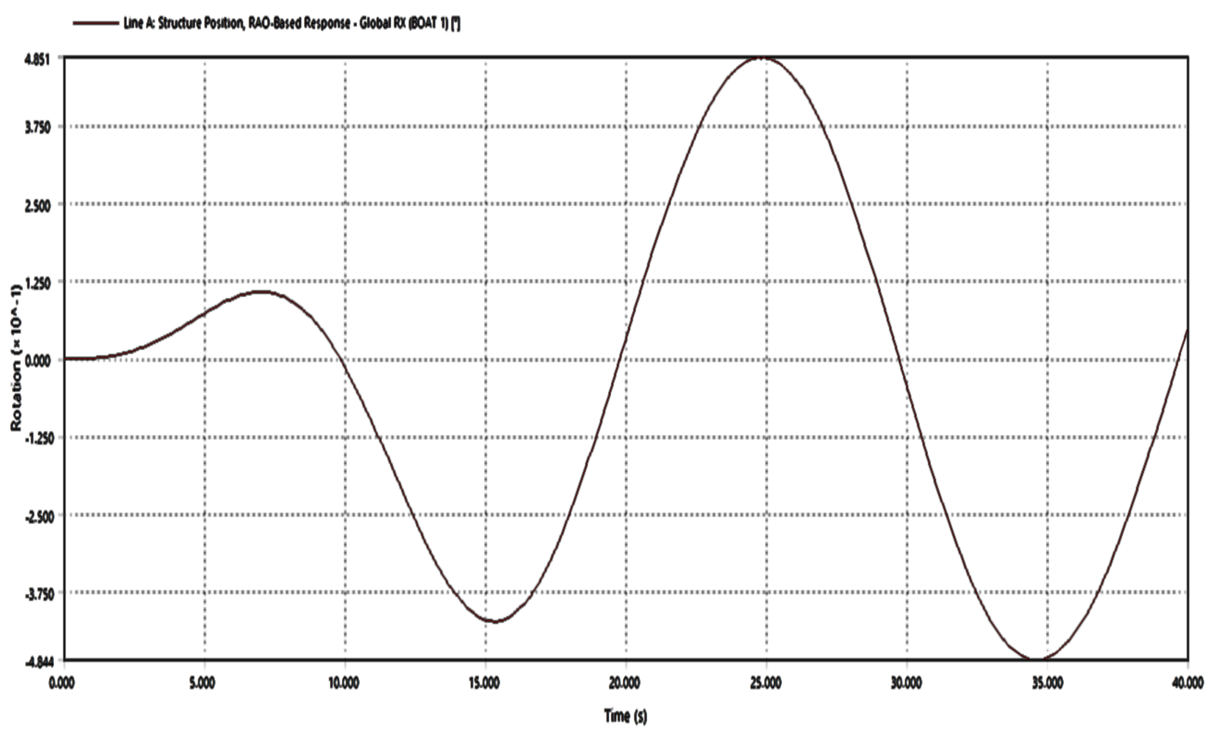

Figure B- 6. Roll in beam Seas for the mass of 2800kg

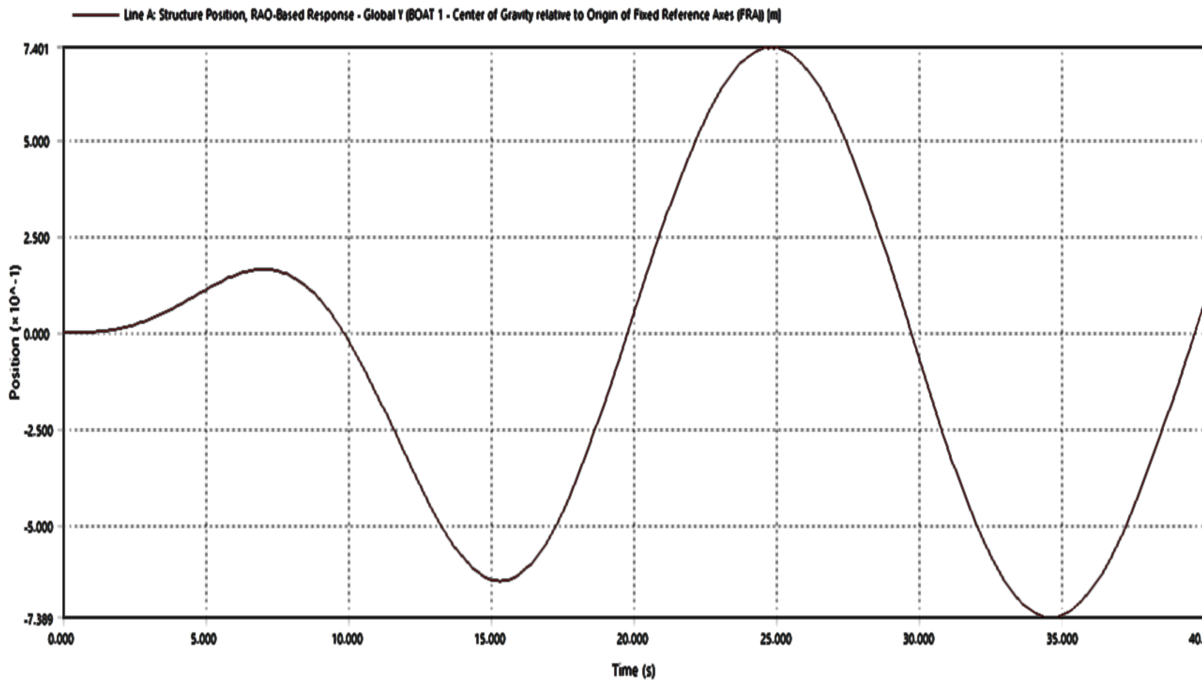

Figure B- 7. Sway in beam Seas for the mass of 2800 kg

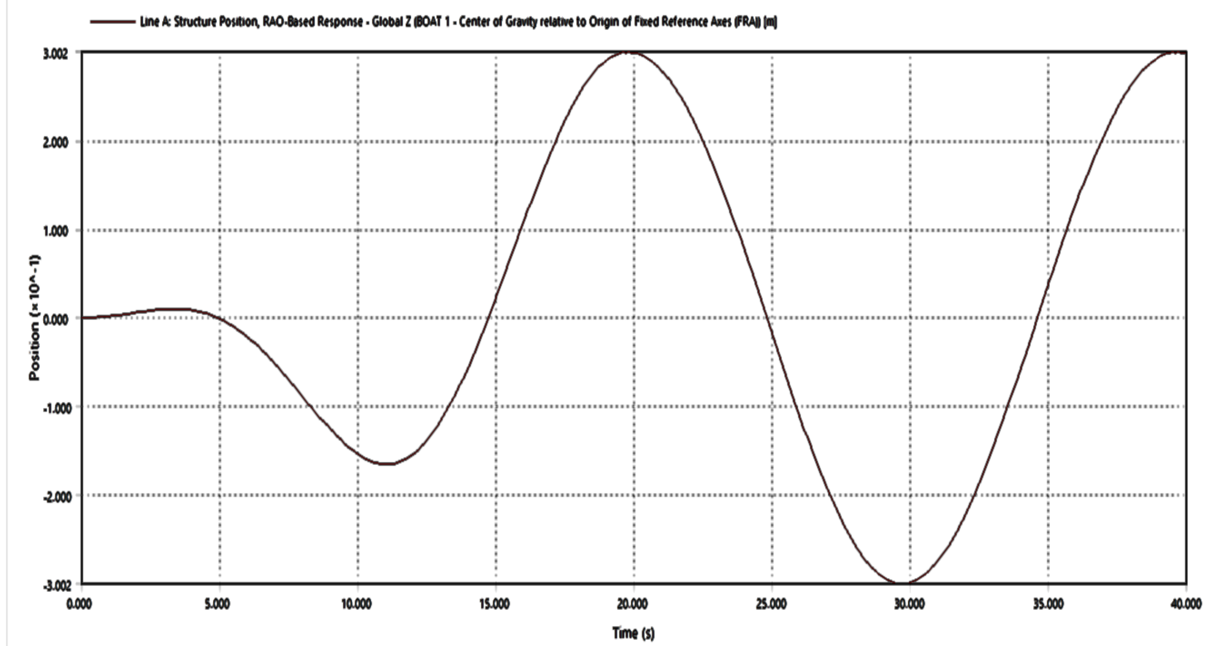

Figure B- 8. Heave in beam Seas for the mass of 2800kg

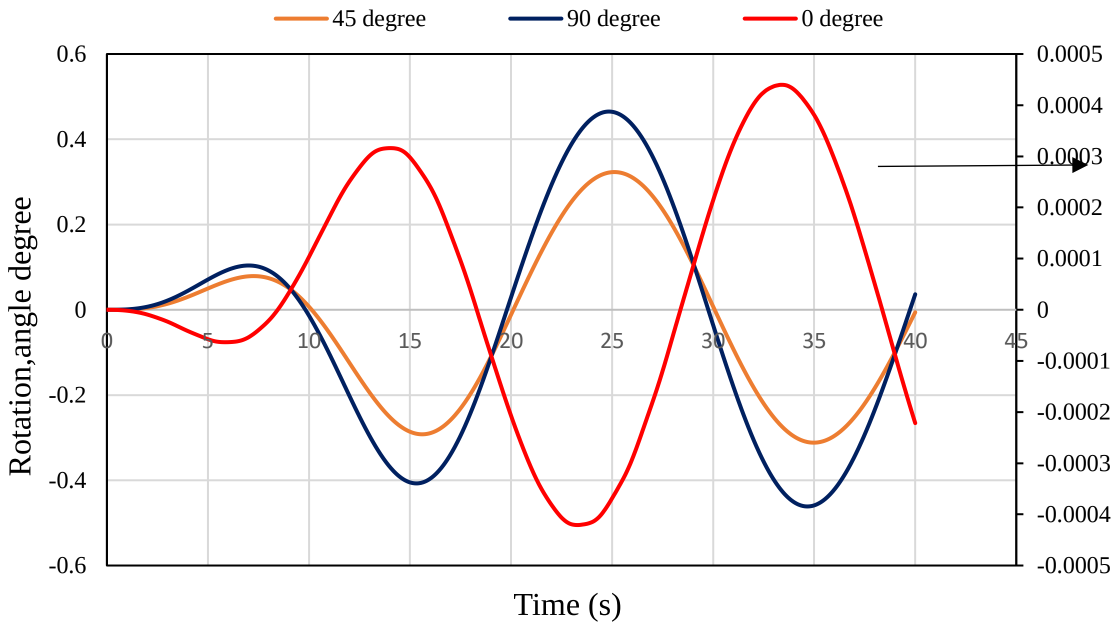

Figure B- 9. Roll in different wave directions for 800 kg

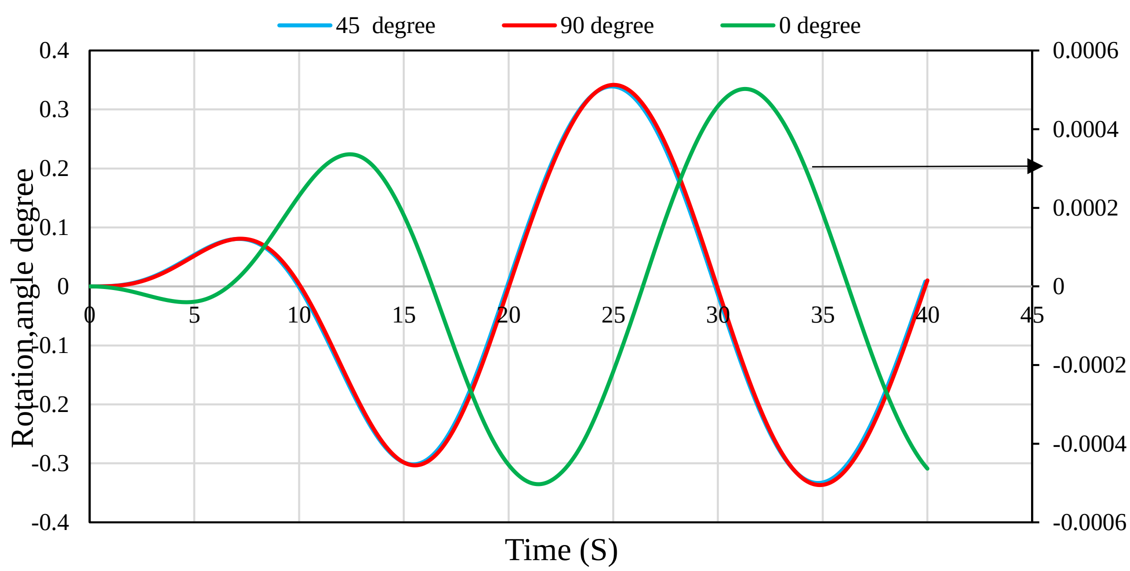

Figure B- 10. Roll in different wave directions for 2300 kg

Appendix C: Residual Coefficient Curve According to ITTC 57

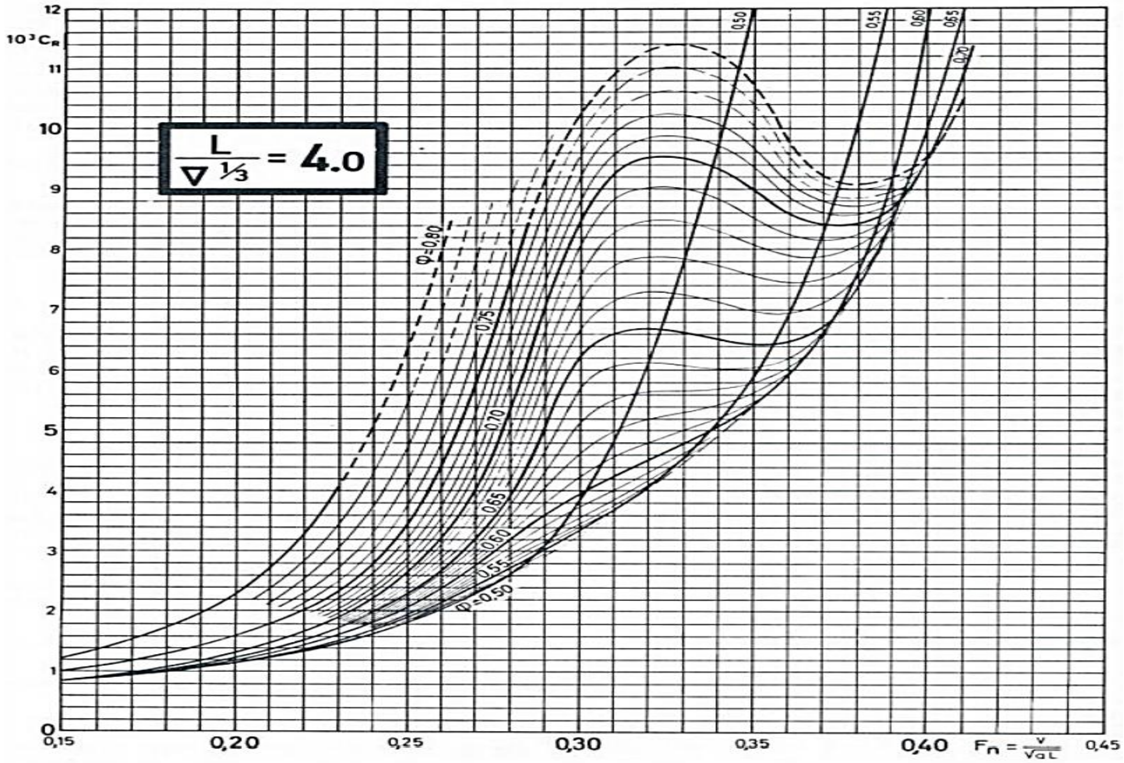

Figure C- 1. Residual Coefficient Curve for the Froude number 4.0

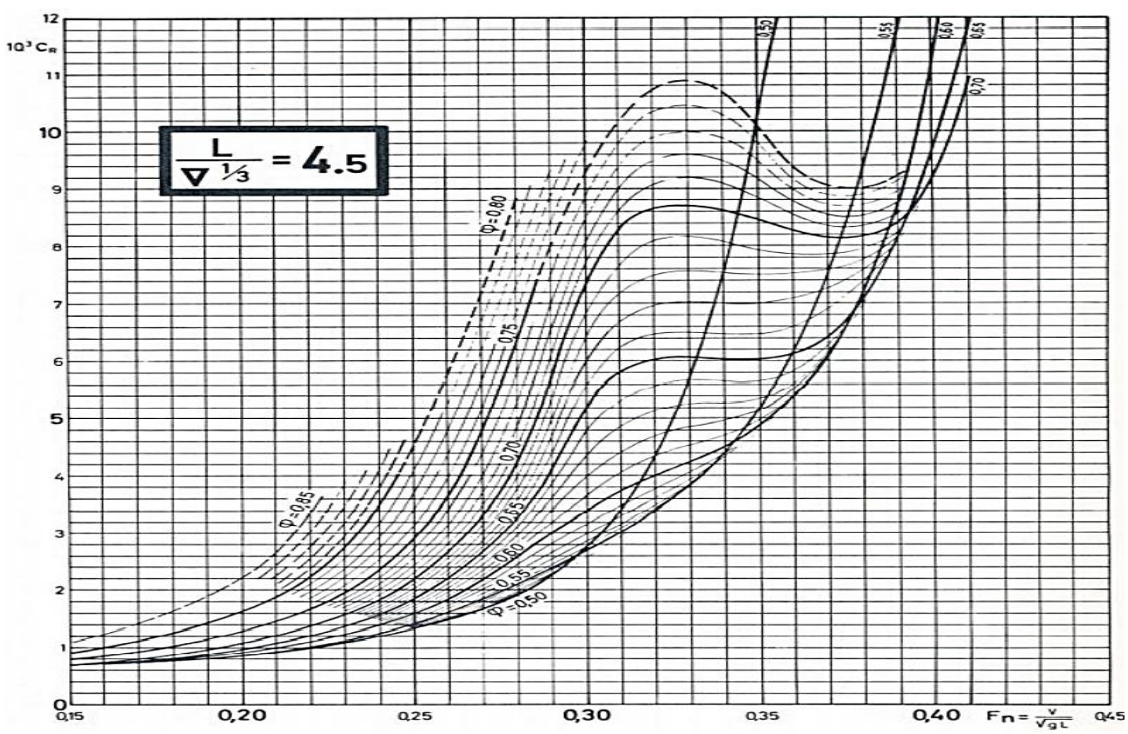

Figure C- 2. Residual Coefficient Curve for the Froude number 4.5

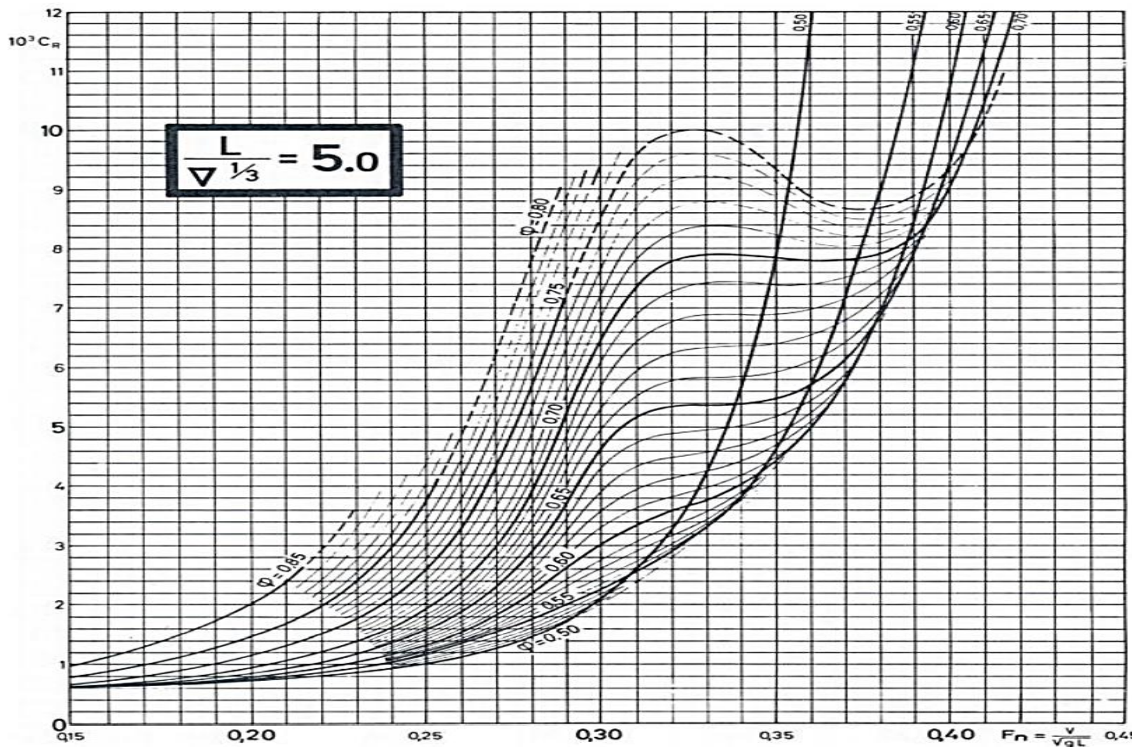

Figure C- 3. Residual Coefficient Curve for the Froude number 5.0

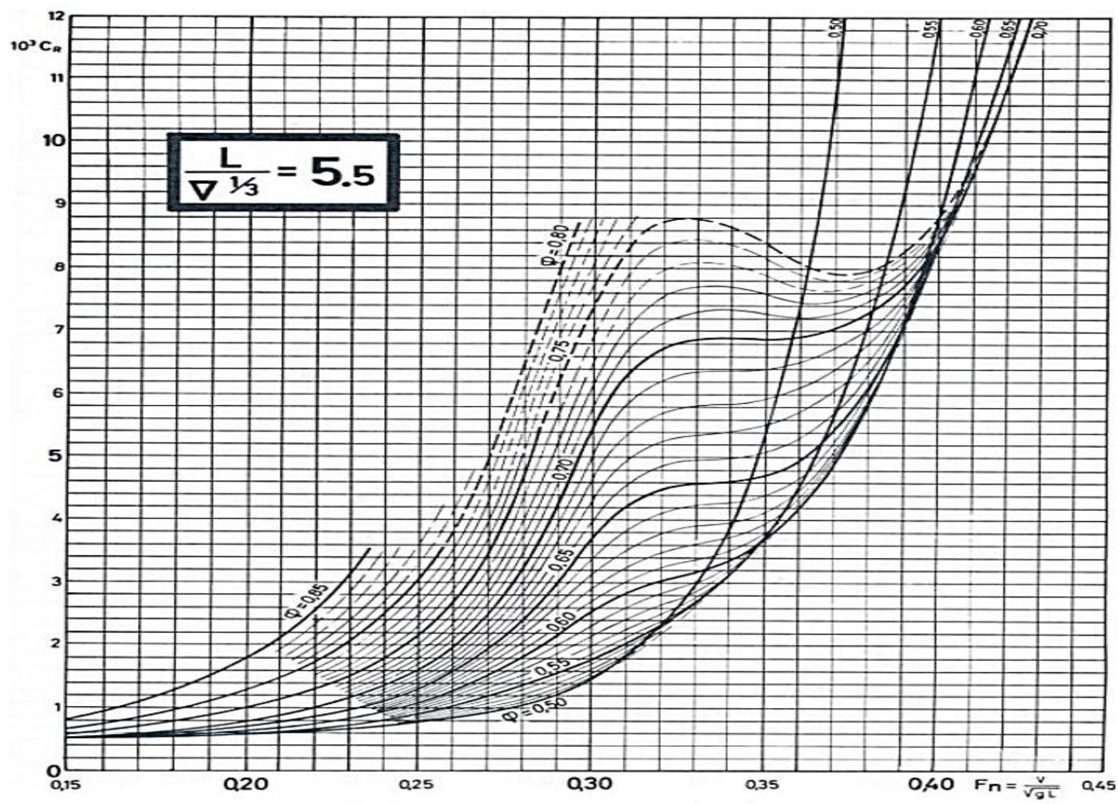

Figure C- 4. Residual Coefficient Curve for the Froude number 5.5

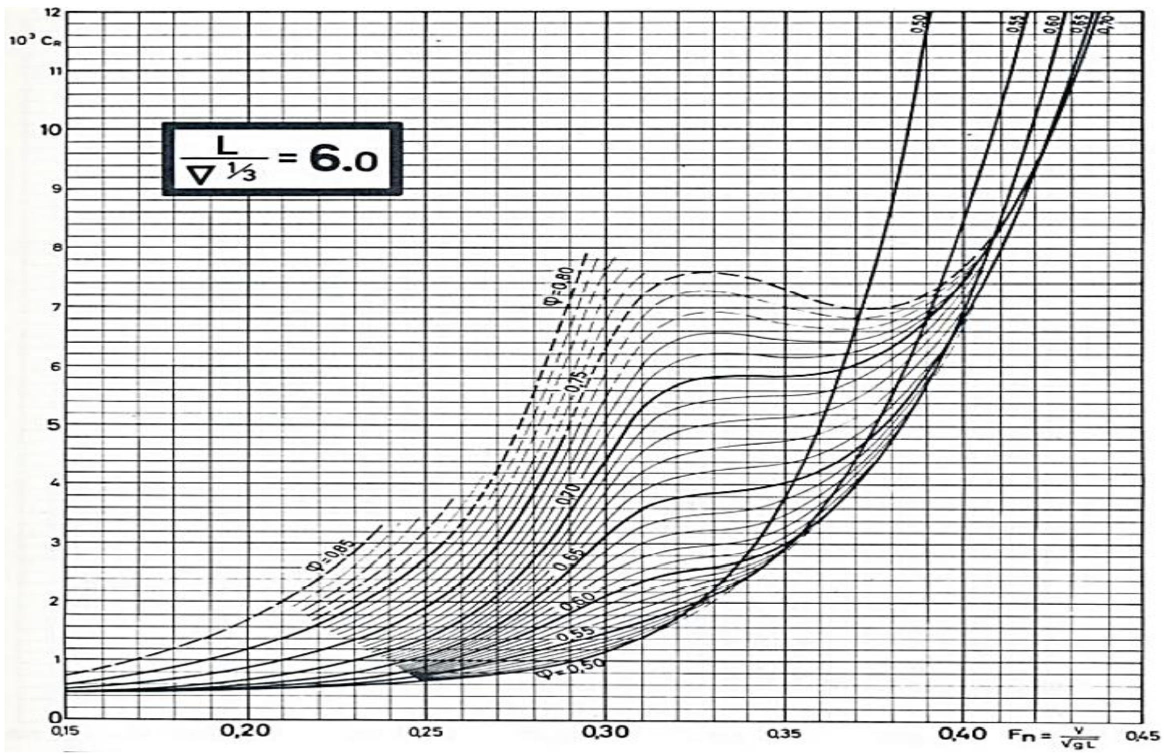

Figure C-5. Residual Coefficient Curve for the Froude number 6.0

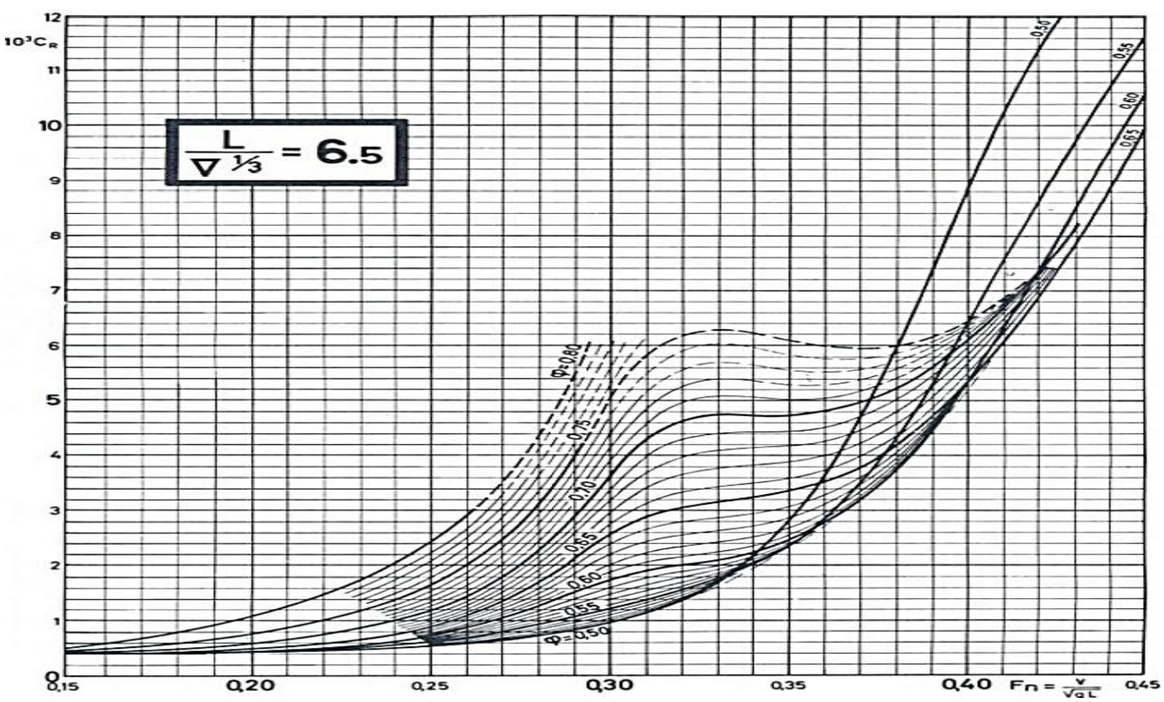

Figure C-6. Residual Coefficient Curve for the Froude number 6.5

Appendix D: Wind Force Coefficient for Standard River Boat (Grm A, 2017).

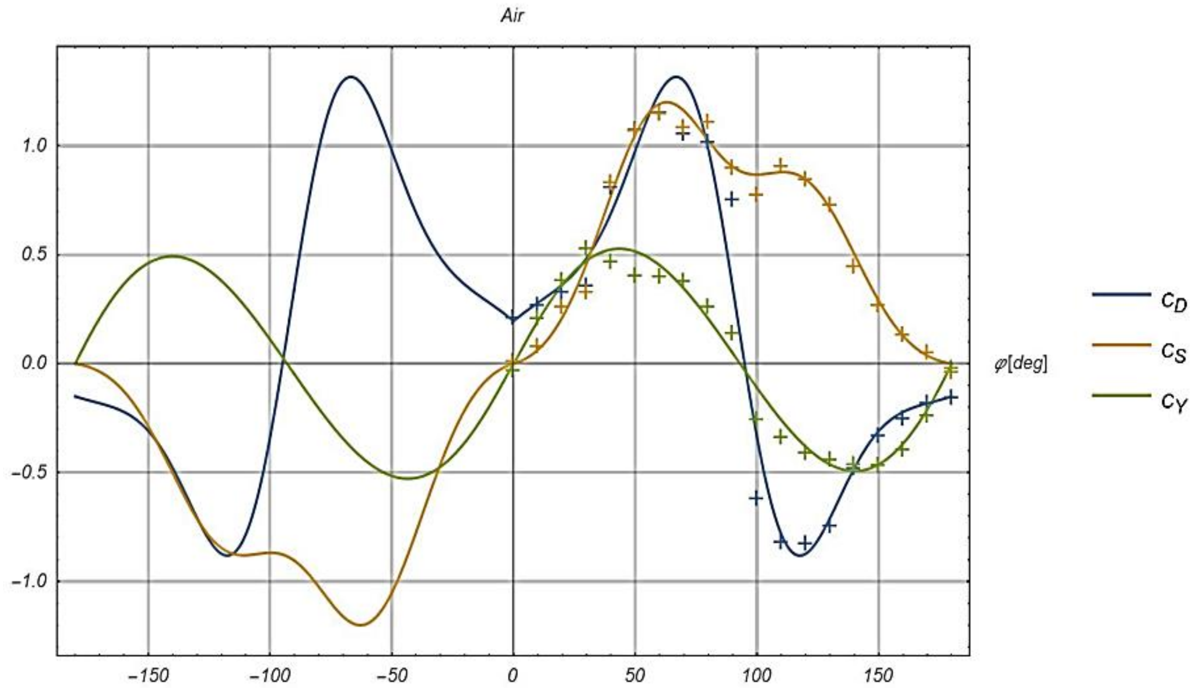

Figure D-1.Wind Force Coefficient

Appendix E: Boat Motor Catalog specifications and Propellers

Elco ELECTRICOUTBOARD

EP-9.9 ELECTRIC OUTBOARD FEATURES AND BENEFITS

- Reliable and durable construction with minimal maintenance required
- Available in tiller or top- and side-mount throttle control
- All motors available in long- or short shaft models
- Traditional design with standard aluminum casting so replacement parts are readily available
- Water-cooled system that prevents over-heating
- Multiple safety precautions including over-speed protection, overload protection, temperature protection, over-voltage and over-current protection
- Consistent power throughout the speed range
- Brushless PMAC motor that is over 90-percent efficient
- Cruise with peace of mind thanks to our "Get Home Safe" battery alert system
- Motors ranging from 5-HP to 50-HP
- Clean cruising without the hassles and hazards of gasoline
- Low cost of operation when compared to traditional gas motors

Table E-1. Boat Motor Catalog specifications

INPUT POWER (WATTS)	4,704 watts
VOLTAGE	48 vdc
MAXIMUM CURRENT	98 amps DC
MOTOR	Brushless PMAC
COOLING SYSTEM	Water cooled
WEIGHT	65 lbs

Table E-2.Propellers specifications for boat

Aluminum 4 Deluxe-8 HP Pin Drive, 2-Stroke

- 4 & 4.5 HP, 1980 - 1986
- 6 / 7.5 / 8 HP, 1980 - 2005
- 7 HP Commercial, 1991 - 2000

RH P/N	LH P/N	Description	Blades	Dia.	Pitch
778796		Aluminum	3	8"	7"

Aluminum 6 HP Pin Drive, 2-Stroke

- 1966 - 1979

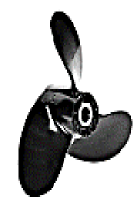

RH P/N	LH P/N	Description	Blades	Dia.	Pitch
763745		Aluminum	2	8"	7 1/4"
763588		Aluminum	3	8 1/4"	8"
763586		Aluminum	3	8 1/4"	9"

Appendix F: Assembly Drawings

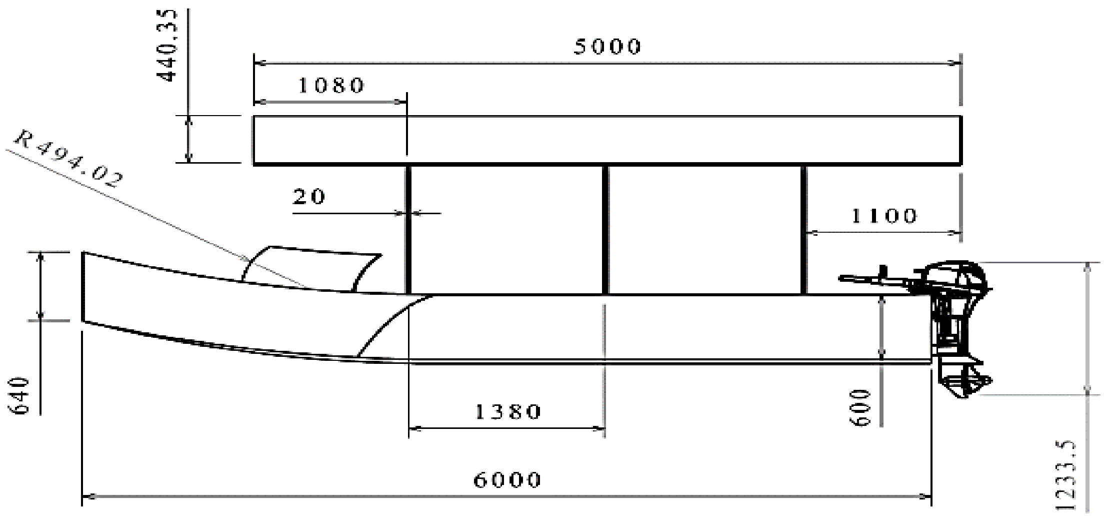

Dimensions are in mm.

Side View of the Boat	ASTU	
Drawn By Tigist Andarge	Side View	
Advisor Dr. Addisu Bekele	Size A4	Drawing Number 1
Scale 1:1	Sheet 1/3	

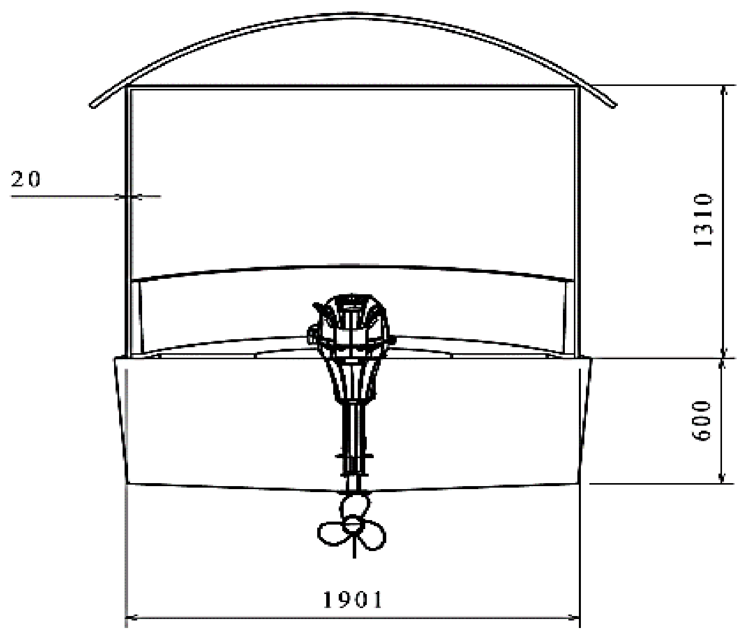

Dimensions are in **mm**.

Rear View of the Boat	ASTU		
Drawn By Tigist Andarge	Rear View		
Advisor Dr. Addisu Bekele	Size A4	Drawing Number 2	
Scale 1:1	Sheet	2/3	

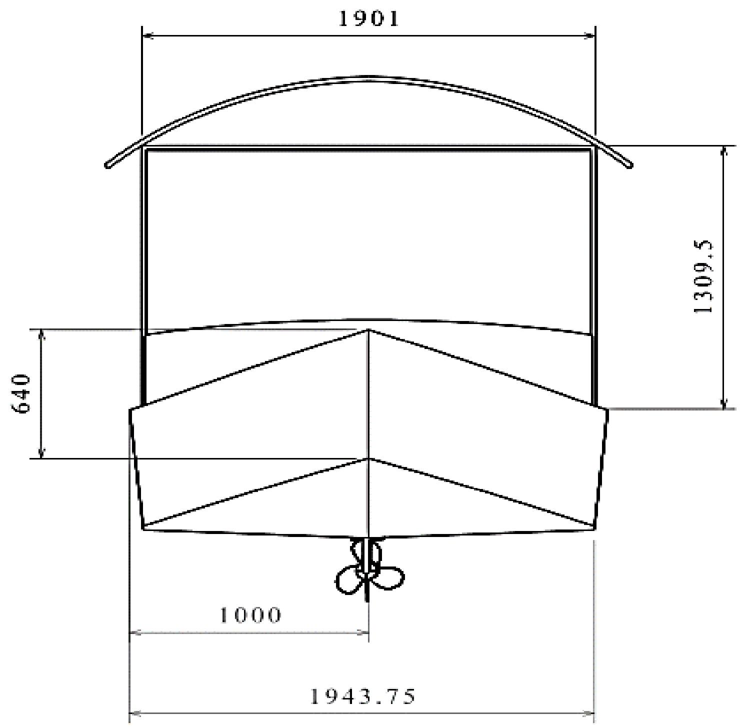

Dimensions are in **mm**.

Front View of the Boat	ASTU	
	Front View	
Drawn By Tigist Andarge		
Advisor Dr. Addisu Bekele	Size A4	Drawing Number 3
Scale 1:1	Sheet 3/3	